Fisheries and Oceans Canada | Pêches et Océans Canada
Ecosystems and Oceans Science | Sciences des écosystèmes et des océans

Canadian Science Advisory Secretariat (CSAS)

Research Document 2024/039

Quebec Region

Describing the Seasonal and Spatial Distribution of *Calanus* Species and North Atlantic Right Whale Potential Foraging Habitats in Canadian Waters Using Species Distribution Models

S. Plourde[1], C. Lehoux[1], J.J. Roberts[2], C.L. Johnson[3], N. Record[4], P. Pepin[5], C. Orphanides[6], R.S. Schick[2,7], H. J. Walsh[6], C.H. Ross[4,8]

[1] Fisheries and Oceans Canada, Maurice-Lamontagne Institute, 850 Route de la Mer, Mont-Joli, Québec Canada G5H 3Z4

[2] Marine Geospatial Ecology Lab, A328 Levine Science Research Center, Duke University, Durham, NC 27708, USA

[3] Fisheries and Oceans Canada, Bedford Institute of Oceanography, PO Box 1006, Dartmouth, Nova Scotia Canada B2Y 4A2

[4]Tandy Center for Ocean Forecasting, Bigelow Laboratory for Ocean Sciences, East Boothbay, ME 04544, USA

[5] Fisheries and Oceans Canada, Northwest Atlantic Fisheries Centre, 80 White Hills Road, PO Box 5667, St. John's, Newfoundland and Labrador, Canada A1C 5X1

[6] NOAA Fisheries, Northeast Fisheries Science Center, 28 Tarzwell Drive, Narragansett, Rhode Island, 02882

[7] Southall Environmental Associates, Inc., 9099 Soquel Drive, Suite 8, Aptos, CA United States 95003

[8] Darling Marine Center, University of Maine, School of Marine Sciences, Walpole, ME United States 04573

August 2024

Foreword

This series documents the scientific basis for the evaluation of aquatic resources and ecosystems in Canada. As such, it addresses the issues of the day in the time frames required and the documents it contains are not intended as definitive statements on the subjects addressed but rather as progress reports on ongoing investigations.

Published by:

Fisheries and Oceans Canada
Canadian Science Advisory Secretariat
200 Kent Street
Ottawa ON K1A 0E6

http://www.dfo-mpo.gc.ca/csas-sccs/
csas-sccs@dfo-mpo.gc.ca

ISSN 1919-5044
ISBN 978-0-660-72875-9 Cat. No. Fs70-5/2024-039E-PDF

Correct citation for this publication:

Plourde, S., Lehoux, C., Roberts, J.J., Johnson, C.L., Record, N., Pepin, P., Orphanides, C., Schick, R.S., Walsh, H.J., Ross, C.H. 2024. Describing the Seasonal and Spatial Distribution of *Calanus* Prey and North Atlantic Right Whale Potential Foraging Habitats in Canadian Waters Using Species Distribution Models. DFO Can. Sci. Advis. Sec. Res. Doc. 2024/039. v + 71 p.

Aussi disponible en français :

Plourde, S., Lehoux, C., Roberts, J.J., Johnson, C.L., Record, N., Pepin, P., Orphanides, C., Schick, R.S., Walsh, H.J., Ross, C.H. 2024. Description de la répartition saisonnière et spatiale des proies du genre Calanus *et des habitats potentiels d'alimentation de la baleine noire du nord de l'Atlantique dans les eaux canadiennes à l'aide de modèles de répartition des espèces. Secr. can. des avis sci. du MPO. Doc. de rech. 2024/039. v + 75 p.*

TABLE OF CONTENTS

ABSTRACT

The goal of this study was to describe the seasonal and spatial variations of *Calanus* species abundance and North Atlantic Right Whale (henceforth NARW) potential foraging habitat in Canadian waters during 1999-2020. We took advantage of oceanographic monitoring programs in Canada and USA to develop an integrated modelling approach including the following elements: (1) Species Distribution Models (SDMs) of *Calanus finmarchicus*, *C. glacialis* and *C. hyperboreus* to predict their abundance, (2) predicted abundance converted in biomass to account for differences in body size among *Calanus* species, (3) Generalized Additive Models (GAMs) describing the seasonal variations in *Calanus* vertical distribution, (4) a multispecies 3-D prey layer combining species-specific water column biomass and vertical distribution, and (5) a right whales bioenergetic model to assess prey suitability and describe the seasonal and spatial distribution of potential foraging habitat. Using GAMs, we built a suite of SDMs based on different mechanistic assumptions about the drivers of *Calanus* species populations across Canadian and US waters. The best performing models included a seascape 'connectivity' term in addition to other key covariates (temperature, bathymetry) and assumed that *Calanus* species responses to covariates were generally the same across the domain (no local adaptation) with strong influence of transport in specific locations. The temperature and 'connectivity' terms captured realistic patterns of influence of different temperature regimes and waters masses on *Calanus* across Canadian waters. Our integrated modelling approach successfully identified known (ex: Roseway Basin) and newly identified (ex: southern GSL) NARW foraging habitats as well as other potential foraging habitats across Canadian waters. Our results showed that NARW potential foraging areas in Canadian waters are determined by an assemblage of multiple *Calanus* species that varies across space and time. Therefore, inferences about past, current and future resilience of NARW foraging habitats to variations in environmental conditions and climate change should be carefully made due to species-specific responses to these changes.

1. INTRODUCTION

The subarctic *Calanus finmarchicus* and the arctic *C. glacialis* and *C. hyperboreus* dominate zooplankton biomass in Canadian Atlantic waters with region-specific differences in their contribution (Sorochan et al. 2019, DFO 2023). *Calanus* species have a complex life cycle and use different habitats during their annual cycle (Conover 1988). Active growth, development and lipid accumulation predominantly occur in the upper layer of the water column, whereas lipid-rich late development stages generally overwinter in a resting state at greater depths associated with lower local temperature (Wishner et al.1995, Plourde et al. 2001, Plourde et al. 2003, Baumgartner et al. 2017, Krumhansl et al. 2018). Individual vital rates (e.g., respiration, feeding, development, growth, egg production) and population dynamics parameters (production, mortality, survival, abundance) are affected by temperature but with different species-specific optima (Plourde et al. 2009, Moller et al. 2012, Chust et al 2014, Pasternak et al. 2013, Alcaraz et al. 2014, Albouy-Boyer et al. 2016).

The eastern Canadian and northeast USA continental shelf is characterized by a predominantly southward circulation and anticlockwise currents pattern in the Gulf of St. Lawrence (GSL, see Table 1 for the full list of acronyms) and in the Gulf of Maine (GOM) (Loder et al. 1998, Figure 2). In general, the inner shelf is influenced by fresher water originating from the Arctic or from rivers such as the St. Lawrence River, while the outer shelf is more influenced by saltier water originating from the continental shelf slope and ocean basin (Loder et al. 1998). The origin (water masses) and the timing of transport events could vary among *Calanus* species because of the interplay between variations in circulation patterns and in species phenology (presence in the surface layer). Advection has been shown to play a key role in sustaining *Calanus* populations at different spatial and temporal scales across the Ecosystem Monitoring Program (EcoMon)-Atlantic Zone Monitoring Program (AZMP) spatial domain, including Cape Cod Bay (CCB), Scotian Shelf (SS), southern GSL (sGSL) and the eastern Newfoundland shelf (eNL) (Miller et al. 1998, Head et al. 2003, Zakardjian et al. 2003, Jiang et al. 2007, Maps et al. 2011, Brennan et al. 2021, Pepin et al. 2013).

North Atlantic Right Whale (NARW henceforth) seasonal foraging migrations occur at large scales. During its main foraging season (spring to fall), NARW aggregate in regions characterized by high abundance of their preferred prey, the lipid-rich *C. finmarchicus*, on which they feed either in the surface or deep layers depending on locations and seasons (see Baumgartner et al. 2017 and references therein). In the early 2010s, occurrence of NARW markedly decreased in traditionally used foraging habitats in Great South Channel (Spring), Grand Manan and Roseway basin (Summer-Fall) in response to a decrease in prey availability (Record et al. 2019, Meyer-Gutbrod et al. 2023). Following this, about one third of the NARW population have used the sGSL since the late 2010s likely because of the combined high abundance of *C. hyperboreus* and relatively shallow bathymetry in the region (Simard et al. 2019, Plourde et al. 2019, Lehoux et al. 2020). The observed change in NARW distribution, the results from previous work on prey in the sGSL, and sightings in other areas in summer and fall suggest that NARW could forage on prey aggregations dominated by species other than *C. finmarchicus* and that other potential foraging habitats could exist elsewhere in Canadian waters.

Despite previous studies based on *Calanus* abundance data covering spatial and temporal scales relevant to NARW seasonal migrations (Plourde et al. 2019, Sorochan et al. 2019, Meyer-Gutbrod et al. 2023), a comprehensive description of *Calanus* species spatial and seasonal distribution across regions known or hypothesized to be visited by NARW during their foraging season is still lacking. In this context, the goal of this study was to describe the seasonal and spatial variations of *Calanus* species abundance and NARW potential foraging

habitat in Canadian waters during 1999-2020. We took advantage of different monitoring programs and tools to develop an integrated modelling approach including the following elements: (1) Species Distribution Models (SDMs) of *C. finmarchicus*, *C. glacialis* and *C. hyperboreus* to predict abundance, (2) a multispecies prey layer estimated from predicted abundance converted into biomass to account for up to a one order of magnitude differences in body size among these *Calanus* species, (3) Generalized Additive Models (GAMs) describing the seasonal variations in *Calanus* vertical distribution, (4) a multispecies 3-D prey layer combining species-specific water column biomass and vertical distribution, and (5) a NARW bioenergetic model to assess prey suitability across space and time. Data collected by monitoring programs in eastern Canada and USA waters were used to develop and assess the performance and accuracy of a suite of *Calanus* SDMs with the goal of identifying the best model for describing NARW foraging habitat. Our results were presented in Canadian waters. Our *Calanus* SDMs' results were discussed in the context of the known drivers of *Calanus* species seasonal and spatial distribution, while our predictions of NARW foraging habitat suitability were compared to traditionally used foraging habitats. Our results highlighted potential new NARW foraging areas in Canadian waters.

2. MATERIAL AND METHODS

2.1. SOURCES OF DATA

2.1.1. *Calanus* species data

The Atlantic Zone Monitoring Program (AZMP) is conducted by the Department of Fisheries and Oceans Canada (DFO) and routinely samples zooplankton across eastern Canadian waters since 1999 with a 200-µm mesh plankton net twice a year in spring and fall. High frequency stations are also visited on a monthly to a weekly basis mainly in spring to fall, and less frequently in winter. Vertical plankton net tows are conducted from 5 metres above the bottom (maximum sampling depth = 1000 m) up to the surface. In AZMP, *Calanus* are identified to species and stages; for more details on zooplankton sampling protocols see Mitchell et al. (2002). Zooplankton on the Northeastern USA shelf are routinely collected as part of the EcoMon program conducted by the National Oceanic and Atmospheric Administration (NOAA, Northeast Fisheries Science Center 2019) since 1977. Zooplankton is sampled using oblique tows with 333 µm mesh Bongo between 0 and 200 m or 5-metres above the bottom. In EcoMon, both *C. glacialis* and *C. hyperboreus* are aggregated in a *Calanus* spp taxon. Because *C. glacialis* shows abundance one order of magnitude lower than *C. hyperboreus* in the nearest region sampled by AZMP (Casault et al. 2022), the western SS, *Calanus* spp. in EcoMon was considered as *C. hyperboreus* in our analyses. For stations positions and seasonal sampling effort in both programs see Figure 1 and Figure A.1. 1 respectively.

The different zooplankton sampling protocols in AZMP and EcoMon implied that a standardization of the zooplankton data was necessary to combine them in the model building. We first restricted our analyses to the late development stages CIV-VI as they are similarly sampled by the 200 and 333 µm mesh nets, and because the filtering efficiency of the NARW baleen is roughly equal to a 333 µm mesh net (filtering efficiency ~1 for *Calanus* > 1.5 mm body length, Mayo et al. 2001). Since maximum sampling depth in EcoMon is 200 m compared to 1000 m in AZMP, we used monthly predictions of vertical distribution by our models in the GOM (*C. finmarchicus*) and western SS (*C. hyperboreus*) (see below) to standardize abundance data in EcoMon and make them comparable to AZMP data. Finally, AZMP regularly sampled stations with bottom depth > 1000 m, which is not the case in EcoMon. These stations were excluded to

maintain homogeneous bathymetric limits across our spatial domain. As a result, 16,333 stations were retained across the AZMP-EcoMon domain (Figure A.1. 1).

2.1.2. Environmental covariates and underlying mechanistic hypotheses

The selection of covariates for SDMs was based on ecological theory and was hypothesis-driven, because of a direct mechanistic causal link between temperature-related covariates and their expected effects on *Calanus* physiology and population abundance. We used temperature in 0-50 m (T_0-50) and the temperature minimum in the water column (Tmin) as a proxy of the thermal envelope during the active growth and overwintering periods with the explicit hypothesis that *C. finmarchicus* would show a different temperature preference and optimum relative to the arctic *C. glacialis* and *C. hyperboreus*. Bathymetry was included as a proxy of the availability of the overwintering habitat and because of its strong effect on *Calanus* abundance across the region (Albouy-Boyer et al. 2016, Grieve et al. 2017, Ross et al. 2023).

We developed candidate SDMs based on two criteria: presence or absence of local adaptations, and processes at the regional level and how the seascape is formulated (see section 2.2.1 below). Given the importance of transport in driving *Calanus* species seasonal distribution across the eastern Canadian shelf, one candidate model formulation aimed at capturing the coarse spatial and seasonal patterns in connectivity by developing a model formulation based on the '*Supply – Aggregation – Availability '* framework (Sorochan et al. 2021, Johnson et al. in preparation[1]) with an emphasis on the elements associated with '*supply*'. In this formulation, Latitude was used as a first level proxy of the distance from a source region (*Regional population levels*) as there are clear north-south species-specific abundance patterns across the spatial domain (Sorochan et al. 2019). Then, we used a spatial climatology of salinity in the 0-50 m layer (climS_0-50sqrt, see below) to structure the salinity seascape and putative pathways of connectivity (*Advective supply*) and source regions along fresher (inner shelf) and saltier (outer shelf) water masses (Figure 2). Finally, our connectivity framework included Month to account for species-specific seasonality in *Calanus* species life cycle. These three covariates were combined in a 'connectivity' interaction term (see section 2.2.1). Local coupled biological-physical processes (a*ggregation*) were therefore not considered as they generally occur at smaller time and spatial scales than the monthly time scale considered in our SDMs, while '*availability*' was taken into account with the use of the 3D prey layer and NARW bioenergetic model (see below) (Sorochan et al. 2021).

T_0-50 and Tmin by month and year during 1999-2020 were used to match the main mode of zooplankton sampling in AZMP and EcoMon, thus addressing our goal to model seasonal (i.e., monthly) and spatial variations in *Calanus* abundance.

GLORYS12v1 data products were considered the best available source of data at the scale addressed in our study, although surface salinity was generally underestimated in the western GSL (see Figure A.1. 3) (Lellouche et al. 2021, Castillo-Trujillo et al. 2023). T_0-50,Tmin, and salinity monthly indices were thus derived from monthly GLORYS12v1 depth-resolved products using the *CopernicusMarine* R package (de Vries 2023). GLORYS12v1 bathymetry is derived from ETOPO1 (Amante and Eakins 2009) for deep ocean and GEBCO8 on the coast and continental shelf.

[1] Johnson, C.L., Plourde, S., Brennan, C.E., Helenius, L.K., Le Corre, N. and Sorochan, K.A. In preparation. The Southern Gulf of St. Lawrence as a Foraging Habitat for the North Atlantic Right Whale. DFO Can. Sci. Advis. Sec. Res. Doc.

The average of S_0-50 across each month for years 1999-2020 was calculated and transformed:

$$climS\_0-50sqrt = \sqrt{34.05306 - S\_0\_50_{x,y}}$$

where 34.05306 was the 99th quantile of all salinity in the climatology. See Figure A.1. 4 for the effect of the transformation on the distribution of salinity values. This transformation is effective for left-tailed covariates, but inverse its scale. Therefore, low (high) values of climS_0-50sqrt represent high (low) salinities.

2.2. *CALANUS* SPECIES DISTRIBUTION MODELS

2.2.1. Species Distribution models: Generalized Additive Mixed Models (GAMM)

SDMs were built for each species separately using abundance data and the monthly GLORYS12v1 product at the zooplankton station position. The transboundary approach (large spatial domain encompassing the northeast USA and Canada shelf) implied that a greater range of environmental covariates and varying habitat quality were considered relative to previous species distribution models performed in some regions (Albouy-Boyer et al. 2016, Grieve et al. 2017, Ross et al. 2023).

We developed a set of candidate SDMs using Generalized Additive Mixed Models (GAMM) to identify which set of covariates provide the better representation of the data across the distributional range of the three species of *Calanus* (Wood 2017). Each species abundance (n m^{-2}) followed a zero-altered Gamma (ZAG) distribution with a log link:

$$Abundance_i = \mathrm{ZAG}(\pi_i \mu_i)$$

$$E(Abundance_i) = \pi_i \times \mu_i$$

$$var(Abundance_i) = \frac{\pi_i \times r + \pi_i - \pi_i^2 \times r}{r} \times \mu_i^2$$

where π_{sy} is the probability of presence for observation *i* and has a Bernoulli error distribution, μ_{sy} is the abundance given presence and has a Gamma error distribution. The model error structure is thus generated by running the model twice (presence/absences, Abundance > 0) and combining predictions. r is a scaling factor.

Model 1 was equivalent to models previously done separately with AZMP (Albouy-Boyer et al. 2016) and EcoMon (Grieve et al. 2017) assuming that *Calanus* species would not adapt to local environmental conditions or that the same environmental relationships hold across the entire spatial domain (no regional factorization):

$$log\,it(\pi_i)\ or\ log(\mu_i) = s(Month) + s(SSS) + s(T\_0\_50) + s(Tmin) + s(log_{10}bathymetry) + fYear_i$$

Model 2 was similar to Model 1 but assumed that *Calanus* species could adapt to local environmental conditions or there are specific environmental processes affecting species abundance in all different regions (with regional factorization, n= 9, see Figure A.3.5):

$$log\,it(\pi_i)\ or\ log(\mu_i) = Region + s(Month \times Region) + s(SSS \times Region) + s(T\_0\_50) + s(Tmin) + s(log_{10}bathymetry) + fYear_i$$

Model 3.1 included the 'connectivity' interaction term described above with no regional factorization (no local adaptation or processes):

$$log\,it(\pi_i)\ or\ log(\mu_i) = ti(Month \times latitude \times climS\_0\_50sqrt) + s(T\_0\_50) + s(Tmin) + s(log_{10}bathymetry) + fYear_i$$

Model 3.2 was similar to 3.1 but included limited regional factorization (n = 4, see Figure 1 left) to account for the dominance of transport in few specific regions not captured by other covariates:

$$log\,it(\pi_i)\ or\ log(I) = Region + ti(Month \times latitude \times climS\_0\_50sqrt) + s(T\_0\_50) + s(Tmin) + s(log_{10}bathymetry) + fYear_i$$

Model 3.3 optimized 3.2 by Winsorizing Tmin (pmin, Dixon et al. 1960) when justified (*C. finmarchicus and C. hyperboreus,* see below):

$$log\,it(\pi_i)\ or\ log(\mu_i) = Region + ti(Month \times latitude \times climS\_0\_50sqrt) + s(T\_0\_50) + s(pmin(Tmin)) + s(log_{10}bathymetry) + fYear_i$$

In models 3.2 and 3.3, the four regions were the sGSL, GB, CCB and a large region encompassing the rest of the study area (MAB, SNE, GOM, Fundy-GOM, SS, nGSL, eNL and LAB) (see Figure 1 and Figure A.3. 5).

In all models, Year was a random intercept. Region was an intercept to capture the effect that local circulation processes not captured by other variables could have on abundance. *s* is a thin plate regression spline (Wood et al. 2003) and *ti* is a tensor product interaction for which we included the main effects and the lower-level interactions (Wood et al. 2006). The dimensional basis used to represent the smooth term (k) was reduced to avoid overfitting (Tmin <= 8, T_0_50 <=5, bathymetry <=5, month, latitude and climS_0_50sqrt <= 6 for main effects and <=3 for the interaction).

Tmin > 20°C (*C. finmarchicus*) and >10°C (*C. hyperboreus*) were Winsorized in model 3.3 (indicated by pmin) to minimize the potential impact of occurrences under warmer conditions than expected (due to their southward transport) on predictions in other regions/months in Canadian waters. It means that the partial effects and associated confidence intervals of Tmin were kept constant at temperature greater than these species-specific thresholds. Temperature covariates were not winsorized for *C. glacialis* as occurrence and abundance in this cold-water species generally showed the expected decreasing relationship with T_min and T_0-50 (see Results). Therefore, model 3.3 was not performed for this species.

GAMs were fitted using the package *mgcv* (Wood 2017) in R.

2.2.1.1. Validation and model selection

Homogeneity of Pearson's residuals of the abundance predictions (π x μ) and accuracy of predictions against observation were verified graphically. We performed 10,000 model simulations of π and μ (ZAG model) to assess if the models were adequate for the zero inflation of abundance data, especially for *C. hyperboreus* and *C. glacialis*. From these simulations, we calculated the 50th, 75th, 85th and 95th percentiles of the combined predictions to compare to the fitted data. The simulations were done by sampling occurrence from a Bernouilli distribution and abundance from a Gamma distribution with distribution parameters derived from our SDM (Zuur and Ieno 2016).

Models were refit 100 times using 70% of the original data. From the resulting occurrence predictions, we calculated the average True Skill Statistic (TSS= sensitivity + specificity -1) (Allouche et al. 2006) using the R package "PresenceAbsence" (Freeman and Moisen 2008). For the abundance model, we calculated the out of sample deviance for the 30% of data held out using code from Pederson et al. (2019). TSS and deviance explained were also calculated on the model fitted with 100% of data.

Region-specific validation was performed using Pearson's correlation coefficient between the monthly/yearly averages of predictions and observations. Model selection was conducted using AIC and region-specific correlations. The best model should perform well in most regions.

Abundance predictions were made at a monthly-yearly temporal scale using the GLORYS12v1 spatial grid (0.083 x 0.083 degrees). The year's random intercept was included in predictions.

2.2.2. Uncertainty in SDMs parameters

We estimated the uncertainty of total *Calanus* spp. predicted abundance using a simulation-based approach (Miller et al. 2022). For each species, GAMMs parameters were simulated 1000 times using the Metropolis Hastings sampler available in the mgcv package (Wood 2017). From the original models, we extracted the linear predictor matrix (lpmatrix) for each time slice (n = 264;12 months*22 years) of the GLORYS12v1 prediction grids. For each simulation and time slice, we obtained the expected response (π x μ) for each cell of the prediction grid by the multiplication of the lpmatrix and the simulated parameters. The multiplication of π and μ assumed that they were independent (no covariance). For each cell, the 1000 simulations for all years were aggregated by month, then the variance was calculated for each month for each species. To provide the uncertainty on the total *Calanus* spp. abundance, we summed the variance of the three species assuming that species-specific GAMMs were independent. The resulting uncertainty was expressed as the coefficient of variation (CV) and considered both the uncertainty around parameters and inter-annual variation around the climatology.

2.3. NARW BIOENERGETIC FORAGING MODEL

2.3.1. Converting multispecies water column abundance into a common currency: biomass.

C. finmarchicus, *C. glacialis* and *C. hyperboreus* differ in size with the individual body weight of *C. hyperboreus* being 6-10 times greater than that of *C. finmarchicus*. To build a multispecies prey layer from species-specific abundance predictions, GAMMs abundance predictions must be therefore converted into a common currency, biomass. We used the T_0-50 from GLORYS12v1 and used equations between temperature and *C. finmarchicus* CIV, CV, and CVI carbon weight from Campbell et al. (2001) (Table A.2. 1). We considered T_0-50 during the period of development of the new generation during which body size in late stages is determined: May to August for *C. finmarchicus*, and May and June for *C. hyperboreus* and *C. glacialis*. We then determined individual carbon weight of the two larger *Calanus* species using scaling factors calculated from differences in averaged species- and stage specific individual body weight, which ranged between 1.6-2.5 and 5-8 for *C. glacialis* and *C. hyperboreus* respectively (Plourde et al. 2019, Helenius et al. 2023). To convert carbon weight into total individual dry weight (IDW), we assumed that carbon represents 52% of IDW for *C. finmarchicus* and *C. glacialis* and 60% for *C. hyperboreus* (Runge et al. 2006, Brey et al. 2010, Helenius et al. 2023).

In order to avoid estimating unrealistic IDW at extremely high or low temperature, estimated body weights were constrained to not exceed the lower 10% and upper 90% quantiles of field observations (Helenius et al. 2023, 2024).To account for variations in stage composition on the CIV-CVI dry weight, we used the monthly stage-specific relative abundance (%) of CIV, CV and CVI of the three *Calanus* species in the 7 Canadian regions (r in eq. below) (Figure A.2. 2).

The resulting species-specific biomass, *s*, for each cell, c, at month, m, and year, y, was:

$$DW_{s,c,m,y} = IDWCIV_{s,c,m,y} \times \%CIV_{s,r,m} + IDWCV_{s,c,m,y} \times \%CV_{s,r,m} + IDWCVI_{s,c,m,y} \times \%CVI_{s,r,m}$$

2.3.2. Calanus species vertical distribution model

Vertical distribution of *Calanus* spp. was previously described using GAMs in GSL and in eastern and western SS (Plourde et al. 2019, Lehoux et al. 2020). As *C. finmarchicus* and *C. glacialis* were not always differentiated in the early sample analysis, they were combined in the vertical distribution GAMs to maximize the use of the existing data set. GAMs were fitted for each region separately following this equation with a beta distribution:

$$pDW_{cum} = ti(\%Z \times Month) + ti(Z) + ti(\%Z \times Z)$$

where pDW_{cum} is the cumulative proportion of dry weight from the top of the water column, Z is the station depth and %Z is the percentage of the water column sampled.

In this study, data in the GOM were added and a GAM was also fitted for the GOM (Table A.4.1, Krumhansl et al. 2018). In this GAM, Z was log-transformed to account for the larger range of bathymetry covered by vertically stratified sampling in the GOM. We did not build a GAM for eNL-LAB as stations were mostly located in the slope area with a coarse vertical sampling resolution (>100 m thick). For the seasonal and depth-stratified sampling coverage, see Figure A.1.2. The period of the day (day/night) was not considered because the number of stations in each month was sometimes too low to add this factor to the model.

2.3.3. Building the 3-D preyscape

The 3D preyscape was used to consider the 'availability' of prey (see Sorochan et al. 2021) as prey depth is predicted to constrain NARW foraging success at depths greater than 150 m in the bioenergetic foraging model (Gavrilchuk et al. 2021).The 3D preyscape was built using biomass predictions for each species separately. Species and region-specific vertical distribution model (GAM) were used to predict the monthly vertical distribution in 10 m-thick bins following Plourde et al. (2019) and Lehoux et al. (2020). *C. hyperboreus* vertical distribution in the EcoMon area was predicted using the vertical distribution GAM in the closest region, the western SS (WSS) (Plourde et al. 2019). We used the vertical distributions of the GSL for predictions in the LAB and NFL. 3-D seascapes (Month, geographic position, species density in 10-m thick) of each species depth-specific density (g m^{-3}) were then converted into energy depth-specific density (kJ m^{-3}) using a constant *Calanus* energy density (27.9 kJ g^{-1}, Davies et al. 2012) assuming that latitudinal variation in total energy would depend mostly on differences in abundance and body weight (Helenius et al. 2023).See Figure A.4. 1 for the spatial coverage of region-specific GAMs used to build the preyscape.

2.3.4. Applying the NARW foraging bioenergetic model

We used the NARW bioenergetic foraging model developed by Gavrilchuk et al. (2020, 2021). The model summarized the available knowledge about NARW foraging behaviour and bioenergetics. The model accounts for the energy gained (E_{in}) which can vary with prey density and time spent foraging at depth. Energy gained is predicted to decrease at depth > 150 m because foraging time (hours d^{-1}) decreases (see Figure 6 in Gavrilchuk et al. 2020). Energy cost (E_{out}) is determined by female state with resting, pregnant and lactating having gradually greater energy requirements. In our study, we used the mean parameters of pregnant females in the E_{out} equation (see Lehoux et al. 2020 for details) and thus E_{out_preg} was spatially and temporally invariant in our approach. Using parameters for resting or lactating females would only have scaled down (resting) or up (lactating) E_{out} .

We calculated E_{in} for each *Calanus* species and summed the E_{in} gained from total *Calanus* biomass in each 10 m-layer *l* of each time step for years *y* and months *m* and cells *c* (E_{in_cal}). The NARW energy balance (E_{net}) was calculated as followed:

$$E_{net} = \frac{E_{in\_cal} - E_{out\_preg}}{E_{out\_preg}} + 1$$

We reported E_{net} at the depth layer where E_{net} was maximized for each cell and time step (optimal E_{net}) (Lehoux et al. 2020) and calculated the average and coefficient of variation of the E_{net} for each cell and month over the 1999-2020 period. We added a constant of 1 to E_{net} to facilitate interpretation.

Since our SDMs predicted the mean response of *Calanus* species to covariates and did not account for local aggregation processes (see above, Sorochan et al. 2021), the E_{net} presented in this document should be considered as relative and be used to identify areas and months during which prey quantities available to being aggregated and therefore foraging conditions would be better than elsewhere. To highlight these areas and their seasonal persistence, we also selected sites where E_{net} were larger than the 90% quantities of E_{net} by regions (7 Canadian regions) and month over the 1999-2020 climatology.

3. RESULTS

3.1. *CALANUS* SPECIES DISTRIBUTION AND VERTICAL DISTRIBUTION MODELS

3.1.1. Performance and accuracy of candidate models

Model 1 [no regional factorization and no 'connectivity' term] showed the worst performance metrics in both the Bernoulli and Gamma models for the three *Calanus species* (Table 2). Model 2 [9 regions and no 'connectivity' term] showed slightly better performance for some metrics in comparison to models 3.1-3.3, which included the 'connectivity' term, for *C. finmarchicus*. Model 3.2 and 3.3 (4 regions, 'connectivity' term) demonstrated superior performance metrics for *C. hyperboreus* (Table 2). Model 3.3 (winsorizing T_min) improved the 'Out of sample' metric relative to Model 2 for *C. finmarchicus* and *C. hyperboreus* (Table 2). Therefore, Model 3.3 (4 regions, 'connectivity' term, winsorizing T_min) showed the overall better performance metrics. Model 3.1 and 3.2 were similar for *C. glacialis*.

Models 1 and 3.1 (no regional factorization) were in general the lowest performing models for predicting the average level of observed abundance of the three *Calanus* species with the largest differences in GB, CCB, sGSL and nGSL (Figure A.3. 5). Model 2 (9 regions) was the best in predicting the average abundance in most regions, but resulted in region-specific intercepts, which would generate unrealistic sharp interregional boundaries in abundance predictions (not shown). Predictions with Model 3.2 and 3.3 (4 regions with 'connectivity' term) generally compared favorably with those of Model 2 in Canadian waters with the additional benefit of limiting the problem of unrealistic sharp regional boundaries in predictions (not shown).

Correlation coefficients were computed using annual and monthly averages of observed and predicted abundance for each model and regions (Table 3). For the 7 regions in Canadian waters, Model 3.2 and 3.3 showed similar or higher correlations than Model 2 in 5, 4 and 2 regions for *C. finmarchicus*, *C. hyperboreus* and *C. glacialis* respectively, the latter being in regions of higher abundance (eNL, LAB) (Table3). All candidate models of *C. hyperboreus* showed lower correlations in the nGSL mainly due to large discrepancies between observed and predicted abundance in January to March, a period with very low sampling effort in the region (Figure A.1. 1). The same exercise revealed that the poorer correlation for *C. finmarchicus* in the sGSL by models 1, 3.2, and 3.3 was related to an underestimation of abundance in May to July (Figure A.3. 6). Examination of the interannual patterns showed that

Model 3 captured the low-frequency interannual patterns but failed to predict large year-to-year changes sometimes observed (Figure A.3. 7). Note that these large differences can arise as much from variations in sampling effort and uncertainty in observations as from processes not considered in model's formulation.

Overall, Model 3.3 showed performance metrics similar or better than Model 1, Model 2, models 3.1 and 3.2, and improved the accuracy of the predictions in most regions for *C. finmarchicus* and *C. hyperboreus* while limiting the occurrence of sharp discontinuities at the regions' boundaries associated with Model 2. In *C. glacialis*, model 3.1 was equivalent to models 2 and 3.2 while also avoiding generating sharp boundaries in predictions among regions. Models 3.3 (*C. finmarchicus*, *C. hyperboreus*) and 3.1 (*C. glacialis*) were therefore selected as the best models and used for predicting the seasonal climatology of *Calanus* species abundance and NARW potential foraging habitat across Canadian waters.

3.1.2. Covariate effects in best model

Model 3.3 terms and covariates were generally significant, the 'connectivity' term being the only covariate not significant in the *C. finmarchicus* Bernoulli model. There were some patterns in the Gamma models' residuals, resulting in overestimation at very low abundance values, and an underestimation of abundance (Figure A.3. 1) most notably in the < 50^{th} and > 95^{th} percentiles (expected due to the smoothing effect). Simulations of the ZAG distribution showed that these over or underestimations were < 5000, < 500, < 3000 N m^{-2} for *C. finmarchicus, C. glacialis* and *C. hyperboreus* respectively (Figure A.3. 2-A.3.4). All models complied with the assumption of residuals homogeneity (Figure A.3. 2-A.3.4).

The form of the T_0-50 and Tmin smoothed functions differed among *Calanus* species (Figure 3, Table 4). T_0-50 lower than 11.8 °C had a positive effect on the probability of *C. finmarchicus* occurrence (Bernoulli), whereas the effect on abundance was dome shaped and positive between 3.3-14.8 °C. Tmin showed a positive effect on occurrence and abundance above 3.4 °C and between 3.7-8.7 °C, respectively. In the *C. glacialis* and *C. hyperboreus* models, the positive effect of both T_0-50 and Tmin was observed at considerably lower values than in *C. finmarchicus*, but smoothed functions showed a larger uncertainty at high temperature for the Bernoulli models in *C. glacialis*. This larger uncertainty and the fact that the Tmin smoothers in many models showed positive effects at high temperatures should be interpreted as an indication of southward transport of *Calanus* species in sub-optimal environmental conditions.

The effect (smoothers) of Latitude, Month and ClimS_0-50sqrt generally varied among species (Figure 4, Table 4). The main positive effect of Latitude on abundance occurred at lower values for *C. finmarchicus* (43-44°N) than for *C. hyperboreus* (> 47°N) and *C. glacialis* (centered at 50°N). The positive effect of ClimS_0-50sqrt also showed marked differences between species, with *C. finmarchicus* and *C. hyperboreus* being positively associated with saltier (32.5-34.0, climS_0_50sqrt = 1.25-0.25) and fresher (< 31.9 PSU, climS_0_50sqrt = 1.47) water masses respectively, and with *C. glacialis* sharing both affinities (29.4-31.8 PSU, climS_0_50sqrt = 2.15-1.5). As a result, the 'connectivity' term (Latitude*Month*ClimS_0-50sqrt) showed species-specific and spatial-temporal patterns often encompassing several regions and indicating different 'connectivity' pathways (Gamma models, Figure 5). For example, the 'connectivity' term showed a positive effect on *C. finmarchicus* abundance from the Grand Bank (eNL), on the SS and in USA waters from May to August. In *C. glacialis*, the positive effect was mostly observed in the LAB, eNL and nGSL regions from May to October and restricted to the outer shelf of LAB and northern eNL in winter and late Fall. Finally, the 'connectivity' term was positive for *C. hyperboreus* in late Spring to October in nGSL-sGSL-SS region, but also on the inner shelf of LAB, and eNL from May to September.

3.1.3. Spatial and seasonal patterns in uncertainty of best Calanus SDMs' parameters and prediction

Monthly spatial variations of uncertainty in the SDMs' parameters and in monthly abundance predictions across the transboundary modelling domain are shown in Figure 6. In Canadian waters, uncertainty was markedly larger at the northern portion of the spatial domain in the LAB region (Figure 6). Very high uncertainty also persisted across months at the southern limit of the transboundary spatial domain (i.e., outside of Canadian waters) and in a coastal area in the sGSL (Figure 6). Elsewhere in Canadian waters, uncertainty was low and rather uniformly distributed across time and space, with slightly higher values on the SS, sGSL, nGSL and eNL in September-October relative to other months (Figure 6).

Examination of the uncertainty for each covariate helps explain the causes of the high uncertainty associated with the 'connectivity' term in some regions. In particular, a large uncertainty was common at the extreme ends of the spatial domain (Latitude) and at extreme high/low ClimS_0-50sqrt (low/high salinity) values (Figure 4).

3.1.4. Vertical distribution models

The vertical distribution GAM for *C. finmarchicus* CIV-CVI in the GOM performed similarly to models built in other regions (Plourde et al. 2019). The deviance explained was high at 92.5% with model diagnostics similar to those of previous models (Table A.4. 1). The GAM performed well during cross-validation. Correlation and a linear model between predictions and observations showed similar performance when the GAM was fitted on 70% or 100% of the data suggesting that the GAM was not overfitted. The %Z was significant for each month and the Z and interaction between %Z and Z were mostly significant during the fall, when *C. finmarchicus* is overwintering and thus more limited by bottom depth (Table A.4. 1). The GAM's smoothers are presented in Figure A.4. 3 and Figure A.4. 4. The GAM conformed to the residuals homogeneity assumption and the response was generally accurately predicted with no obvious bias.

3.2. MONTHLY AND SPATIAL VARIATIONS IN *CALANUS* ABUNDANCE AND BIOMASS

There were marked seasonal and regional variations in the three *Calanus* species water column predicted abundance during 1999-2020 (Figure 7). *C. finmarchicus* abundance generally decreased from the south (Fundy-GOM, GB) to the north (eNL) with a notable exception in LAB in the spring (Figure 7, top panel). Peaks in abundance generally occurred earlier (late spring-early summer) in the south than in the north (late summer-fall), with again a departure from this pattern being observed in LAB in the spring. Note that LAB showed the greatest uncertainty in the models' parameters (predictions) (see above, Figure 6). *C. glacialis* and *C. hyperboreus*, the two arctic species, showed the opposite pattern with lower abundance in the south (Fundy, GB, SS) relative to the north (sGSL, nGSL, eNL, LAB) (Figure 7, middle and bottom panels). These species also showed a delayed timing of the seasonal peak in abundance in the north (Figure 7, bottom panel). Beyond the general patterns described above, a key feature of the distribution of *Calanus* species was the greater abundance of *C. hyperboreus* in the GSL than in other regions, including eNL and LAB in the north (Figure 7, bottom panel).

Regional and seasonal differences in *Calanus* water column biomass (g m^{-2}) showed similar patterns previously described using species-specific abundance (Figure 8). *Calanus* water column biomass was higher in nGSL, LAB and Fundy-GOM, somewhat lower in sGSL, SS and eNL, and was the lowest in GB (Figure 8). Again, there was a general south to north gradient in

the timing of the seasonal maximum in *Calanus* biomass from GB (May) to nGSL (July), whereas a different seasonal pattern occurred in eNL and LAB (Figure 8).

3.3. MULTISPECIES 3D PREY LAYER AND NARW POTENTIAL FORAGING HABITAT

3.3.1. Seasonal and regional variations in *Calanus* vertical distribution

The predicted vertical distribution of *Calanus* species biomass varied among seasons (months), regions and bathymetric range (Figure 9). The occurrence of a bimodal vertical distribution was a common feature in *C. finmarchicus* and *C. glacialis* across regions and seasons, with the proportion of the population associated with the shallow mode generally decreasing as the season progress (Figure 10). Bimodal vertical distribution in *C. hyperboreus* was uncommon and limited to early summer (Figure 10). In all regions and species, the depth of the deep mode in vertical distribution increased with bottom depth of the site, but the deep mode of *C. finmarchicus* and *C. glacialis* was generally observed shallower in the GSL relative to ESS, WSS and GOM, a pattern not observed in *C. hyperboreus* (Figure 9). Bottom depth showed a strong effect on the maximum relative density of the deep mode with 4-5 times greater maximum occurring in shallow (60-100 m) compared to deep (300-450 m) locations (Figure 9).

3.3.2. Seasonal pattern in depth of optimal prey density and in foraging suitability

We compared the performance of our 3-D prey and NARW bioenergetic modelling approach to estimate optimal depth with results reported at various feeding sites during the early 2000's (Baumgartner et al. 2017) (Table 5). Our modelling approach predicted realistic foraging depth in Cape Cod Bay in March, Bay of Fundy (Grand Manan) in August, Roseway Basin in September-October, and Jeffreys Ledge in late Fall (Table 5). However, our model did not perform well at predicting foraging depth in the Great South Channel in May-June (Table 5).

NARW potential foraging habitat suitability (Enet) was generally greater in the sGSL and nGSL year-round, with equivalent high values in LAB in late winter-early Spring, and somewhat lower values in Fundy-GOM and SS (Figure 10). Enet generally peaked in June-July across Canadian waters, but with an earlier seasonal maximum in April and May in Lab and nGSL respectively (Figure 10). Note that abundance predictions at the northern end of the LAB region showed the largest level of uncertainty. Enet in eNL was generally low, but was higher relative to GB, Fundy-GOM, SS and LAB in October-November (Figure 10).

The contribution of *C. finmarchicus* to NARW potential foraging suitability (Enet) varied among regions and seasons (Figure 11). *C. finmarchicus* contribution to Enet was nearly 100% in GB and Fundy-GOM, the lowest (21-42%) in the nGSL and sGSL, and intermediate (65-70%) in SS, eNL and LAB (Figure 11). Seasonally, *C. finmarchicus* contribution was generally the lowest from May to September but with regional variations in timing and duration. It increased afterward across Canadian waters, reaching its seasonal maximum between September (SS, sGSL) and November (LAB) (Figure 11).

3.3.3. Monthly spatial climatology and variability of foraging habitat suitability

In GB and Fundy-GOM (Figure 12), Enet was higher in deep areas of the northeast part of the GOM (including just northeast of GB) in June to August with slightly higher Enet in Grand Manan relative to the rest of the outer Bay of Fundy. This period of high Enet corresponded to low and high interannual variability in June and July-August respectively (Figure 15). In SS, Enet was higher on the inner eastern SS along Cape Breton and in the Northeast Channel northeast of GB in May and June (Figure 12). Later in the season, Enet was generally greater

on the western SS and in Roseway Basin in July-August -September, and to a lesser extent off southwest NL (Figure 12). In SS, interannual variability in Enet was greater in July to December at the outer shelf boundary and off the southern NL coast (Figure 15).

In GSL (Figure 13), highest Enet was restricted to the northwest in April and May with somewhat greater values south of Anticosti Island in May. Enet was then greater in the sGSL (Gaspé and Shediac Valley) in June to August, and north of Anticosti Island in July to September. In September, Enet was the greatest around the western half of Anticosti Island and along the northwest GSL coast; high Enet was then mainly restricted to the estuary and north of wGSL in somewhat deeper areas along the slope of the deep channels. In general, Enet varied more in shallow coastal areas in sGSL and along northwest eNL, corresponding to regions of very low Enet values. Conversely, areas of high Enet generally corresponded to low interannual variability (Figure 15).

In eNL (Figure 14), Enet was generally greater offshore in April through June, including Flemish Cap in May. Enet was then greater inshore off northeast NFL in June to August (Figure 14). Higher Enet in the Fall occurred on the northeast slope of the Grand Banks. In LAB (Figure 14), Enet was high in March through May on the outer shelf at the northern end of the region, a region characterized by a large uncertainty in models' parameters and predictions (see Figure 6). Enet was then high on the inner shelf in May to August in continuity with eNL in the south and remained low thereafter. Variability was the greatest on the Grand Banks, an area of low Enet for most of the year, and in some areas on the slope of Flemish Cape in April to September (Figure 15).

4. DISCUSSION

4.1. SPECIES DISTRIBUTION MODELS

The best SDMs (Model 3.3) included the 'connectivity' term and assumed that *Calanus* species responses to covariates were generally the same across the domain (no adaptation at the region level) with some factorization in regions where transport is known to be a dominant driver of abundance. Model 3.3 resulted in good prediction accuracy in most regions while showing similar or better performance than Model 2 without the problem of creating artificial boundaries in predictions between regions. In particular, Model 3.3 performed well while considering a vast area including MAB, SNE, GOM, SS, nGSL, eNL and LAB as a single 'transboundary' region. Therefore, the superior performance of Model 3.3 demonstrated the importance of considering covariates such as 'connectivity' on scales corresponding to those at which processes and environmental covariates affecting *Calanus* species populations operate. Building the models across the Canadian and USA domains (transboundary) also allowed a wider range of environmental conditions such as T_0-50 and Tmin to be considered relative to previous SDMs (Albouy-Boyer et al. 2016, Grieve et al. 2017), which should minimize the level of uncertainty in models' predictions (Austin 2007, Waldock et al. 2022).

The 'connectivity' term appeared to capture realistic patterns of influence of different water masses across Canadian waters. The effect of Latitude strongly differed among species, suggesting distinct source regions with patterns of 'connectivity' corresponding to our understanding of pathways of transport of *Calanus* species on the eastern Canadian shelf. Our results suggested that *C. finmarchicus* and *C. glacialis* on the eNL shelf and in the nGSL were mainly linked to sources and transport originating on the Labrador Shelf (Pepin et al. 2013). In sharp contrast, *C. finmarchicus* on the central and western SS was shown to be more associated with offshore sources originating from the outer shelf or slope water (Head et al.1999). Finally, patterns of connectivity showed for *C. hyperboreus* highlighted the nGSL as

the main source for sGSL and SS in a highly connected system under the influence of the freshwater outflow from the St. Lawrence River (Sameoto and Herman 1992, Brennan et al. 2021, Le Corre et al. 2023), and the inner Labrador Shelf as the main upstream sources for this species in eNL (Head et al. 2003). The 'connectivity' term therefore captured some aspects of the large-scale advective processes that would have been explicitly taken into account when using more complex coupled bio-physical models (see Zakardjian et al. 2003, Maps et al. 2011, Pepin et al. 2013).

The best SDMs (Model 3.3) however included an intermediate level of regional factorizing necessary to predict realistic abundance levels in specific regions where transport is a dominant driver of *Calanus* abundance (sGSL, CCB). However, the model formation was not always sufficient to predict discrete and large interannual variations in abundance as exemplified by the lower correlations obtained between predicted and observed abundance in the sGSL (*C. finmarchicus*) and nGSL (*C. hyperboreus*) (Figure A.3. 7, Figure A.3. 8). Surface currents and transport of *Calanus* in highly advective systems such as the nGSL-sGSL and in western GOM-CCB are driven by atmospheric-ocean surface forcing operating at higher temporal and spatial resolutions than those that can be realistically accounted for by our SDMs (Jiang et al. 2007, Maps et al. 2011, Brennan et al. 2021, Le Corre et al. 2023). This ‘disconnection’ between predictions and observations was particularly important early in the season when transport is the strongest, with our SDMs yielding much better results later in the season.

SDMs are useful tools to infer patterns in periods and areas where data are scarce. However, it is recommended to perform predictions and inferences at scales within those considered to be well resolved by the models, which are determined by the temporal and spatial characteristics of the data used to build them (Austin et al. 2007, Waldock et al. 2022). Sampling effort in AZMP is highly uneven, with most effort occurring during spatial surveys performed two or three times per year on sparsely distributed hydrographic sections, while few high-frequency sampling stations are visited once or twice a month (Figure 1, Figure A.1. 1). In EcoMon, sampling effort is better distributed in space but still substantially uneven among months, years and regions (Figure A.1. 1). Based on these characteristics, we determined that predicting *Calanus* species abundance at the monthly scale was reasonable and within our SDM’ capacity. The same precautionary approach limiting predictions to a monthly scale was applied to the GAMs describing the vertical distribution of *Calanus* species.

Despite the conservative use of our SDMs at the monthly scales, the uncertainty in model parameters (and abundance predictions) was sometimes high at the northern (colder) and southern (warmer) ends of our spatial domain (LAB, MAB) (Figure 6). Larger uncertainties in smoothers and predictions associated with values at the extreme end of the covariates space is a common feature in SDMs (see Albouy-Boyer et al. 2016, Grieve et al. 2017), which indicates that predictions in such areas should be interpreted with caution.

4.2. MULTISPECIES 3D PREY LAYER

Our GAMs describing the monthly and regional variations in *Calanus* species vertical distribution conformed well with their life history and phenology at the monthly scale. In *C. finmarchicus*, the bimodal vertical distribution is reflective of the production of multiple generations (presence of active and resting individuals during most months) or an admixture of two species (*C. finmarchicus* and *C. glacialis*) with a different seasonal phenology in the same taxonomic category considered in this historical data set. In *C. hyperboreus*, which produces only one new generation per year, the bimodal vertical distribution observed only in late spring is likely indicative of the transition from a population state characterized by active and developing individuals in the surface layer to a state dominated by resting individuals in deeper waters (Plourde et al. 2003). The vertical distribution model in the GOM yielded similar patterns

as previous studies in Canadian waters, i.e., a bimodal vertical distribution in *C. finmarchicus* and a strong concentrating effect on the deeper mode when bottom depth is shallower than the optimal depth observed in deeper regions (deep basins, channels and slope waters) (Krumhansl et al. 2018, Plourde et al. 2019).

Our 3D modelling approach appeared to perform reasonably well in predicting the depth of optimal NARW foraging, but with some large difference in the GSC in May-June (Table 5). NARW were observed feeding on surface aggregations of *C. finmarchicus* in GSC, although the vertical distribution of *C. finmarchicus* in spring could vary from year-to-year (Beardsley et al. 1996, Durbin et al. 1995, Baumgartner et al. 2017). The GOM vertical distribution model predicted a bimodal vertical distribution in June, which represented the monthly average of all data collected in June over several years in the region (Figure 9). Therefore, the discrepancy between prediction and observations could result from comparing a monthly average value with discrete *Calanus* vertical distribution and NARW foraging events. Additionally, Baumgartner et al. (2017) observed NARW foraging in the surface layer even if similar or greater prey densities were available deeper in the water column, suggesting that NARW may prefer foraging at the surface in such a prey configuration. Such a hypothetical behavioural preference was not parameterized in the NARW bioenergetic foraging model and could also explain the discrepancy observed between observations and our predictions in the GSC.

4.3. NARW POTENTIAL FORAGING HABITAT

Our integrated modelling approach combining SDMs, prey vertical distribution models and a mechanistic NARW bioenergetic model successfully identified traditionally used (Roseway Basin and to a lesser extent Grand Manan) and more recently used foraging habitats in the sGSL (Shediac Valley and its surroundings) similarly to a previous non-SDM analysis that used a spatial climatology of *Calanus* biomass, constructed from an independent but heterogeneous historical data set and simplistic NARW bioenergetic foraging considerations (Plourde et al. 2019). Our results therefore demonstrated the value of using SDMs of *Calanus* species built with AZMP and EcoMon data collected across Canadian and USA waters and over a large range of covariate values to make spatial predictions about *Calanus* abundance and distribution in data-poor areas. When combined with the seasonal and spatial patterns in model parameter uncertainty, those predictions can be made with an adequate level of confidence and therefore provide useful information about potential foraging areas in the context of the management of NARW.

Because our SDMs and vertical models predict the mean response of *Calanus* species to covariates and do not account for local aggregation processes (see above, Sorochan et al. 2021), the consistent higher Enet values estimated in the western part of nGSL and sGSL mainly resulted from high *Calanus* species biomass driven by markedly higher regional abundance level of the large-bodied *C. hyperboreus* (Figure 7,8), suggesting that aggregation processes occurring at high spatial and temporal resolution might play a larger role in the formation of high prey density in other regions. At the scale of Canadian waters, Enet should therefore be considered as relative and be used to identify areas and months during which foraging conditions are likely to be most appropriate (greater or lower than elsewhere). To highlight these areas and their seasonal persistence (number of months during each quarter), we selected Enet that were larger than the 90% quantities of all monthly values within each region in the 1999-2020 monthly climatology and represented the results by quarter of the year (Figure 16). Several previously unknown and ‘persistent’ areas of potentially high potential foraging suitability for NARW were predicted across Canadian waters in addition to known foraging habitats (Figure 16). In January-March, the most persistent new areas of Enet values > 90^{th} quantile were predicted in the western GSL and in LAB, with some areas with a lesser

persistence off southern NL, along the northeast and southern slope of the Grand Banks, and on Flemish Cap (Figure 16). In April-June, the most persistent new areas were predicted in the Northeast Channel off the tip of GB, along the coast of Cape Breton and eastern SS, off the southern tip of Grand Banks (eNL), and offshore in eNL (Figure 16). In July-September when Enet was generally high (Figure 11), the most persistent new areas were in the Northeast Channel (GB), western SS, and on the inner shelf near the coast in wNL and LAB (Figure 16). Finally, the most persistent new areas in October-December (period of decreasing/low Enet, Figure 11) were predicted in the western GSL, off southern eNL, along the northeast slope of the Grand Banks, and on Flemish Cap (Figure 16). Because of the marked seasonal and spatial patterns in predicted Enet across Canadian waters (Figure 10, Figure 17), new areas identified between April and September in the GSL should be considered as potentially more significant for NARW foraging, while those in LAB being more uncertain than elsewhere (Figure 6, Figure 17).

NARW potential foraging areas in Canadian waters are determined based on *Calanus* species assemblages that vary across space and time. Our 3D multispecies prey layer and Enet estimates integrated this complexity. In the warmer Fundy-GOM and SS, *C. finmarchicus* is the dominant species year-round producing a strong spring generation followed by a second yet smaller second generation in late summer (Casault et al. 2022). In the colder nGSL and eNL, the development of *C. finmarchicus* is delayed with the main spring generation developing in summer (Plourde et al. 2001, Blais et al. 2021, Maillet et al. 2019). *C. hyperboreus* dominates the mesozooplankton biomass in the GSL with abundance levels greater than elsewhere in Canadian waters mainly associated with the deep channels typical of the region (Plourde et al. 2003, Plourde et al. 2019). It produces one new generation per year developing in surface waters in spring when it is transported in shallow areas such as the sGSL and across the Canadian shelf (Maillet et al. 2019, Blais et al. 2021, Casault et al. 2022). In those areas, the abundance of *C. hyperboreus* sharply decreases in summer when *C. finmarchicus* becomes predominant. Therefore, inferences about the resilience of known and new NARW potential foraging habitats to variations in environmental conditions and climate change should be carefully made due to species-specific responses to these changes.

4.4. SOURCES OF UNCERTAINTY

Species identification: *C. finmarchicus* vs *C. glacialis*. There is an uncertainty in the species identification with their prosome length frequency distribution overlapping (Parent et al. 2011, Gabrielsen et al. 2012).

The presence of *Calanus helgolandicus*, which has a higher temperature optimum than *C. finmarchicus* (Moller et al. 2012), has been detected in MAB using morphometric and genetic approaches (Fleminger and Hulsemann 1977, Bucklin et al. 2022). The late stages of these two species are only distinguishable using fine morphometric characteristics of the basipod of the fifth leg (Fleminger and Hulsemann 1977), a time-consuming approach not part of the EcoMon (and AZMP) sample analysis protocol. If present, the relative importance of *C. helgolandicus* in MAB is unknown but could potentially affect our *C. finmarchicus* SDMs at the upper end of temperature values (warmer conditions).

There is a need for additional field work aimed at describing the vertical distribution of *C. finmarchicus* in SNE-MAB (EcoMon) and on the shelf in eNL-LAB. Because of a lack of taxonomic resolution in the vertical distribution data collected in the past, little is known about the difference (or lack thereof) in vertical distribution between *C. finmarchicus* and *C. glacialis*. Sampling at a higher vertical resolution is likely needed to parse them out.

The necessity of using a coarse stage category CIV-CVI to limit the number of SDMs and simulations may have impacted our SDMs. *C. finmarchicus* CIV and CVI females are mostly active in the surface layer, whereas CV spend most of its life in deep waters as a resting stage. It means that stage-specific abundance was not always 'directly' connected with T_0-50 and Tmin. It was not the case for *C. hyperboreus* and *C. glacialis* in which CIV-CV-CVI are all resting stages in Canadian waters. The departure of some of the smoothers describing the effect of T_0-50 on *C. glacialis* and *C. hyperboreus* from the expected temperature-*Calanus* relationships could have been associated to this disconnection between abundance and covariates on the vertical dimension.

Local or high-resolution aggregation mechanisms, as described by Sorochan et al. (2021), were not considered.

GLORYS12v1 products are an approximation of reality. GLORYS temperatures deviate from direct CTD observations. The predictions can diverge from the physiological response if GLORYS temperatures diverge locally. Differences between GLORYS and CTD are similar across large regions but not necessarily throughout the area at smaller scales.

5. CONCLUSION

Our suite of SDMs based on different mechanistic assumptions and a seascape 'connectivity' term captured realistic patterns of influence of different temperature regimes and waters masses on *Calanus* across Canadian waters. The good performance of the 'connectivity' covariate in representing large-scale pathways of *Calanus* species transport shows potential for using connectivity proxies in a SDMs framework that could represent some aspects of advective processes explicitly taken into account in coupled bio-physical models (see Zakardjian et al. 2003, Maps et al. 2011, Pepin et al. 2013). Our integrated modelling approach successfully identified known historical (ex: Roseway Basin) and new (sGSL) foraging habitats as well as new potential foraging habitats across Canadian waters. Newly identified potential foraging habitats could be considered as candidate locations for additional survey effort when resources are available. Our results showed that NARW potential foraging areas in Canadian waters are determined by an assemblage of multiple *Calanus* species that varies across space and time with a latitudinal negative (positive) gradient in the contribution of *C. finmarchicus* (*C. hyperboreus/C. glacialis*). Because of the marked seasonality in predicted Enet across Canadian waters, new areas identified between April and September should be considered as potentially more significant for NARW foraging with those at the northern end of the domain being more uncertain. Consequently, inferences about past, current and future resilience of known and new NARW potential foraging habitats to variations in environmental conditions and climate change should be carefully made due to likely species-specific responses to these changes. As right whales might likely continue to expand their foraging range, prey SDMs considering the largest possible geographic and data range will become essential for successful management.

6. REFERENCES CITED

Albouy-Boyer, S., Plourde, S., Pepin, P., Johnson, C.L., Lehoux, C., Galbraith, P.S., Hebert, D., Lazin, G., et Lafleur, C. 2016. Habitat modelling of key copepod species in the Northwest Atlantic Ocean based on the Atlantic Zone Monitoring Program. J. Plank. Res. 38: 589–603. Doi:10.1093/plankt/fbw020.

Alcaraz, M., Felipe, J., Grote, U., Arashkevich, E., et Nikishina, A. 2014. Life in a warming ocean: thermal thresholds and metabolic balance of arctic zooplankton. J. Plank. Res. 36: 3-10.

Allouche, O., Tsoar, A., et Kadmon, R. 2006. Assessing the accuracy of species distribution models: prevalence, kappa and the true skill statistic (TSS). J. Appl. Ecol. 43: 1223–1232. doi:10.1111/j.1365-2664.2006.01214.x.

Amante, C., et Eakins, B. W. 2009. ETOPO1 Global Relief Model converted to PanMap layer format. NOAA-National Geophysical Data Center, PANGAEA.

Austin, M. 2007. Species distribution models and ecological theory: a critical assessment and some possible new approaches. Ecol. model. 200: 1-19.

Baumgartner, M.F., Wenzel, F.W., Lysiak, N.S.J. et Patrician, M.R. 2017. North Atlantic right whale foraging ecology and its role in human-caused mortality. Mar. Ecol. Prog. Ser. 581 : 165−181.

Beardsley, R. C., Epstein, A. W., Chen, C., Wishner, K. F., Macaulay, M. C., et Kenney, R. D. 1996. Spatial variability in zooplankton abundance near feeding right whales in the Great South Channel. Deep Sea Res. II, 43: 1601-1625.

Blais, M., Galbraith, P.S., Plourde, S., Devred, E., Clay, S., Lehoux, C. and Devine, L. 2021. Chemical and Biological Oceanographic Conditions in the Estuary and Gulf of St. Lawrence during 2020. DFO Can. Sci. Advis. Sec. Res. Doc. 2021/060. iv + 67 p.

Brennan, C. E., Maps, F., Gentleman, W. C., Lavoie, D., Chassé, J., Plourde, S., and Johnson, C. L. 2021. Ocean circulation changes drive shifts in *Calanus* abundance in North Atlantic right whale foraging habitat: a model comparison of cool and warm year scenarios. Prog. Oceanogr. 197: 102629.

Brey, T., Müller-Wiegmann, C., Zittier, Z.M.C., and Hagen, W. 2010. Body composition in aquatic organisms - A global data bank of relationships between mass, elemental composition and energy content. J. Sea Res. 64: 334–340.

Bucklin A., Batta-Lona P.G., Questel J.M., Wiebe P.H., Richardson D.E., Copley N.J. et O'Brien T.D. 2022. COI Metabarcoding of Zooplankton Species Diversity for Time-Series Monitoring of the NW Atlantic Continental Shelf. Front. Mar. Sci. 9: 867893. doi 10.3389/fmars.2022.867893

Campbell, R.G., Wagner, M.M., Teegarden, G.J., Boudreau, C.A., and Durbin, E.G. 2001. Growth and development rates of the copepod *Calanus finmarchicus* reared in the laboratory. Mar. Ecol. Prog. Ser. 221 : 161–183. doi:10.3354/meps221161.

Casault, B., Johnson, C.L., Devred, E., Head, E., and Beazley, L. 2022. Optical, Chemical, and Biological Oceanographic Conditions on the Scotian Shelf and in the eastern Gulf of Maine during 2020. DFO Can. Sci. Advis. Sec. Res. Doc. 2022/018. v + 74 p.

Castillo-Trujillo, A.C., Kwon, Y.-O., Fratantoni, P., Chen, K., Seo, H., Alexander, M.A., et Saba, V.S. 2023. An evaluation of eight global ocean reanalyses for the Northeast U.S. Continental shelf. Prog. Oceanogr. 219: 103126. doi:10.1016/j.pocean.2023.103126.

Chust, G., Castellani, C., Licandro, P., Ibaibarriaga, L., Sagarminaga, Y., and Irigoien, X. 2014. Are *Calanus* spp. Shifting poleward in the North Atlantic? A habitat modelling approach. ICES J. Mar. Sci. 71: 241-253.

Conover, R. J. 1988. Comparative life histories in the genera *Calanus* and Neocalanus in high latitudes of the northern hemisphere. Hydrobiologia, 167: 127-142.

Davies, K.T.A., Ryan, A., et Taggart, C.T. 2012. Measured and inferred gross energy content in diapausing *Calanus* spp. in a Scotian shelf basin. J. Plankton Res. **34**: 614–625. doi:10.1093/plankt/fbs031.

de Vries, P. 2023. CopernicusMarine: Search Download and Handle Data from Copernicus Marine Service Information.

DFO. 2023. Oceanographic Conditions in the Atlantic Zone in 2022. DFO Can. Sci. Advis. Sec. Sci. Advis. Rep. 2023/019.

Dixon W.J. 1960. Simplified Estimation from Censored Normal Samples. Ann. Math. Stat. 31:385–391.

Durbin, E. G., Gilman, S. L., Campbell, R. G., and Durbin, A. G. 1995. Abundance, biomass, vertical migration and estimated development rate of the copepod *Calanus finmarchicus* in the southern Gulf of Maine during late spring. Cont. Shelf Res., 15: 571-591.

Fleminger, A., and Hulsemann, K. 1977. Geographical range and taxonomic divergence in North Atlantic *Calanus* (*C. helgolandicus*, *C. finmarchicus* and *C. glacialis*). Mar. Biol. 40: 233-248.

Freeman, E. A. and Moisen, G. 2008. PresenceAbsence: An R Package for Presence-Absence Model Analysis. J. Stat. Soft. 23:1-31.

Gabrielsen, T. M., Merkel, B., Søreide, J. E., Johansson-Karlsson, E., Bailey, A., Vogedes, D., Nygard, H., Varpe, O. and Berge, J. 2012. Potential misidentifications of two climate indicator species of the marine arctic ecosystem: *Calanus glacialis* and *C. finmarchicus*. Polar biol. 35: 1621-1628.

Gavrilchuk, K., Lesage, V., Fortune, S., Trites, A.W., and Plourde, S. 2020. A mechanistic approach to predicting suitable foraging habitat for reproductively mature North Atlantic right whales in the Gulf of St. Lawrence. DFO Can. Sci. Advis. Sec. Res. Doc. 2020/034. iv + 47

Gavrilchuk, K., Lesage, V., Fortune, S.M.E., Trites, A.W., et Plourde, S. 2021. Foraging habitat of North Atlantic right whales has declined in the Gulf of St. Lawrence, Canada, and may be insufficient for successful reproduction. End. Species Res. 44: 113–136. doi:10.3354/ESR01097.

Grieve, B. D., Hare, J. A., et Saba, V. S. 2017. Projecting the effects of climate change on *Calanus finmarchicus* distribution within the US Northeast Continental Shelf. Scient. Rep. 7: 1-12. Doi:10.1038/s41598-017-06524-1.

Head, E. J., Harris, L. R., and Petrie, B. 1999. Distribution of *Calanus* spp. on and around the Nova Scotia Shelf in April: evidence for an offshore source of *Calanus finmarchicus* to the central and western regions. Can. J. Fish. Aquat. Sci. 56: 2463-2476.

Head, E. J. H., Harris, L. R., and Yashayaev, I. 2003. Distributions of *Calanus* spp. and other mesozooplankton in the Labrador Sea in relation to hydrography in spring and summer (1995–2000). Prog. Oceanogr. 59: 1-30.

Helenius, L.K., Head, E.J.H., Jekielek, P., Orphanides, C.D., Pepin, P., Perrin, G., Plourde, S., Ringuette, M., Runge, J.A., Walsh, H.J., Johnson, C.L. 2023. Spatial variability of *Calanus* spp. size and lipid content in the northwest Atlantic – Compilation and brief summary of historical observations, 1977-2020. Can. Tech. Rep. Fish. Aquat. Sci. 3549: iv + 58 p .

Helenius, L. K., Head, E. J., Jekielek, P., Orphanides, C. D., Pepin, P., Perrin, G., Plourde, S., Ringuette, M., Runge, J.A. and Johnson, C. L. 2024. Spatial variability in size and lipid content of the marine copepod *Calanus finmarchicus* across the Northwest Atlantic continental shelves: implications for North Atlantic right whale prey quality. J. Plank. Res. 46: 25-40.

Jiang, M., Brown, M. W., Turner, J. T., Kenney, R. D., Mayo, C. A., Zhang, Z., and Zhou, M. 2007. Springtime transport and retention of *Calanus finmarchicus* in Massachusetts and Cape Cod Bays, USA, and implications for right whale foraging. Mar. Ecol. Prog. Ser. 349: 183-197.

Krumhansl, K.A., Head, E.J.H., Pepin, P., Plourde, S., Record, N.R., Runge, J.A., et Johnson, C.L. 2018. Environmental drivers of vertical distribution in diapausing *Calanus* copepods in the Northwest Atlantic. Prog. Oceanogr. 162: 202–222. doi:10.1016/j.pocean.2018.02.018.

Le Corre, N., Brennan, C. E., Chassé, J., Johnson, C. L., Lavoie, D., Paquin, J. P., Soontiens, N. and Plourde, S. 2023. A biophysical model of *Calanus hyperboreus* in the Gulf of St. Lawrence: Interannual variability in phenology and circulation drive the timing and location of right whale foraging habitat in spring and early summer. Progr. Oceanogr. 219: 103152.

Lehoux, C., Plourde S., and Lesage, V. 2020. Significance of dominant zooplankton species to the North Atlantic Right Whale potential foraging habitats in the Gulf of St. Lawrence: a bio-energetic approach. DFO Can. Sci. Advis. Sec. Res. Doc. 2020/033. iv + 44 p.

Lellouche, J.-M., Greiner, E., Bourdallé-Badie, R., Garric, G., Melet, A., Drévillon, M., Bricaud, C., Hamon, M., Le Galloudec, O., Regnier, C., Candela, T., Testut, C.– E., Gasparin, F., Ruggiero, G., Benkiran, M., Drillet, Y., et Le Traon, P.– Y. 2021. The Copernicus Global 1/12° Oceanic and Sea Ice GLORYS12 Reanalysis. Front. Earth Sci. 9: 698876. doi:10.3389/feart.2021.698876.

Loder, J. W., Petrie, B., and Gawarkiewicz, G. 1998. The coastal ocean off northeastern North America: a large scale view. In The Sea, 11, pp. 105–133. Ed. by A. R. Robinson, and K. H. Brink. John Wiley, New York.

Maillet, G., Bélanger, D., Doyle, G., Robar, A., Fraser, S., Higdon, J., Ramsay, D. and P. Pepin. 2019. Optical, Chemical, and Biological oceanographic conditions on the Newfoundland and Labrador Shelf during 2016-2017. DFO Can. Sci. Advis. Sec. Res. Doc. 2019/055.viii + 35 p.

Maps, F., Zakardjian, B. A., Plourde, S., and Saucier, F. J. 2011. Modeling the interactions between the seasonal and diel migration behaviors of *Calanus finmarchicus* and the circulation in the Gulf of St. Lawrence (Canada). J. Mar. Syst. 88: 183-202.

Mayo, C.A., Letcher, B.H., and Scott, S. 2001. Zooplankton filtering efficiency of the baleen of a North Atlantic right whale, *Eubalaena glacialis*. J. Cetacean Res. Manag. Spec. Special Issue 2: 225–229.

Meyer-Gutbrod, E. L., Davies, K. T., Johnson, C. L., Plourde, S., Sorochan, K. A., Kenney, R. D., Ramp, C., Gosselin, J-F, Lawson, J.W. and Greene, C. H. 2023. Redefining North Atlantic right whale habitat-use patterns under climate change. Limnol. Oceanogr. 68**:** S71-S86.

Miller, C. B., Lynch, D. R., Carlotti, F., Gentleman, W., and Lewis, C. V. 1998. Coupling of an individual-based population dynamic model of *Calanus finmarchicus* to a circulation model for the Georges Bank region. Fish. Oceanogr. 7: 219-234.

Miller, D. L., Becker, E. A., Forney, K. A., Roberts, J. J., Cañadas, A., and Schick, R. S. 2022. Estimating uncertainty in density surface models. PeerJ, 10: e13950.

Mitchell, M.R., G. Harrison, K. Pauley, A. Gagné, G. Maillet and P. Strain. 2002. Atlantic Zonal Monitoring Program Sampling Protocol. Can. Tech. Rep. Hydrogr. Ocean Sci. 223: iv + 23 p.

Møller, E. F., Maar, M., Jónasdóttir, S. H., Nielsen, T. G., and Tönnesson, K. 2012. The effect of changes in temperature and food on the development of Calanus finmarchicus and Calanus helgolandicus populations. Limnol. Oceanogr. 57: 211-220.

Northeast Fisheries Science Center 2019. Zooplankton and ichthyoplankton abundance and distribution in the North Atlantic collected by the Ecosystem Monitoring (EcoMon) Project from 1977-02-13 to 2021-11-15 (NCEI Accession 0187513). NOAA National Centers for Environmental Information. Dataset.

Parent, G. J., Plourde, S., and Turgeon, J. 2011. Overlapping size ranges of *Calanus* spp. off the Canadian Arctic and Atlantic Coasts: impact on species' abundances. J. Plank. Res. 33: 1654-1665.

Pasternak, A. F., Arashkevich, E. G., Grothe, U., Nikishina, A. B., and Solovyev, K. A. 2013. Different effects of increased water temperature on egg production of *Calanus finmarchicus* and *C. glacialis*. Oceanology 53: 547-553.

Pedersen, E.J., Miller, D.L., Simpson, G.L., et Ross, N. 2019. Hierarchical generalized additive models in ecology: An introduction with mgcv. PeerJ 7(e6876). doi:10.7717/peerj.6876.

Pepin, P., Han, G., and Head, E. J. 2013. Modelling the dispersal of *Calanus finmarchicus* on the Newfoundland Shelf: implications for the analysis of population dynamics from a high frequency monitoring site. Fish. Oceanogr. 22: 371-387.

Plourde, S., Joly, P., Runge, J. A., Zakardjian, B., and Dodson, J. J. 2001. Life cycle of *Calanus finmarchicus* in the lower St. Lawrence Estuary: the imprint of circulation and late timing of the spring phytoplankton bloom. Can. J. Fish. Aquat. Sci. 58: 647-658.

Plourde, S., Joly, P., Runge, J. A., Dodson, J., and Zakardjian, B. 2003. Life cycle of *Calanus hyperboreus* in the lower St. Lawrence Estuary and its relationship to local environmental conditions. Mar. Ecol. Prog. Ser. 255: 219-233.

Plourde, S., Pepin, P., and Head, E. J. 2009. Long-term seasonal and spatial patterns in mortality and survival of *Calanus finmarchicus* across the Atlantic Zone Monitoring Programme region, Northwest Atlantic. ICES J. Mar. Sci. 66: 1942-1958.

Plourde, S, Lehoux, C., Johnson, C.L., Perrin, G., et Lesage, V. 2019. North Atlantic right whale (*Eubalaena glacialis*) and its food: (I) a spatial climatology of *Calanus* biomass and potential foraging habitats in Canadian waters. J. Plankton Res. 41: 667–685. doi:10.1093/plankt/fbz024.

Record, N. R., Runge, J. A., Pendleton, D. E., Balch, W. M., Davies, K. T., Pershing, A. J., Catherine L. Johnson, Stamieszkin, K., Ji, R., Feng, Z., Kraus, S.D., Kenney, R.D., Hudak, C.A., Mayo, C.A., Chen, C., Salisbury, J.E. et Thompson, C. R. 2019. Rapid climate-driven circulation changes threaten conservation of endangered North Atlantic right whales. Oceanography 32: 162–169.

Ross, C. H., Runge, J. A., Roberts, J. J., Brady, D. C., Tupper, B., and Record, N. R. 2023. Estimating North Atlantic right whale prey based on *Calanus finmarchicus* thresholds. Mar. Ecol. Prog. Ser. 703: 1-16.

Runge, J.A., Plourde, S., Joly, P., Niehoff, B., et Durbin, E. 2006. Characteristics of egg production of the planktonic copepod, *Calanus finmarchicus*, on Georges Bank: 1994-1999. Deep. Res. Part II Top. Stud. Oceanogr. 53: 2618–2631. doi:10.1016/j.dsr2.2006.08.010.

Sameoto, D. D. and Herman, A. W. 1992. Effect of the outflow from the Gulf of St. Lawrence on Nova Scotia shelf zooplankton. Can. J. Fish. Aquat. Sci. 49: 857-869.

Simard, Y., Roy, N., Giard, S., and Aulanier, F. 2019. North Atlantic right whale shift to the Gulf of St. Lawrence in 2015, revealed by long-term passive acoustics. End. Species Res. 40: 271-284.

Sorochan, K.A., Plourde, S., Morse, R., Pepin, P., Runge, J., Thompson, C., et Johnson, C.L. 2019. North Atlantic right whale (*Eubalaena glacialis*) and its food: (II) interannual variations in biomass of *Calanus* spp. on western North Atlantic shelves. J. Plank. Res. 41: 687–708. doi:10.1093/plankt/fbz044.

Sorochan, K.A., Plourde, S., Baumgartner, M.F., et Johnson, C.L. 2021. Availability, supply, and aggregation of prey (*Calanus* spp.) in foraging areas of the North Atlantic right whale (*Eubalaena glacialis*). ICES J. Mar. Sci. 78: 3498–3520. doi:10.1093/icesjms/fsab200.

Waldock, C., Stuart-Smith, R.D., Albouy, C., Cheung, W.W., Edgar, G.J., Mouillot, D., Tjiputra, J. et Pellissier, L. 2022. A quantitative review of abundance-based species distribution models. Ecography 2022: e05694.

Wishner, K. F., Schoenherr, J. R., Beardsley, R., and Chen, C. 1995. Abundance, distribution and population structure of the copepod *Calanus finmarchicus* in a springtime right whale feeding area in the southwestern Gulf of Maine. Cont. Shelf Res. 15: 475-507.

Wood, S.N. 2003. Thin plate regression splines. J. R. Statist. Soc. B. 65:95-114.

Wood, S.N. 2006. Low rank scale invariant tensor product smooths for generalized additive mixed models. Biometrics 62:1025-1036.

Wood, S.N. 2017. Generalized Additive Models: An Introduction with R (2nd edition). Chapman and Hall/CRC.

Zakardjian, B. A., Sheng, J., Runge, J. A., McLaren, I., Plourde, S., Thompson, K. R., and Gratton, Y. 2003. Effects of temperature and circulation on the population dynamics of *Calanus finmarchicus* in the Gulf of St. Lawrence and Scotian Shelf: Study with a coupled, three-dimensional hydrodynamic, stage-based life history model. J. Geophys. Res. (Oceans). 108 (C11).

Zuur, A. F., and Ieno, E. N. 2016. A protocol for conducting and presenting results of regression-type analyses. Methods Ecol. Evol. 7: 636-645.

7. ACKNOWLEDGEMENTS

We thank all the DFO and NOAA scientists and crew of the research vessels who contributed to the collection of AZMP and EcoMon zooplankton samples. Special thanks are due to the DFO taxonomists and scientists at the Plankton Sorting and Identification Center of the National Marine Fisheries Research Institute, Poland, for processing AZMP and EcoMon plankton samples respectively. We thank F. Cyr, D. Bélanger and B. Casault for providing AZMP environmental and *Calanus* data. V. Lesage, H. Moors-Murphy and K. Sorochan kindly provided comments that helped improving the manuscript. S. Plourde, C. Lehoux, C.L. Johnson and P. Pepin were supported by DFO sciences. C. Orphanides and H.J. Walsh were supported by NOAA. J.J. Roberts and R.S. Schick's participation was funded by NOAA Fisheries (Cooperative Agreement NA20NMF0080246). N. R. Record was supported by National Science Foundation grants 2307754, 1849227.

8. TABLES

Table 1. List of acronyms.

Acronym	Full name
USA	United States of America
GSL	Gulf of St. Lawrence
GOM	Gulf of Maine
EcoMon	Ecosystem Monitoring Program
AZMP	Atlantic Zone Monitoring Program
CCB	Cape Cod Bay
SS	Scotian Shelf
sGSL	southern GSL
eNL	eastern Newfoundland shelf
NARW	North Atlantic Right Whale
SDMs	Species Distribution Models
GAMs	Generalized Additive Models
DFO	Department of Fisheries and Oceans Canada
NOAA	National Oceanic and Atmospheric Administration
T_0-50	temperature in 0-50 m layer
Tmin	temperature minimum in the water column
climS_0-50sqrt	spatial climatology of salinity in the 0-50 m layer
GAMM	Generalized Additive Mixed Models
MAB	Middle Atlantic Bight
SNE	Southern New England Shelf
GB	Georges Bank
GSC	Great South Channel
nGSL	northern GSL
LAB	Labrador Shelf
CIV	copepodid stage IV
CV	copepodid stageV
CVI	copepodid stage VI
DW	dry weight
PSU	Practical Salinity Unit

Table 2. Results of GAMs for Bernoulli and Gamma models. See section 2.2.1 for model equations. The Bernoulli model is validated across the 100 iterations of models refitted with 70% of stations and 30% are used to calculate the TSS (mean ± s.d.). The TSS was also calculated on the resubstitution of the 100% of data used to fit the model. The AIC used for model comparison and the restricted maximum likelihood (REML) are presented for both model distribution. The Gamma model was validated using out-of-sample deviance on 30% of the data (70% for model fitting) and the deviance explained using resubstitution. The combined predictions of the two models (π x μ) was validated using the Spearman's correlation coefficient. See Appendix 3 for further validation. Model 3.3 for C. glacialis was not performed because it was not justified to winzorize smoothers of T_0-50 or Tmin.

		Bernoulli				Gamma				Combined
Species	Model	TSS (30%)	TSS (100%)	AIC	REML	Out of sample deviance (30%)	Deviance explained (100%)	AIC	REML	Spearman's correlation coefficient
C. finmarchicus	Model 1	0.53 ± 0.02	0.55	3016	1526	9086	33.11	318363	159246	0.61
	Model 2	0.55 ± 0.02	0.65	2787	1373	7752	44.71	314823	157529	0.72
	Model 3.1	0.55 ± 0.02	0.63	2787	1425	8054	41.83	315724	157973	0.70
	Model 3.2	0.55 ± 0.02	0.63	2778	1418	7806	43.72	315100	157670	0.71
	Model 3.3	0.55 ± 0.03	0.63	2789	1417	7739	43.91	315035	157641	0.71
C. glacialis	Model 1	0.82 ± 0.00	0.82	6747	3413	1361	27.51	66942	33515	0.69
	Model 2	0.82 ± 0.00	0.82	6411	3244	1327	31.04	66743	33417	0.70
	Model 3.1	0.82 ± 0.00	0.83	6331	3221	1318	33.08	66630	33386	0.70
	Model 3.2	0.82± 0.00	0.83	6334	3222	1286	33.38	66611	33370	0.7
	Model 3.3	-	-	-	-	-	-	-	-	-
C. hyperboreus	Model 1	0.65 ± 0.01	0.65	11775	5927	2906	45.81	106906	53503	0.73
	Model 2	0.68 ± 0.00	0.69	10952	5527	2603	53.59	105875	53004	0.74
	Model 3.1	0.68 ± 0.00	0.69	10779	5468	2651	54.38	105744	52969	0.74
	Model 3.2	0.68 ± 0.00	0.69	10781	5469	2608	55.03	105650	52922	0.74
	Model 3.3	0.68 ± 0.00	0.69	10814	5486	2591	54.96	105659	52929	0.74

*Table 3. Pearson's correlations with YEAR*MONTH averages by regions. Codes for presence of regional boundaries in predictions (cons): none, +++ (highly present), + (present). Codes for accuracy of regional abundance level (pros): + (low), +++ (very high), ++ (high). N = number of YEAR*MONTH averages available in each region for correlation calculation. (-): regions where occurrence and abundance were very low and correlations meaningless. Model 3.3 for C. glacialis was not performed because it was not justified to winzorize smoothers of T_0-50 or Tmin.*

		Region												
Species	**Model name**	**MAB**	**SNE**	**GB**	**CCB**	**GOM**	**Fundy-GOM**	**SS**	**sGSL**	**nGSL**	**eNL**	**LAB**	**Regional boundaries?**	**Accurate regional abundance level?**
C. finmarchicus	Model 1	0.45	0.66	0.65	0.59	0.54	0.68	0.43	0.43	0.21	0.28	0.49	none	+
	Model 2	0.70	0.76	0.78	0.64	0.54	0.65	0.38	0.58	0.58	0.54	0.39	+++	+++
	Model 3.1	0.64	0.79	0.73	0.60	0.50	0.65	0.49	0.45	0.60	0.53	0.43	none	+
	Model 3.2	0.68	0.77	0.75	0.62	0.48	0.65	0.46	0.40	0.61	0.55	0.41	+	++
	Model 3.3	0.68	0.77	0.75	0.60	0.48	0.65	0.46	0.40	0.60	0.54	0.43	+	++
C. hyperboreus	Model 1	-	-	-	-	0.47	0.36	0.78	0.51	0.20	0.66	0.76	none	+
	Model 2	-	-	-	-	0.60	0.41	0.79	0.58	0.32	0.80	0.71	+++	+++
	Model 3.1	-	-	-	-	0.60	0.45	0.79	0.58	0.30	0.76	0.77	none	+
	Model 3.2	-	-	-	-	0.59	0.45	0.80	0.58	0.29	0.77	0.77	+	+++
	Model 3.3	-	-	-	-	0.58	0.45	0.80	0.59	0.29	0.77	0.77	+	+++
C. glacialis	Model 1	-	-	-	-	-	-	0.60	0.55	0.74	0.54	0.23	none	+
	Model 2	-	-	-	-	-	-	0.67	0.61	0.75	0.71	0.20	+++	+++
	Model 3.1	-	-	-	-	-	-	0.63	0.58	0.71	0.78	0.50	+	+++
	Model 3.2	-	-	-	-	-	-	0.63	0.56	0.71	0.78	0.49	+	+++
	Model 3.3	Winzorizing not needed												
	n	113	149	136	87	131	106	245	157	152	215	32		

Table 4. Summary of Model 3.3: covariates values with a positive effect on Calanus species abundance. Model 3.1 was used for C. glacialis.

Species	Covariate	Bernoulli	Gamma
C. finmarchicus	T_0-50	<11.8	3.3-14.8
	Tmin	>3.4	3.7-8.7
	Bathymetry*	>108	>95
	Latitude	35-41.7, >48	35-37,40.4-44.7, >53
	Month	1-2, 9-12	4-9
	climS_0_50*	<32.3	32.5-34-
C. glacialis	T_0_50	<7.40	3.63-8.75, >12
	Tmin	<5.54	<0.57
	Bathymetry*	>128	>166
	Latitude	>41.4	>47.3
	Month	8-11	5-7
	climS_0_50*	<32, >33.17	29.4-31.8
C. hyperboreus	T_0_50	<8.15	2-8.3
	Tmin	>1.77	0.27-4.64, >7.5
	Bathymetry*	>100	>178
	Latitude	<38, > 44	<38.3, 46.7-54
	Month	5-9	4-9
	climS_0_50*	<32.1	<31.9

* Values after back-transformation of logBathymetry and climS_0_50 sqrt

Table 5. Comparison of monthly averaged depth (m) of NARW optimal foraging predicted with the 3D preyscape/bioenergetic model (left, this study) and observed averaged depth (m) of NARW foraging (right, Baumgartner et al 2017) in specific habitats. CCB = Cape Cod Bay, GSC = Great South Channel, BOF = Bay of Fundy (Grand Manan). Corresponding predicted and observed averaged depth during any given month and location are identified by numbers in black.

Transboundary model predictions of optimal foraging depth											Observed foraging depth (Baumgartner et al. 2017)									
Region	Foraging depth (m)										Foraging depth (m)									
	MONTH										MONTH									
	3	4	5	6	7	8	9	10	11	12	3	4	5	6	7	8	9	10	11	12
CCB	18	19	24	17	11	18	13	16	30	17	18	-	-	-	-	-	-	-	-	-
GSC	37	29	121	116	59	91	116	118	125	102	-	-	20	20	-	-	-	-	-	-
Jeffreys Ledge	35	26	107	94	43	77	104	106	109	89	-	-	-	-	-	-	-	-	-	125
BOF	85	94	98	94	94	131	131	129	89	88	-	-	-	-	-	117	-	-	-	-
Roseway	91	114	114	95	92	117	117	117	82	81	-	-	-	-	-	-	103	103	-	-

9. FIGURES

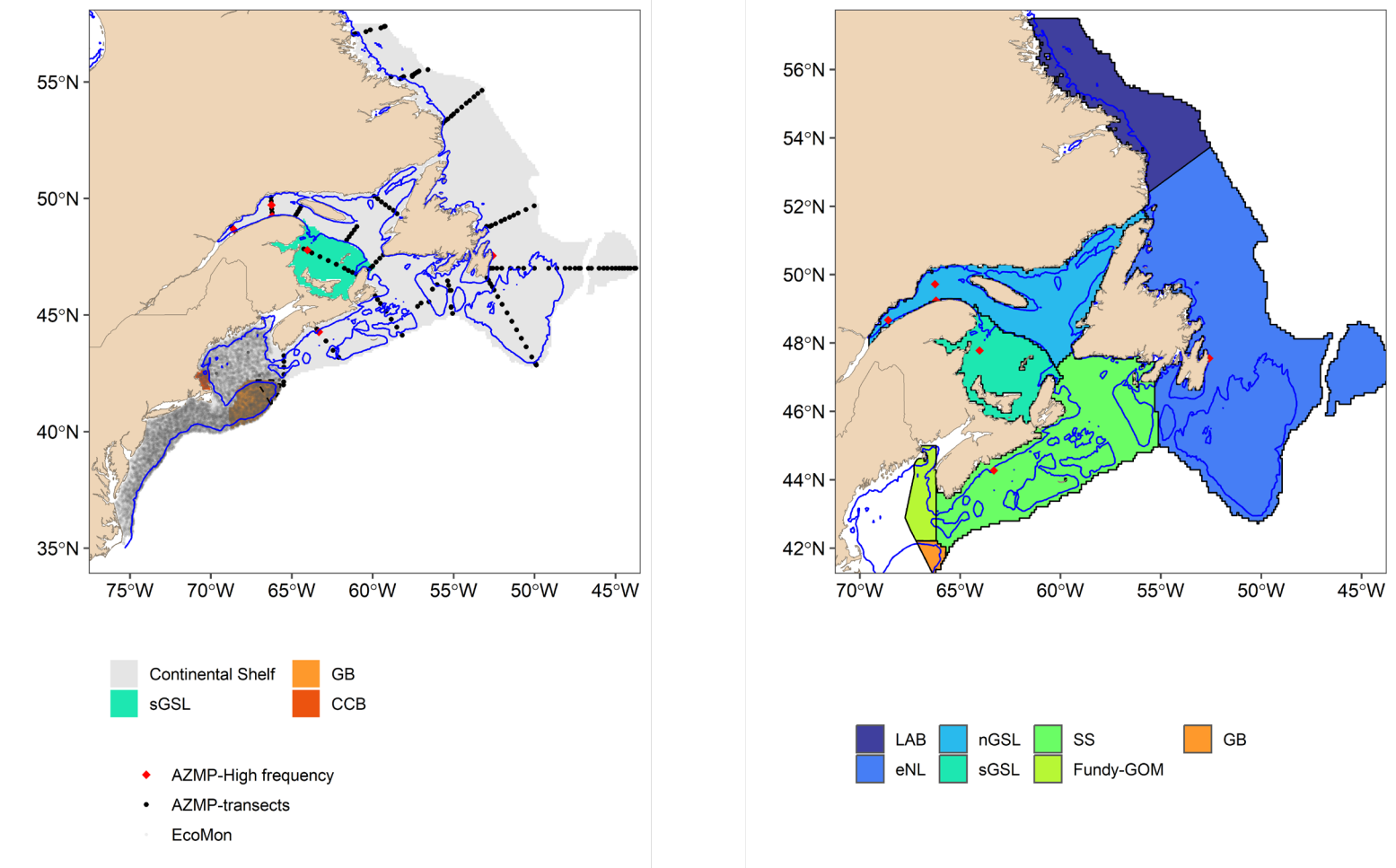

Figure 1. Left panel: Transboundary SDMs spatial domain, zooplankton stations from 1999-2020 (n = 16,333) and sub-regions (n = 4) used as a regional factor in model 3.3: Continental Shelf in grey, sGSL in green, GB in light orange and CCB in dark orange). The black dashed line separates the Canadian part of GB. Right panel: regions in Canadian waters used to report results of the present study. LAB= Labrador shelf, eNL = eastern Newfoundland shelf, nGSL and sGSL= northern and southern Gulf of St. Lawrence, SS = Scotian and southern Newfoundland Shelf, Fundy-GOM = northeast Gulf of Maine and outer Bay of Fundy, GB = northeast tip of Georges Bank. The blue lines show the 100 m-isobath.

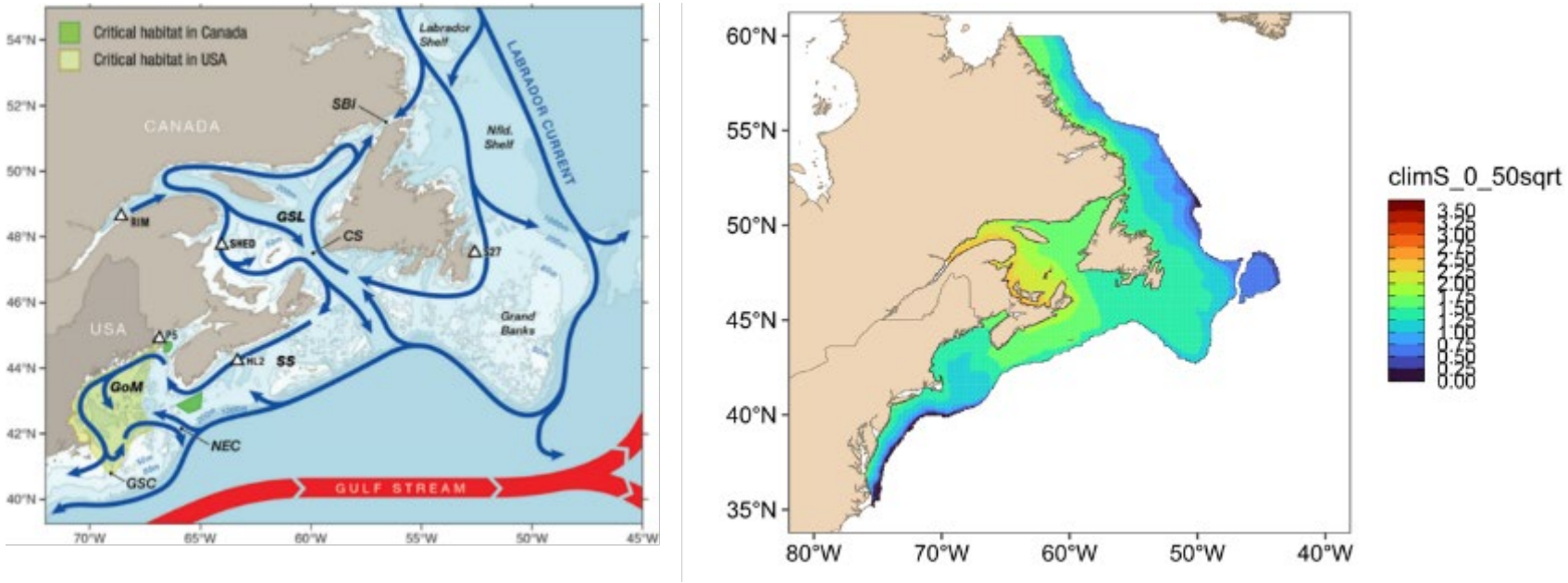

Figure 2. Left panel: Schematic representation of the main surface currents patterns from the Labrador shelf (north) to the southern New England shelf (south) with the anti-clockwise circulation in the Gulf of St. Lawrence (GSL) and Gulf of Maine (GoM) (Adapted from Sorochan et al. 2021). Right panel: Spatial climatology of salinity 0-50 m (S_0-50 m) extracted from GLORYS12v1 1999-2020. S_0-50 was transformed to normalize the data (see text and Figure A.1. 4t) with higher (lower) values on the color scale corresponding to fresher (saltier) water masses. Currents on the inner (outer) shelf generally correspond to fresher (saltier) water masses.

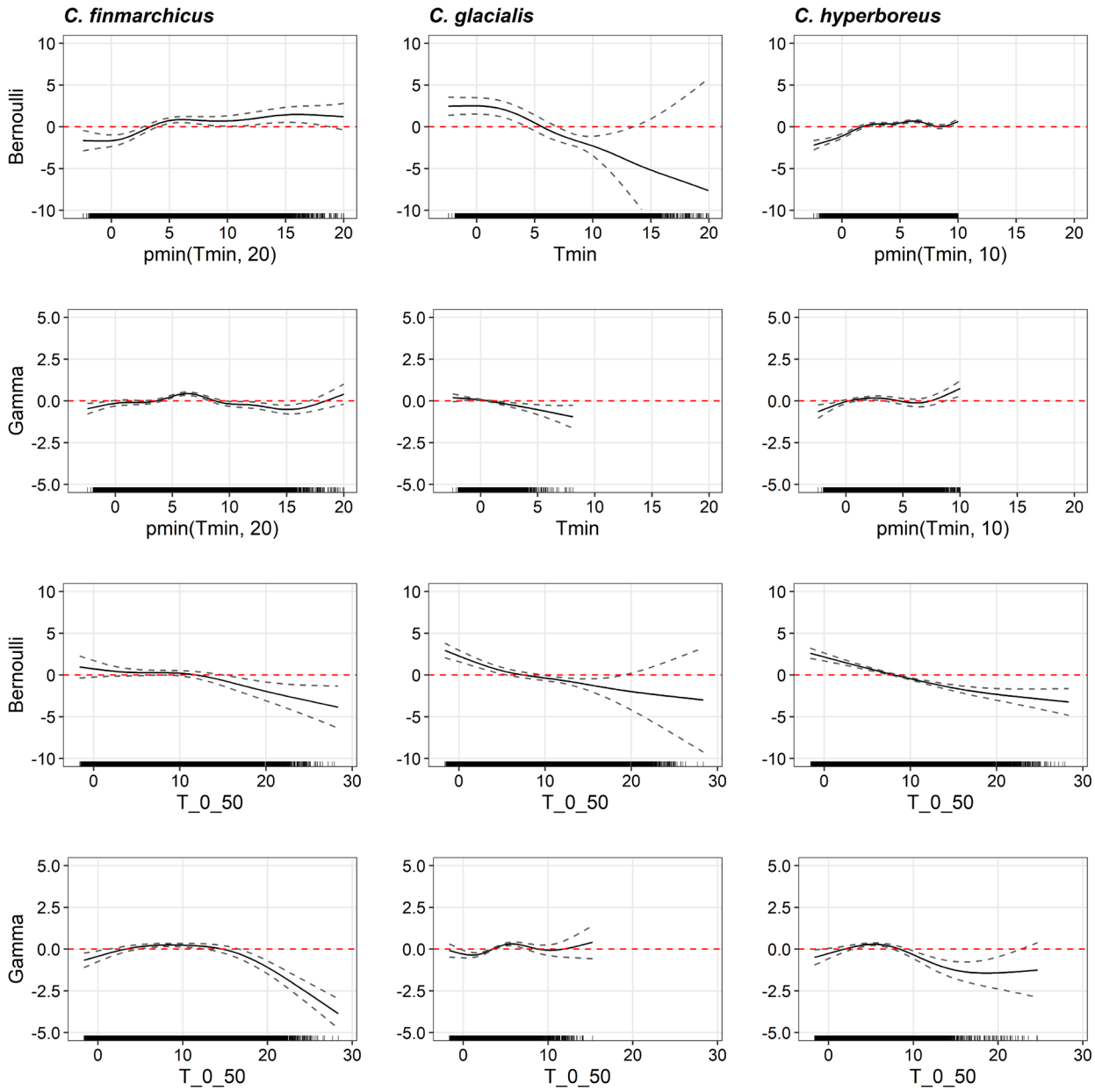

Figure 3. Model 3.3. Smoothers for T_0_50 and Tmin of the Bernoulli and Gamma models for C. finmarchicus, C. glacialis (model 3.1), and C. hyperboreus.

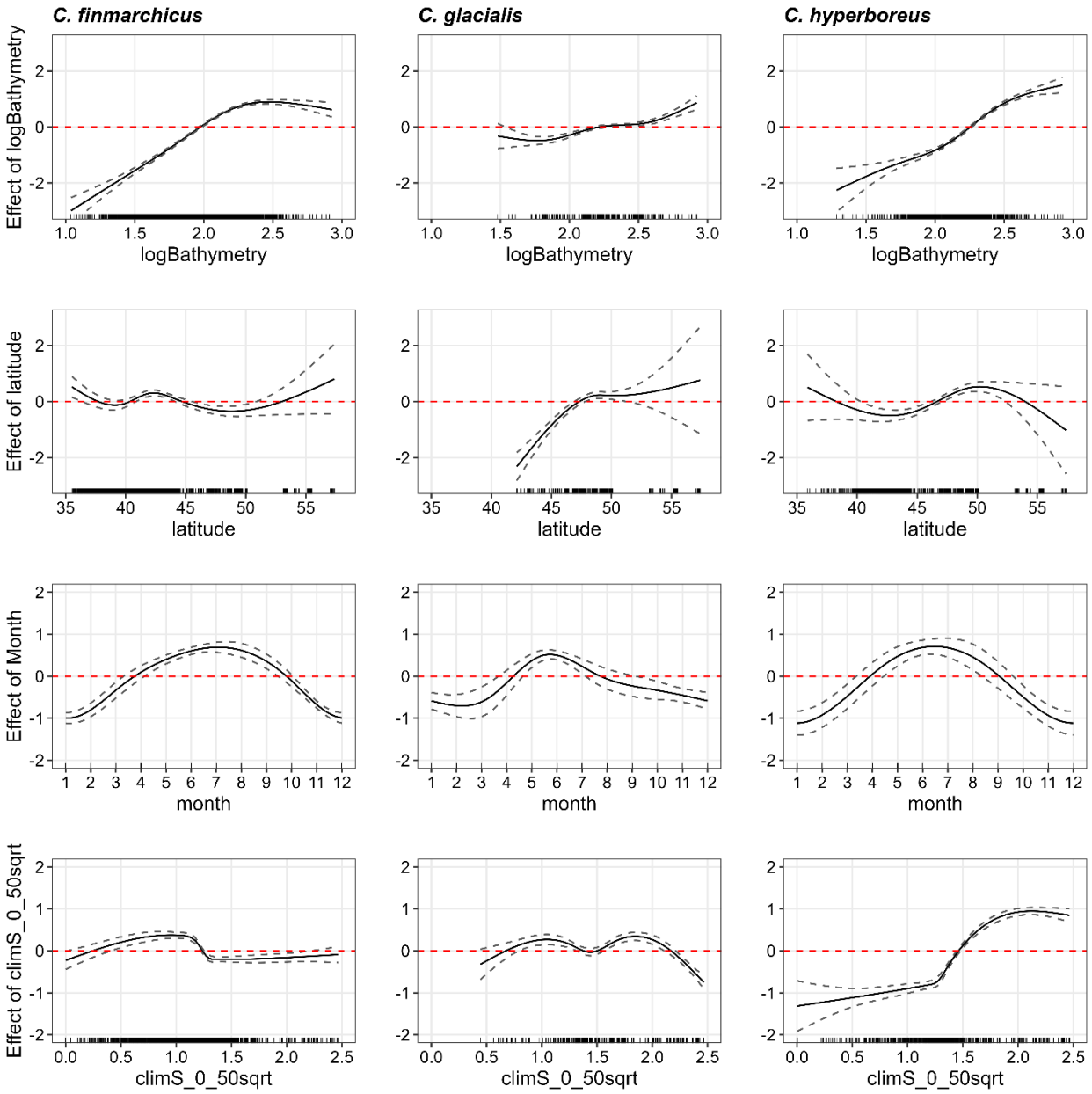

Figure 4. Model 3.3. Smoothers for Bathymetry, Latitude, and ClimS_0-50sqrt of the Gamma model for C. finmarchicus, C. glacialis (model 3.1), and C. hyperboreus.

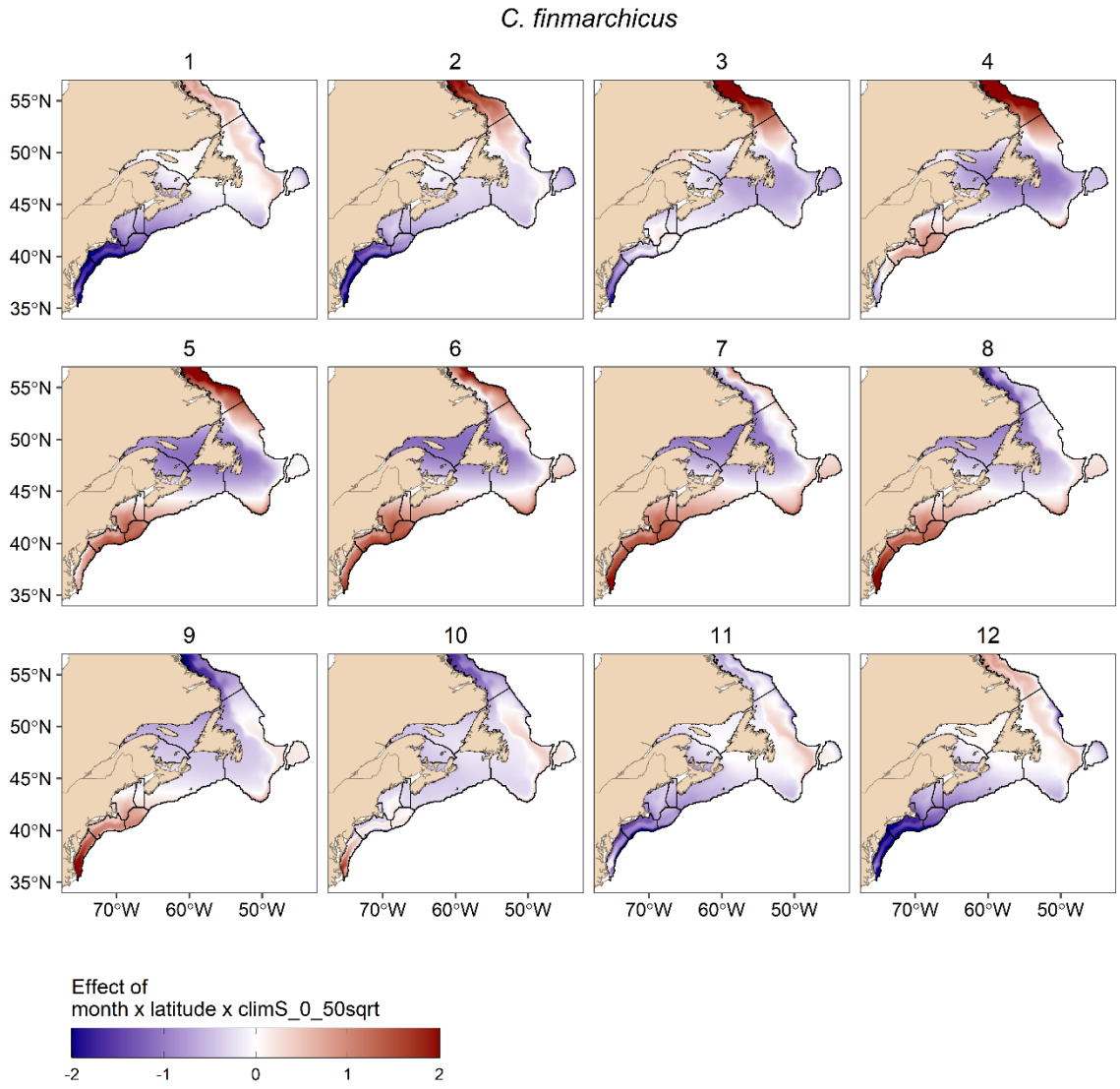

Figure 5. Model 3.3. Monthly summed effect of all covariates included in the ‘ connectivity’ interaction term in the Gamma models for C. finmarchicus during 1999-2020. See next two pages for C. glacialis and C. hyperboreus. Black lines delimit regions used to report results (see right panels in Figure 1 for Canada and Figure A.3. 5 for the transboundary area).

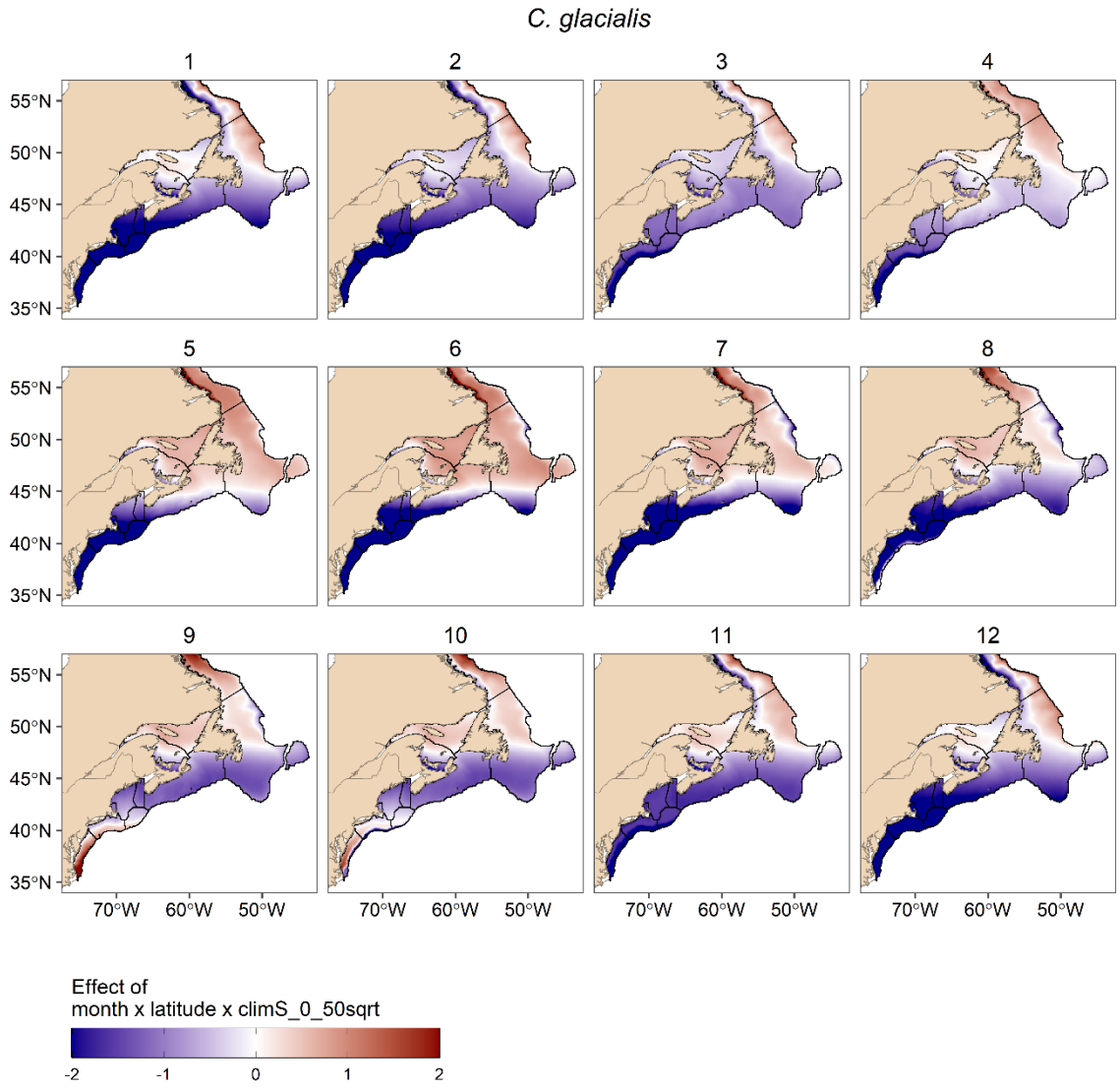

Figure 5 (continued). C. glacialis (model 3.1).

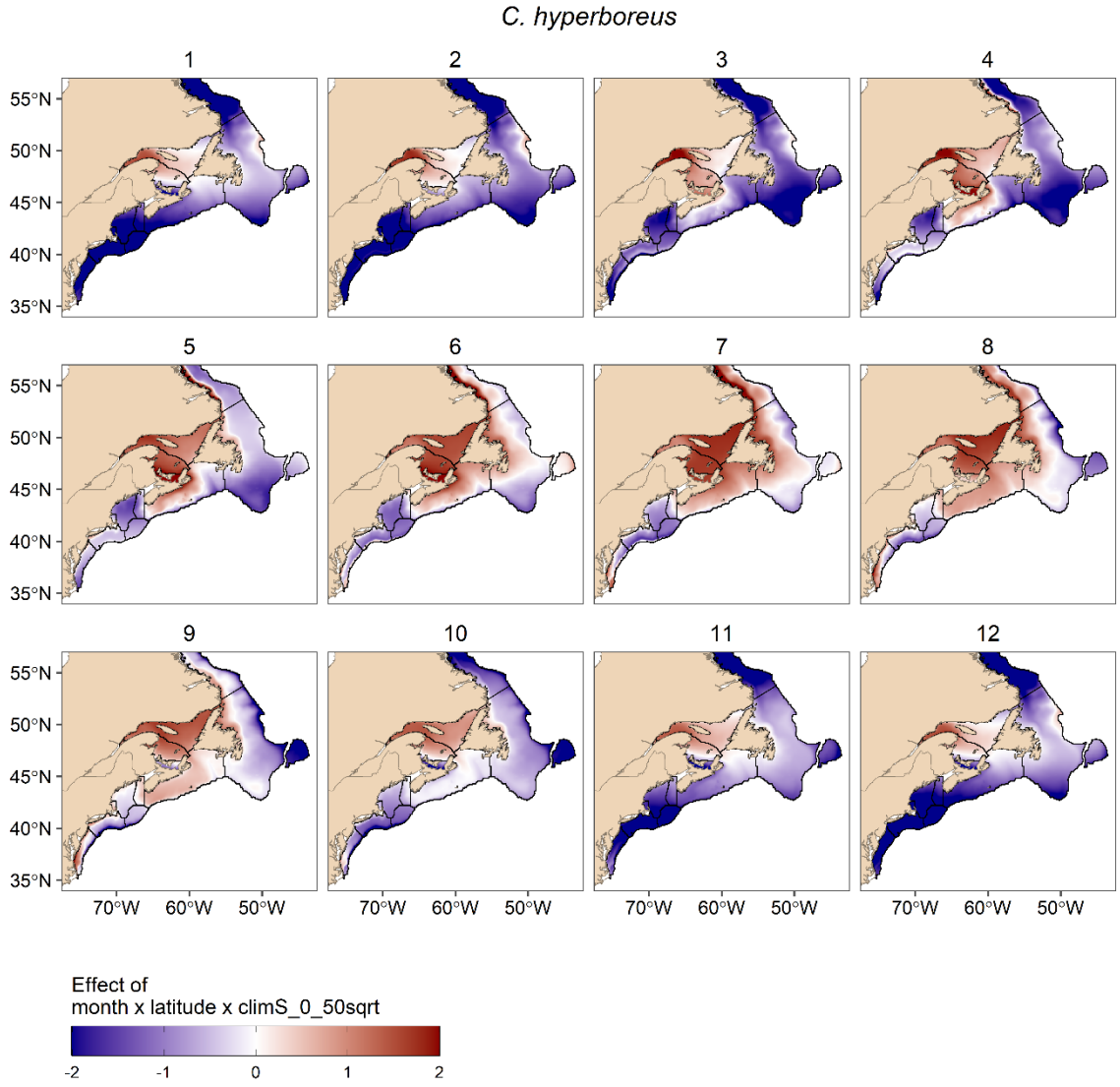

Figure 5 (continued). C. hyperboreus.

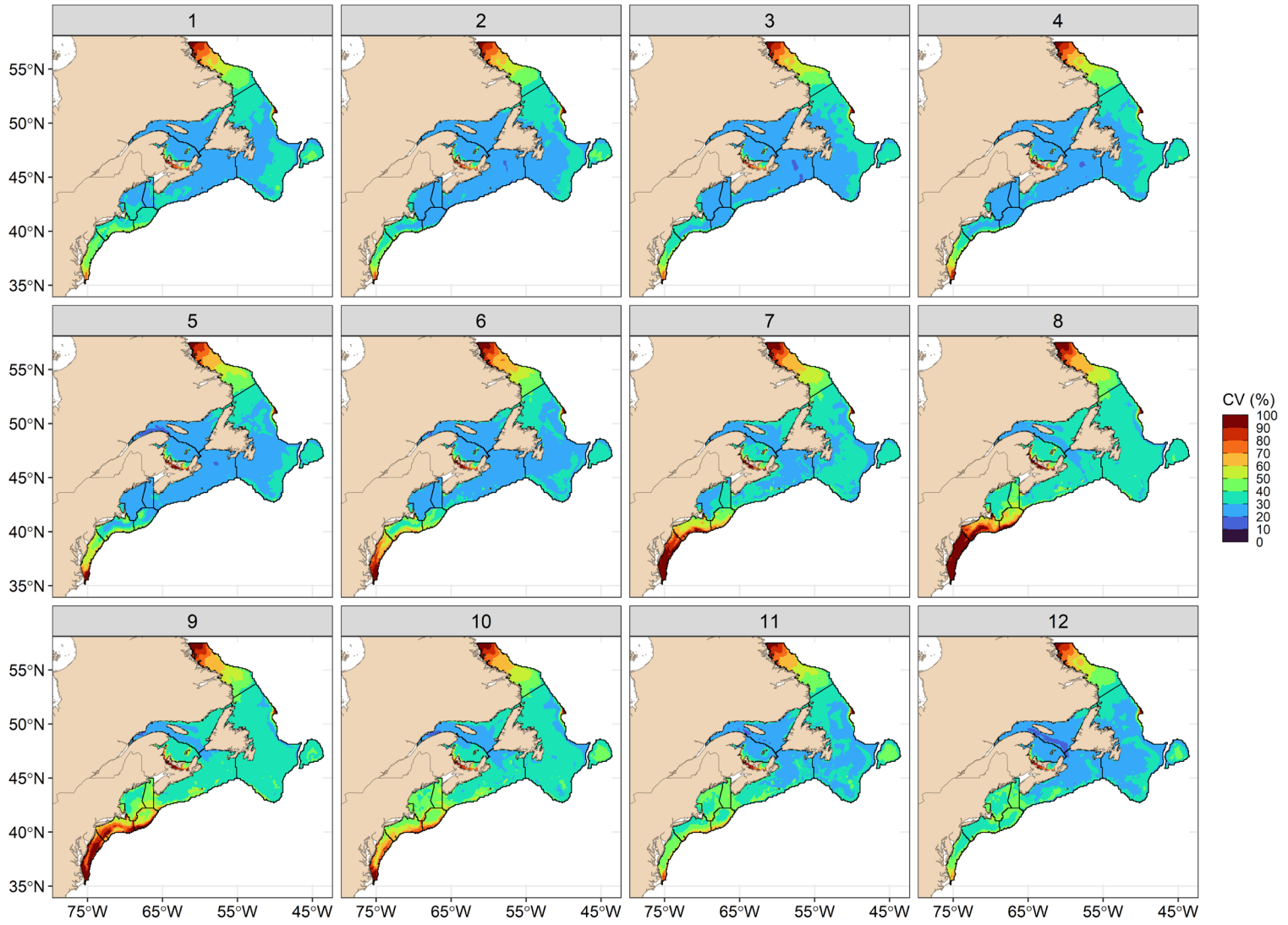

Figure 6. Uncertainty (CV%) of GAMMs' parameters and interannual variability for total abundance predictions of C. finmarchicus, and C. hyperboreus (Model 3.3.) and C. glacialis (model 3.1). Black lines delimit regions used to report results (see right panels in Figure 1 for Canada and Figure A.3. 5 for the transboundary area).

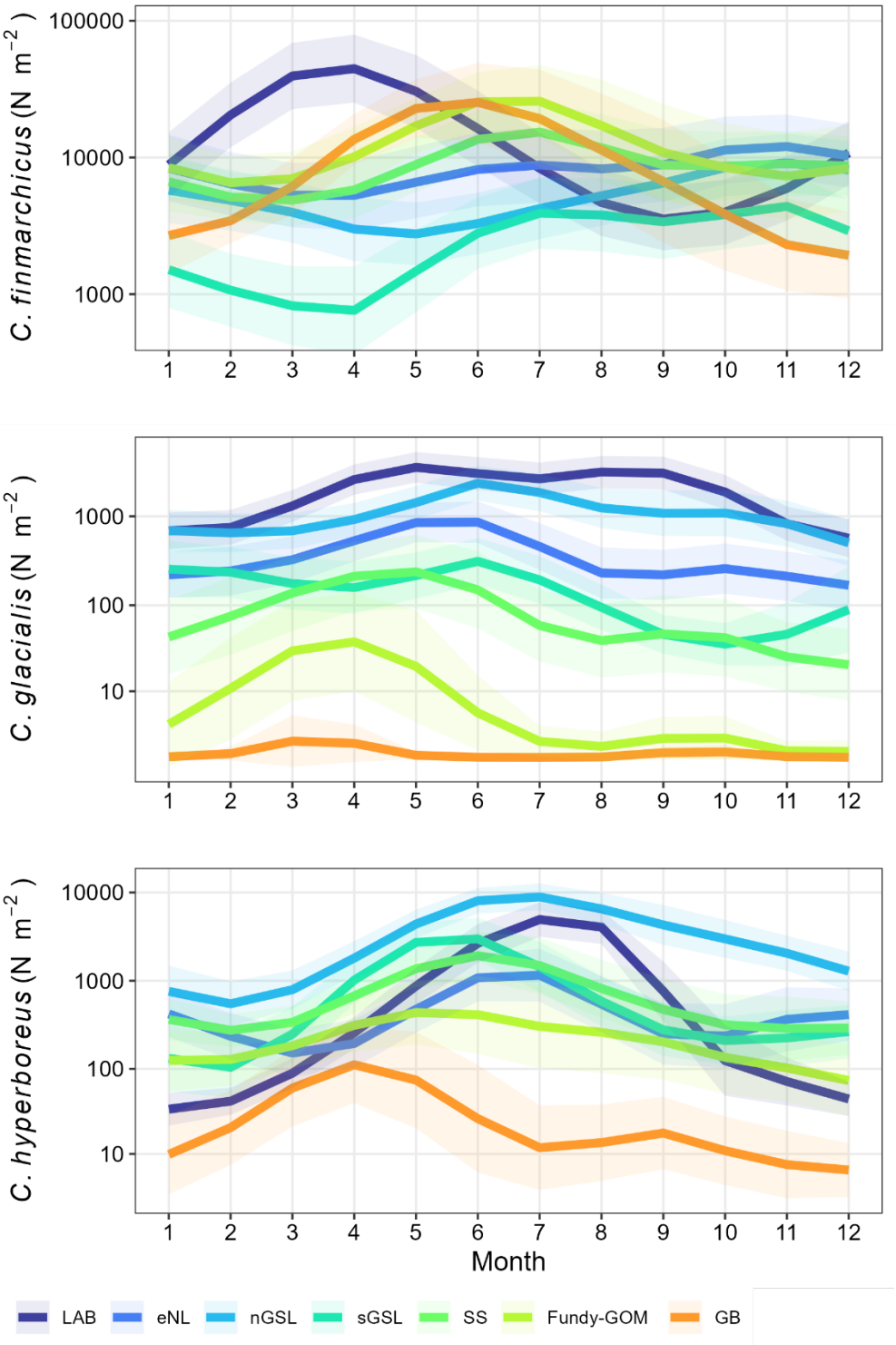

*Figure 7. Monthly predicted abundance of Calanus finmarchicus (top), C. glacialis (middle) and C. hyperboreus (bottom) in the different regions. Shaded areas represent 95% confidence intervals (Mean ±1.96 * sd) of interannual variability during 1999-2020.*

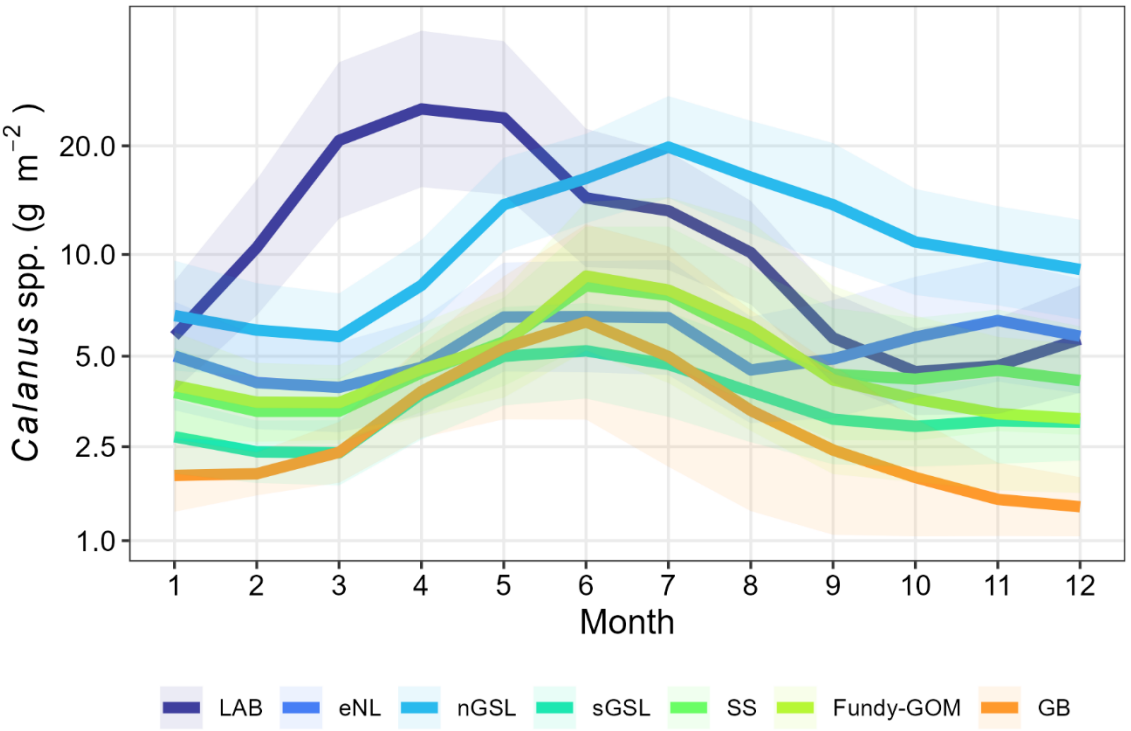

*Figure 8. Monthly average of predicted Calanus water column biomass (g m^{-2}) in the different regions. Shaded areas represent 95% confidence intervals (Mean ±1.96 * sd) of interannual variability during 1999-2020.*

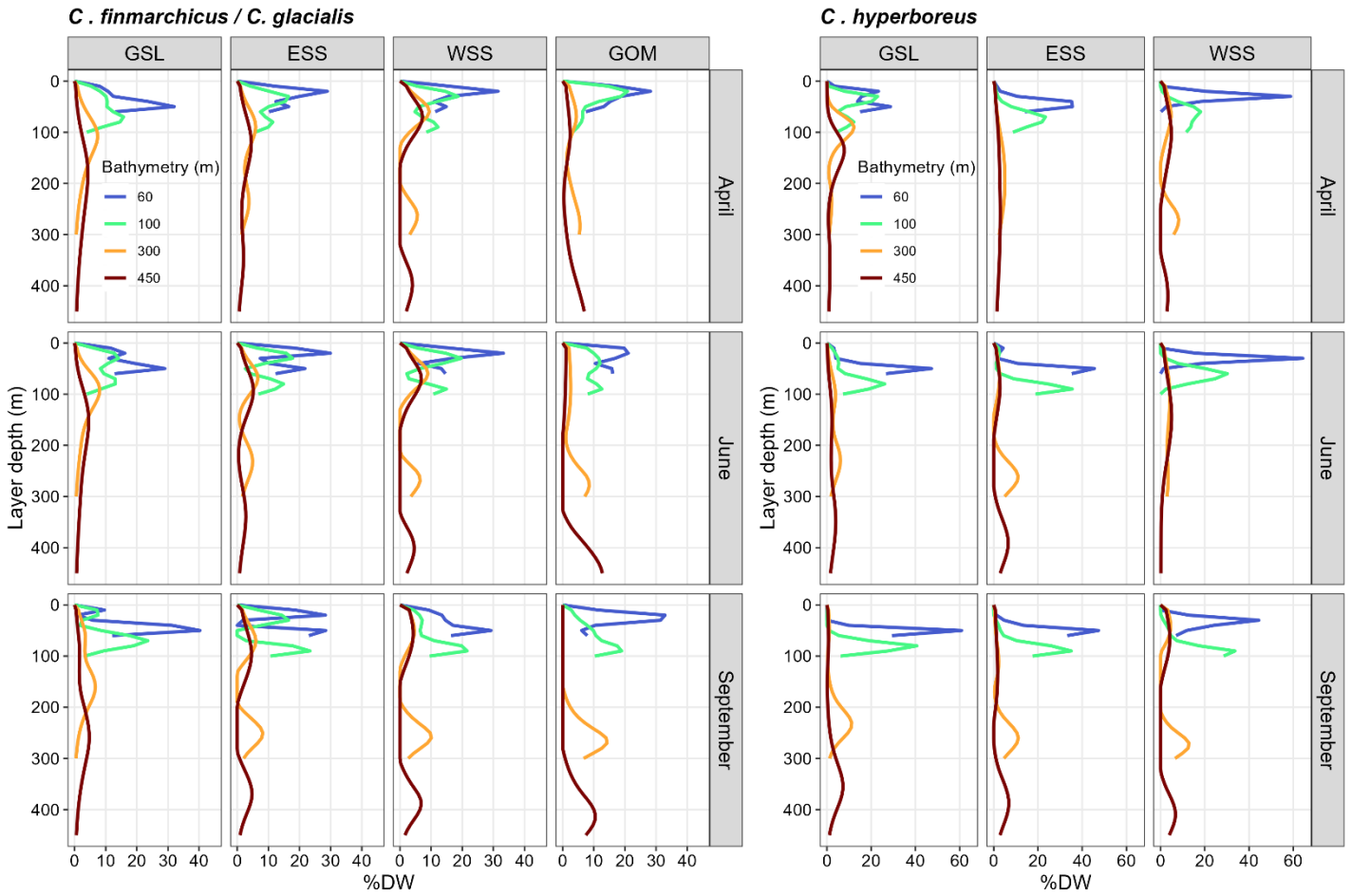

Figure 9. Predicted relative vertical distribution of C. finmarchicus/C. glacialis (left panels) and C. hyperboreus (right panels) in April, June and September for different bathymetry.

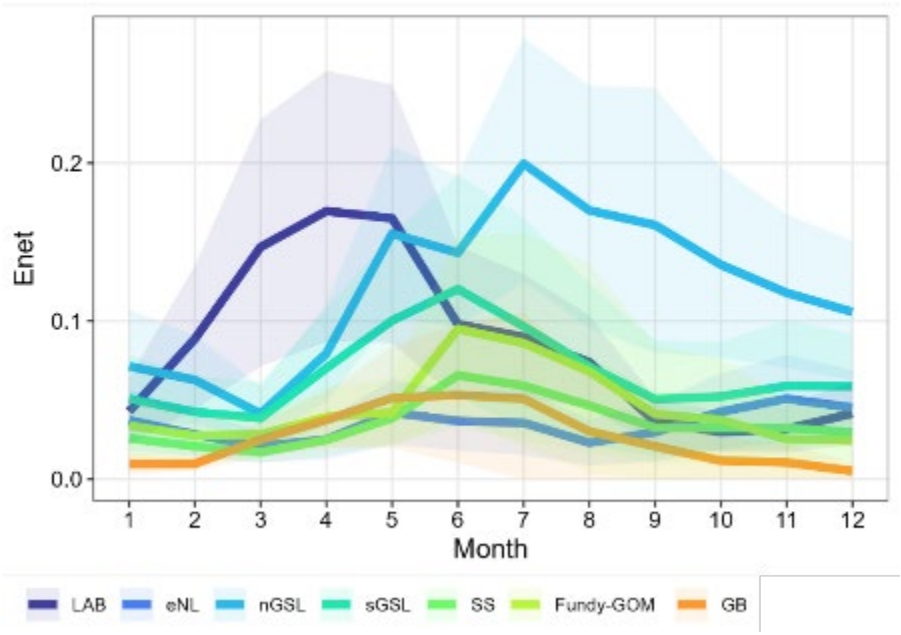

*Figure 10. Monthly averaged Enet in the different regions Shaded areas represent 95% confidence intervals (Mean ±1.96 * s.d.) of interannual variability during 1999-2020.*

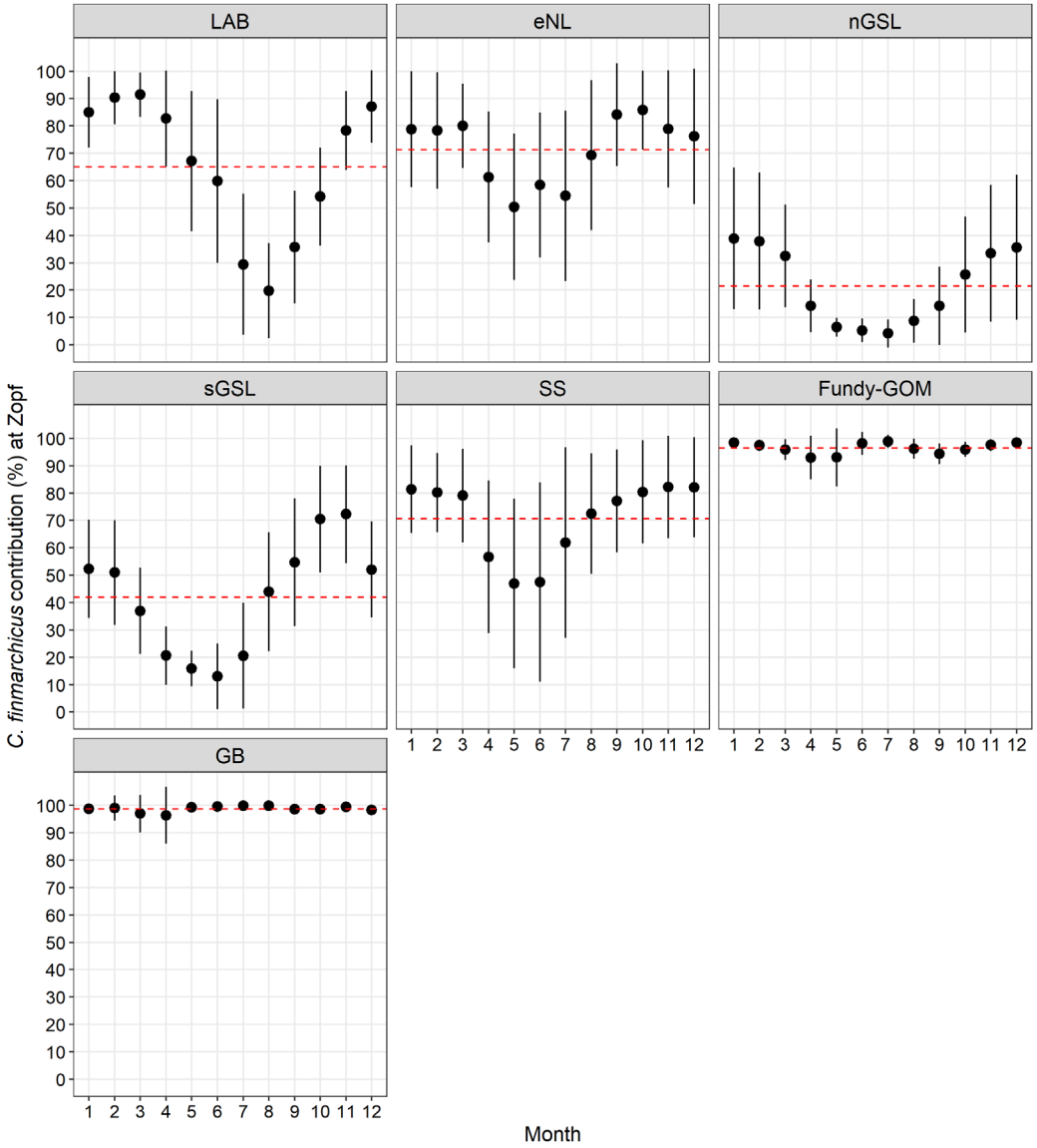

Figure 11. Monthly contribution (%) of C. finmarchicus to Enet in the different regions in Canadian waters. Mean ± s.d . Red line = region average.

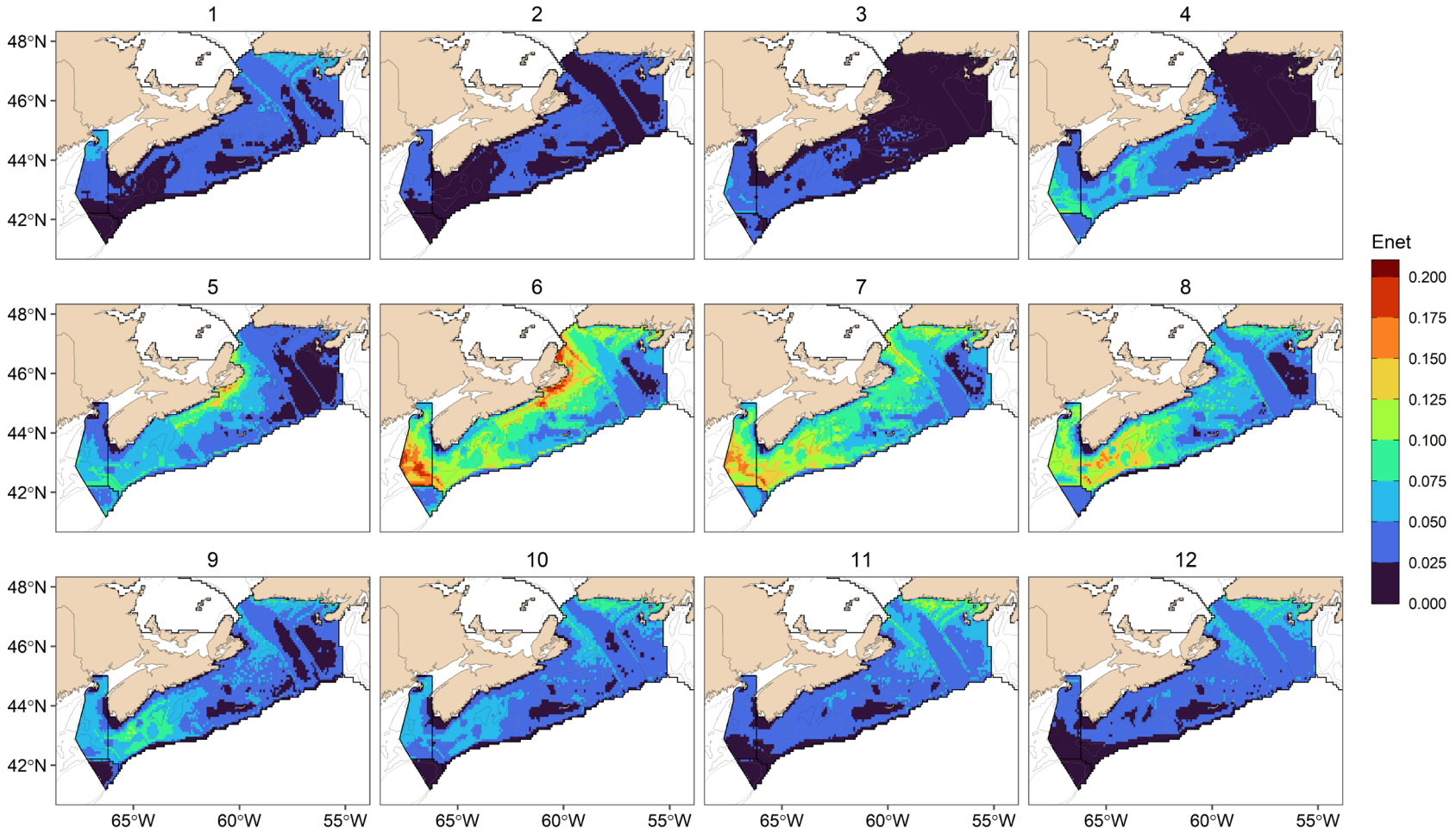

Figure 12. Spatial distribution of monthly predicted Enet in Fundy-GOM and SS during 1999-2020. Light and dark grey lines represent 100 and 200 m isobaths respectively. Black lines delimit regions used to report results in Canadian waters (Figure 1, right panel).

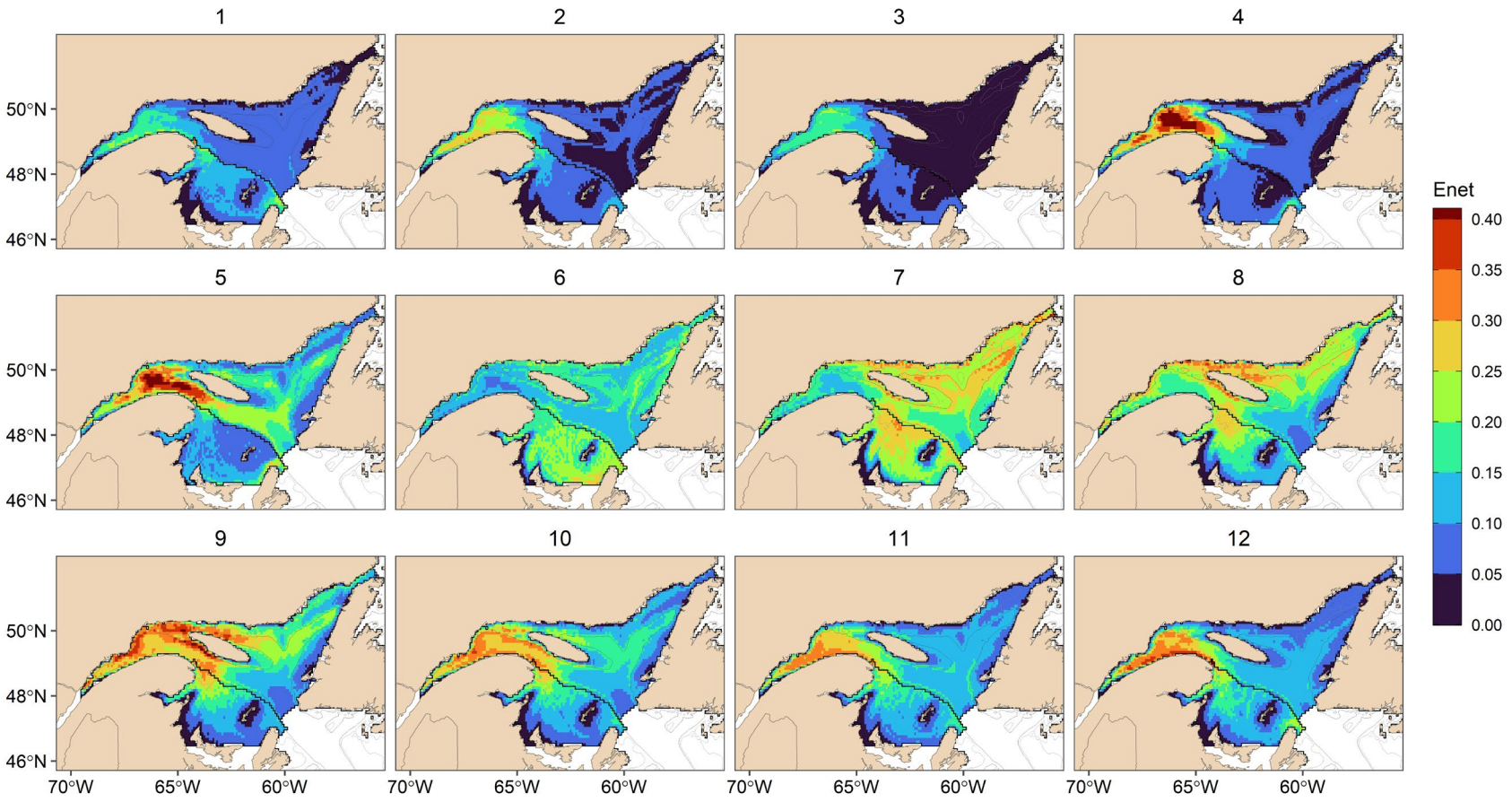

Figure 13. Monthly predicted Enet in sGSL and nGSL during 1999-2020. Light and dark grey lines represent 100 and 200 m isobaths respectively. Black lines delimit regions used to report results in Canadian waters (Figure 1, right panel).

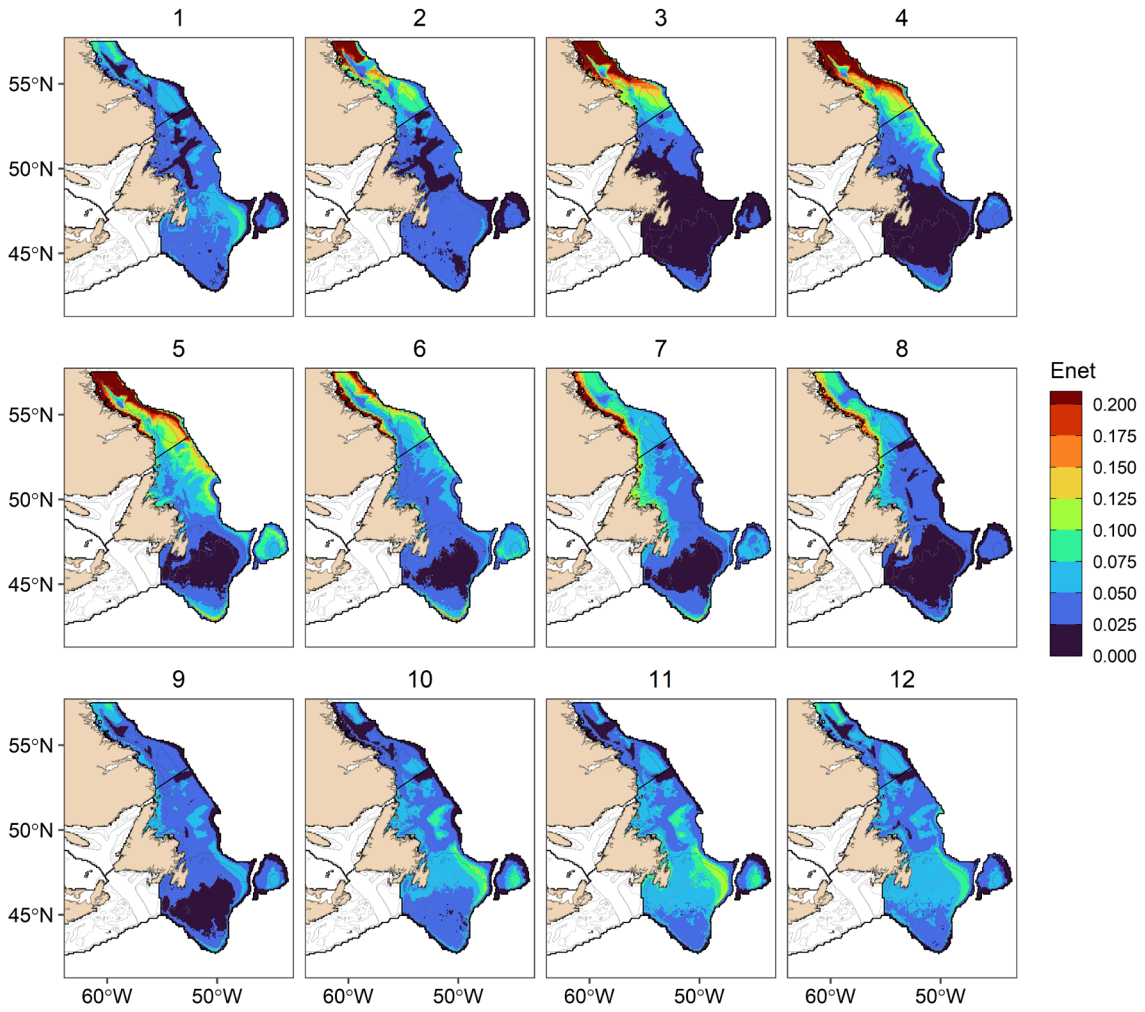

Figure 14. Spatial distribution of monthly predicted Enet in LAB and eNL during 1999-2020. Light and dark grey lines represent 100 and 200 m isobaths respectively. Black lines delimit regions used to report results in Canadian waters (Figure 1, right panel).

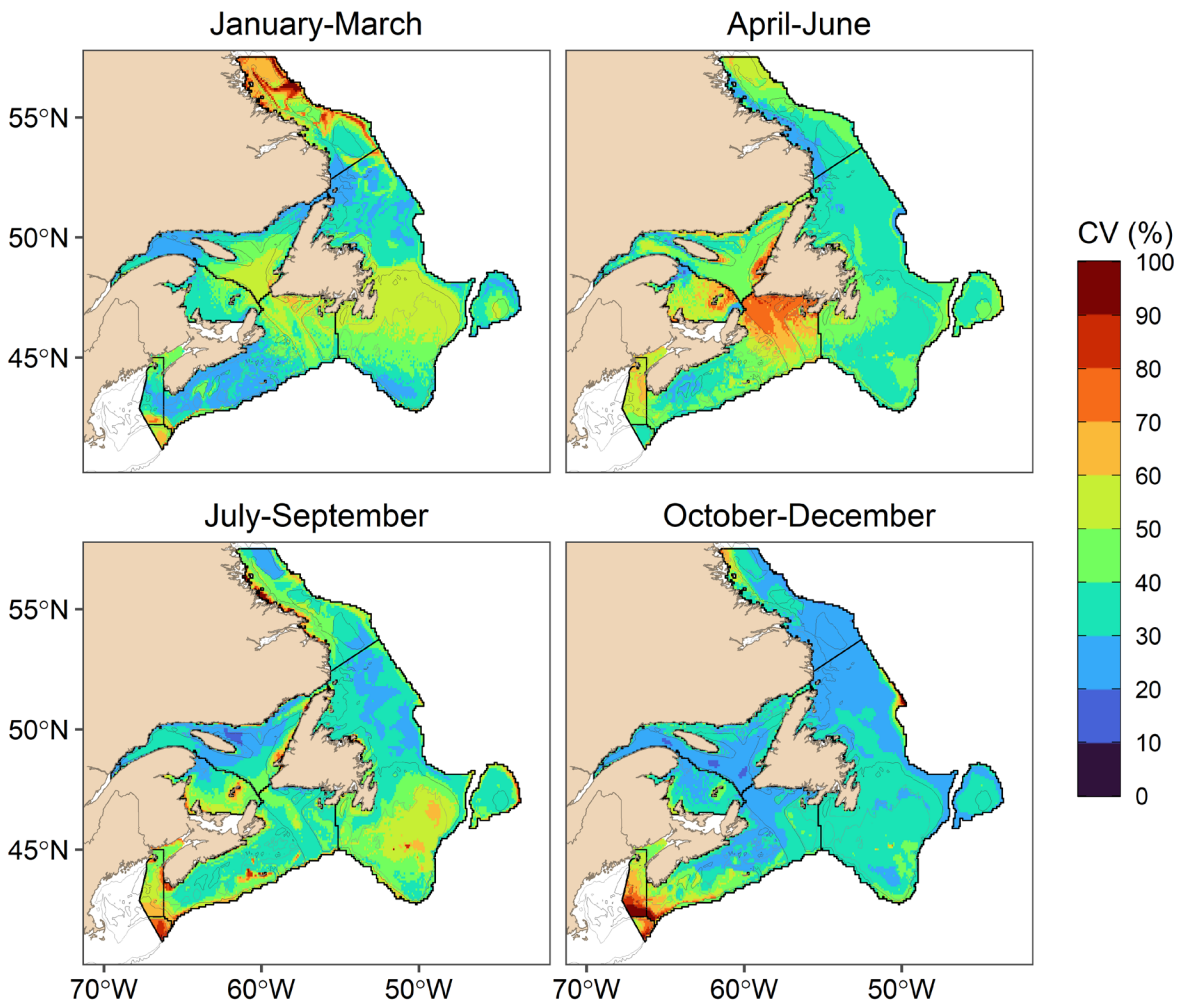

Figure 15. Coefficient of variation (%) on yearly and monthly variability of Enet by quarters during 1999-2020. Light and dark grey lines represent 100 and 200 m isobaths respectively. Black lines delimit regions used to report results in Canadian waters (Figure 1, right panel).

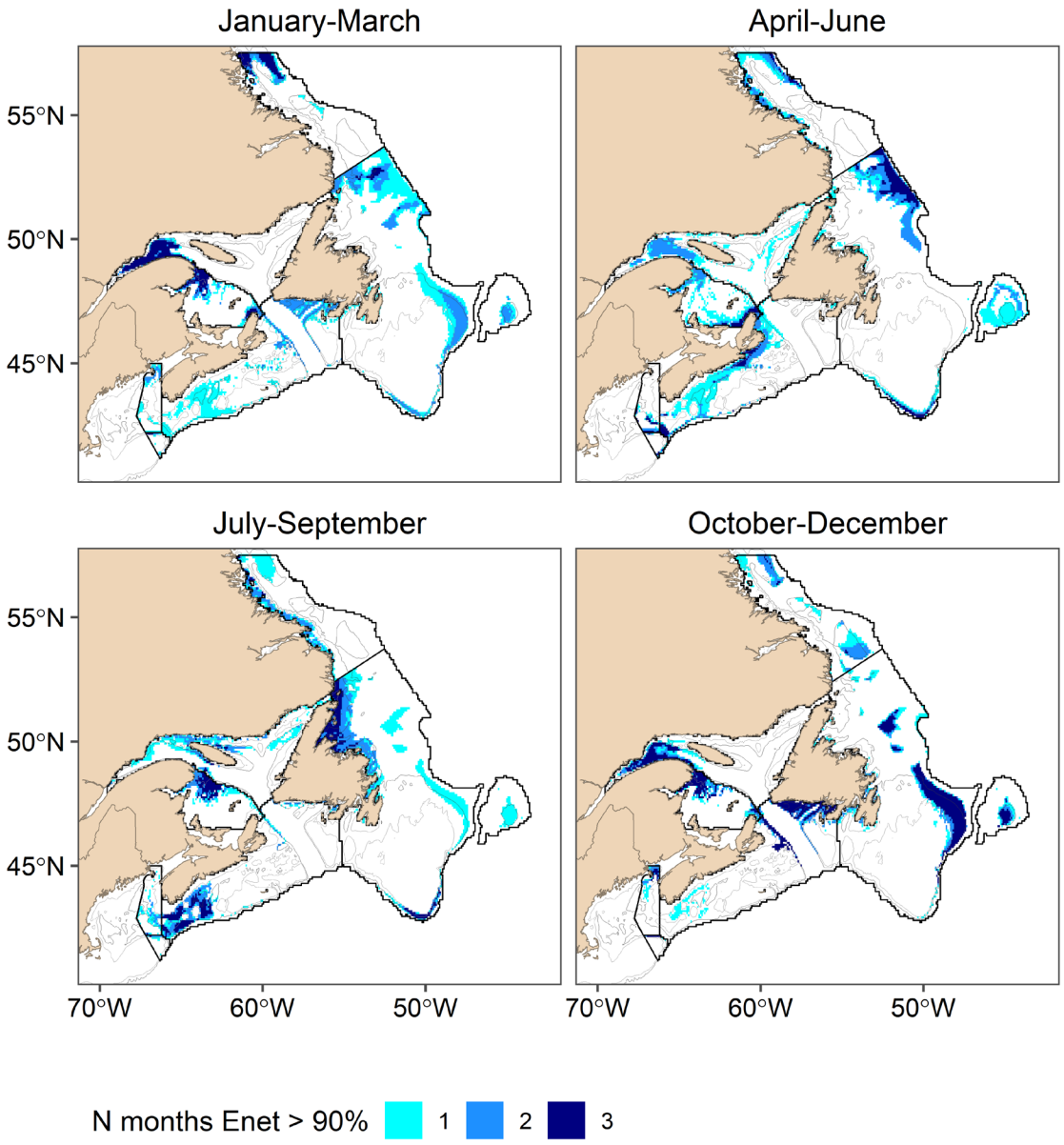

Figure 16. Areas considered to be potentially the most suitable (Enet >90th quantile) for NARW foraging in different regions and quarters of the year. The Color scale represents the persistence of the most suitable areas (1, 2 or 3 months). Light and dark grey lines represent 100 and 200 m isobaths respectively. Black lines delimit regions used to calculate quantiles in Canadian waters (Figure 1, right panel).

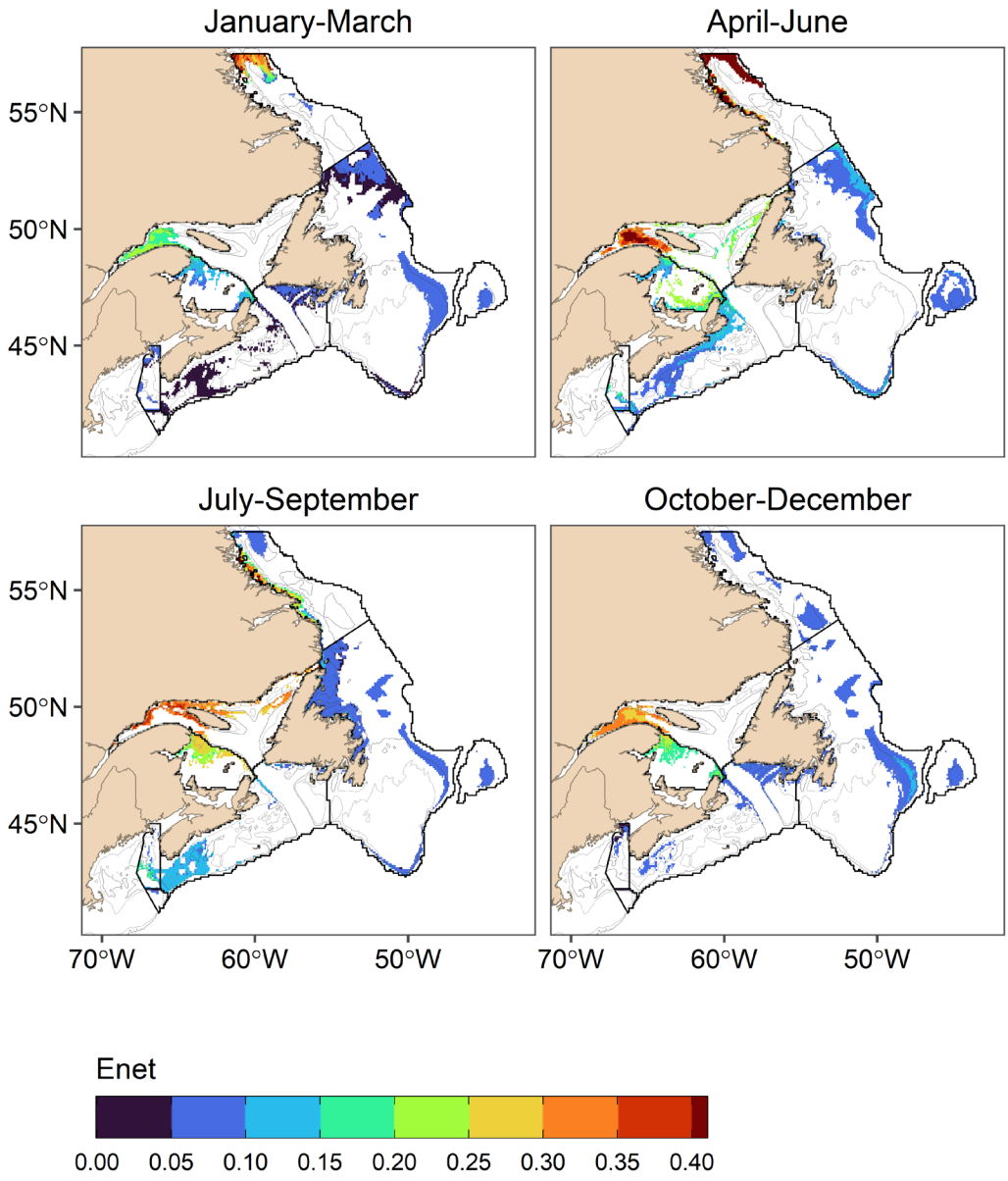

Figure 17. Mean Enet values in areas considered to be potentially the most suitable (Enet >90th quantile) for NARW foraging in different regions and quarters of the year. Black lines delimit regions used to calculate quantiles in Canadian waters (Figure 1, right panel).

APPENDIX 1

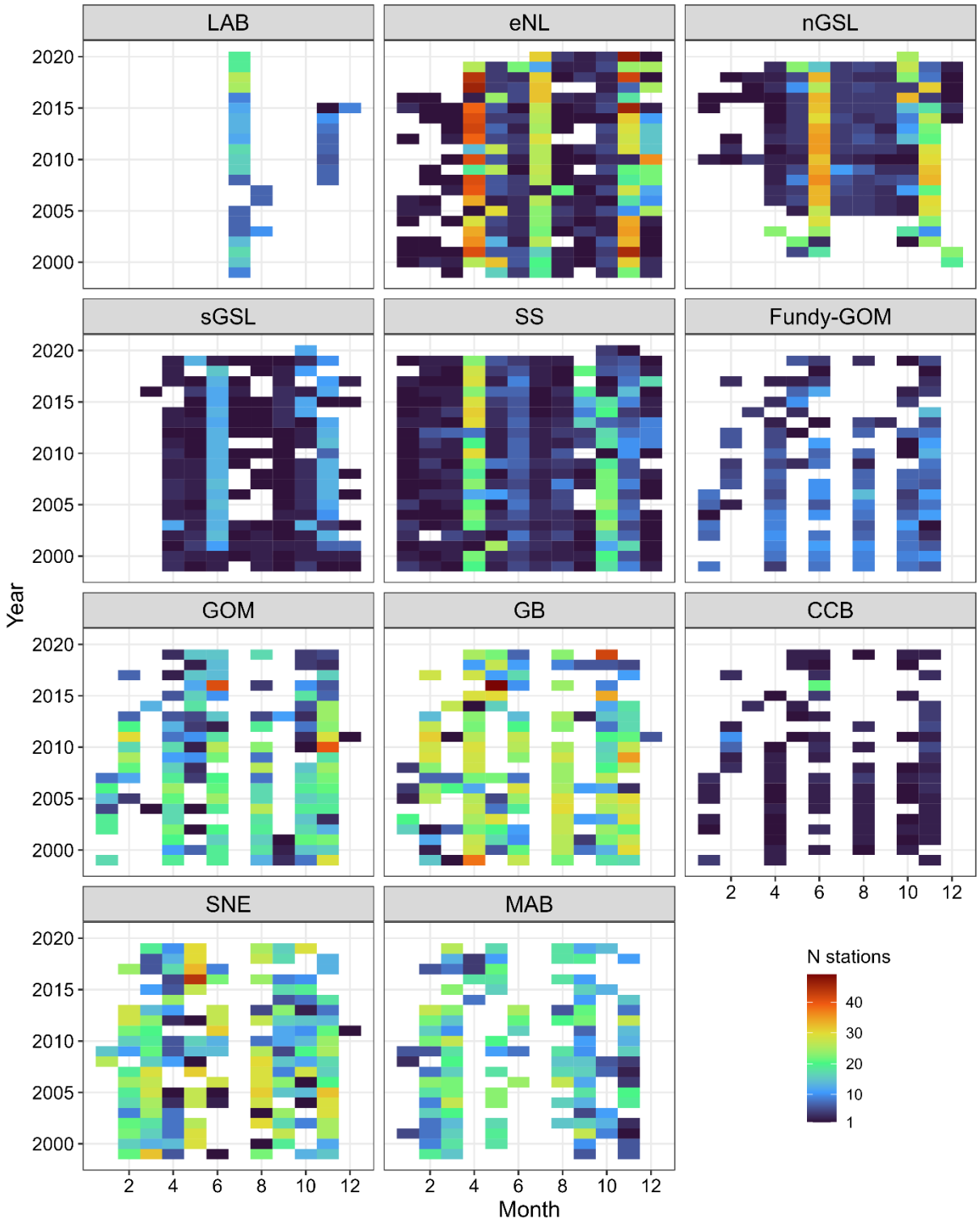

Figure A.1.1. Summary of spatial (by region) and temporal (month x year) coverage of zooplankton stations included in the SDMs.

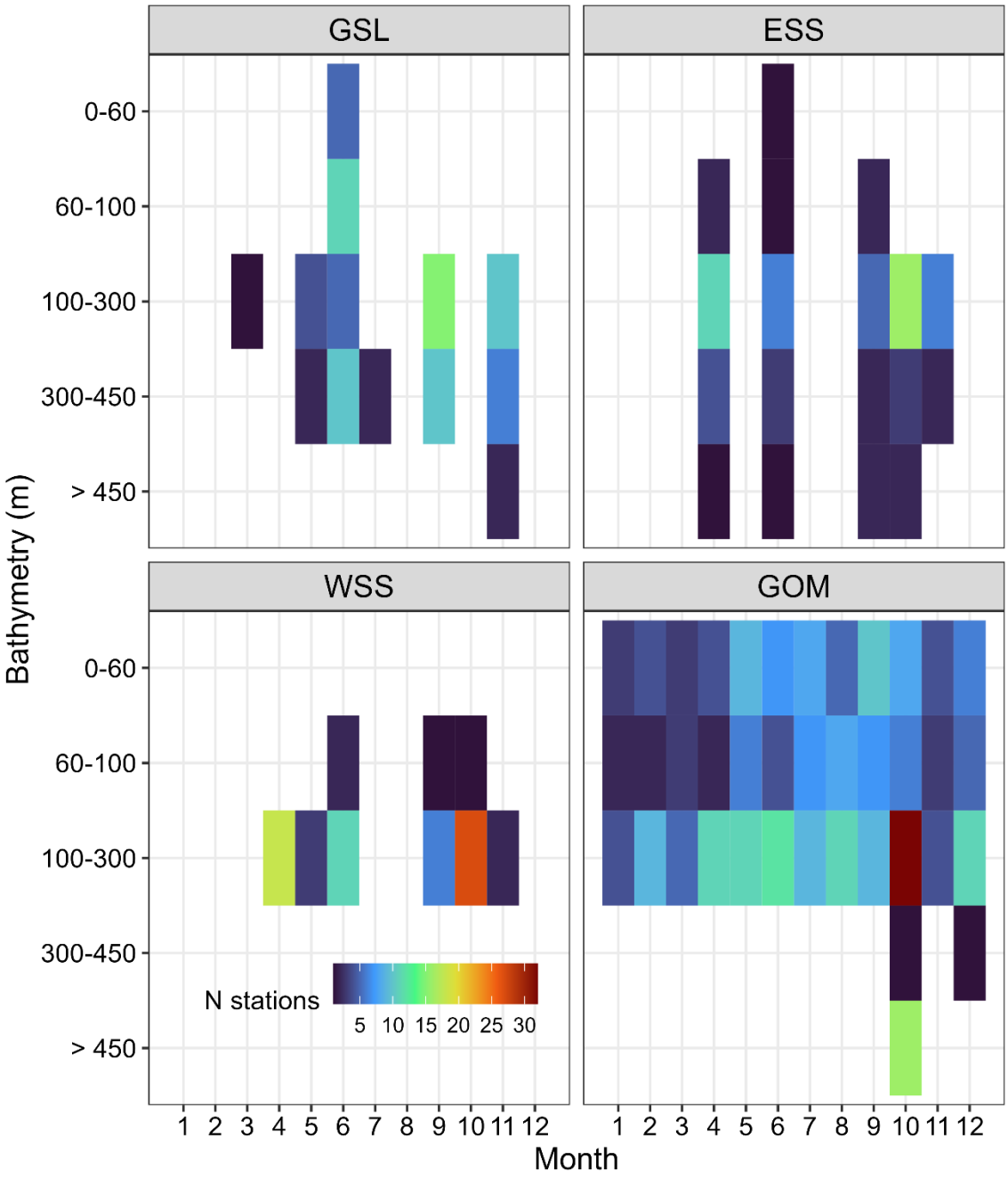

Figure A.1.2. Summary of spatial (by region and bathymetry) and temporal (month) coverage of depth-resolved stations included in the vertical distribution models.

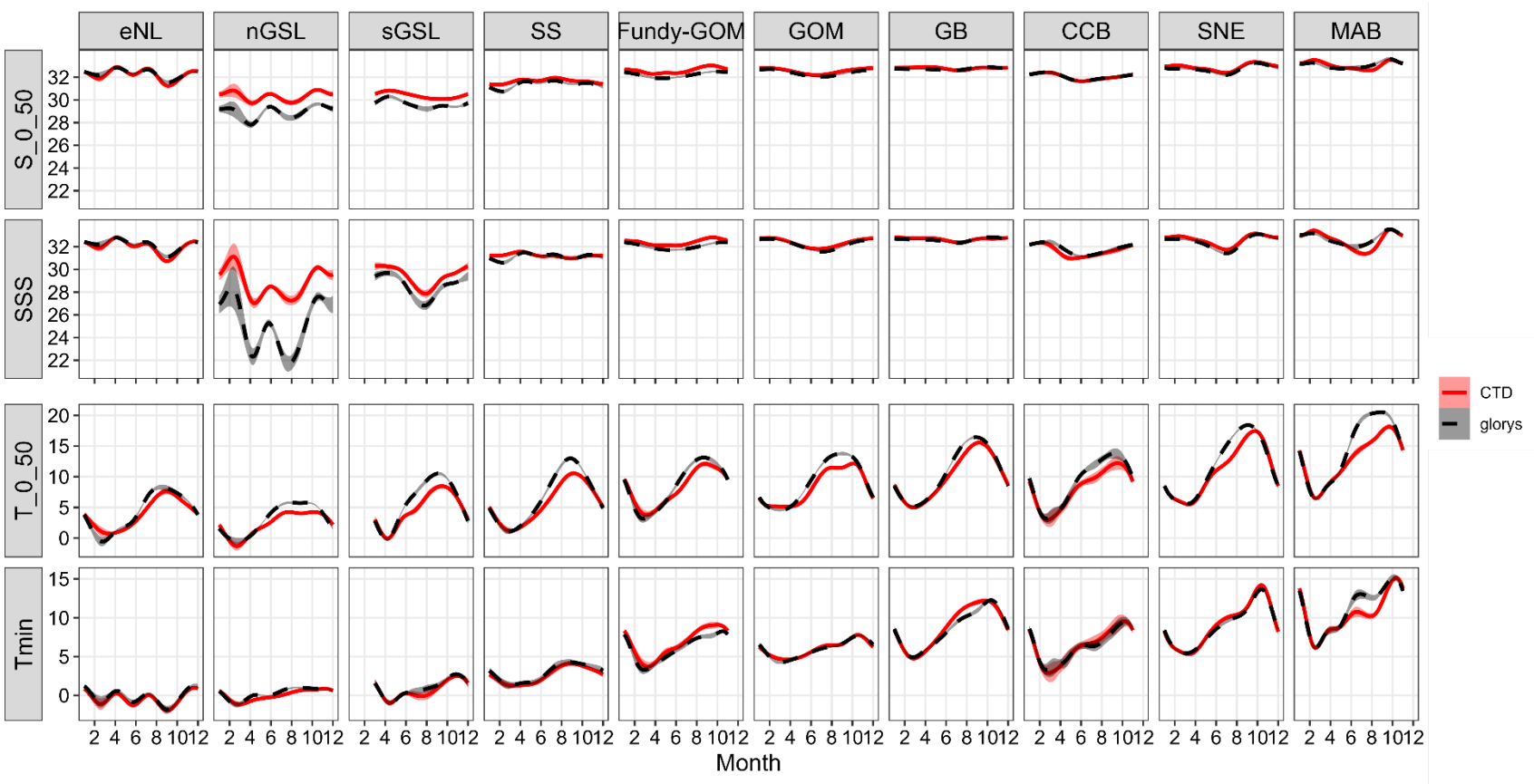

Figure A.1.3. Comparison of the seasonal trends of salinity (S_0_50 and SSS) and temperature (T_0-50 and Tmin) between CTD (red smoothers) and GLORYS12v1 products(black smoothers) at zooplankton stations .

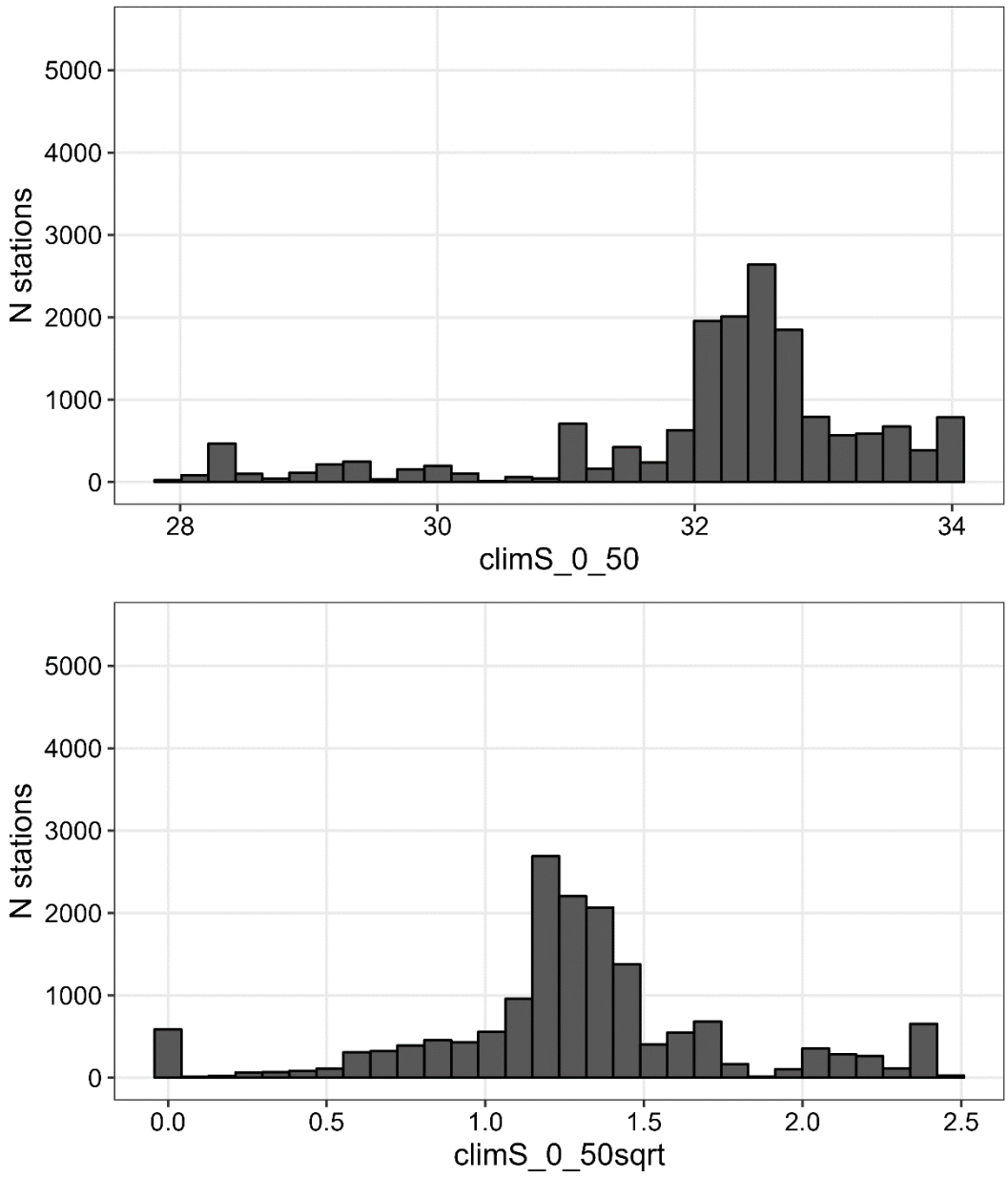

Figure A.1.4. Histograms showing the distribution of climS_0_50 at zooplankton station positions before (upper panel) and after (lower panel) transformation.

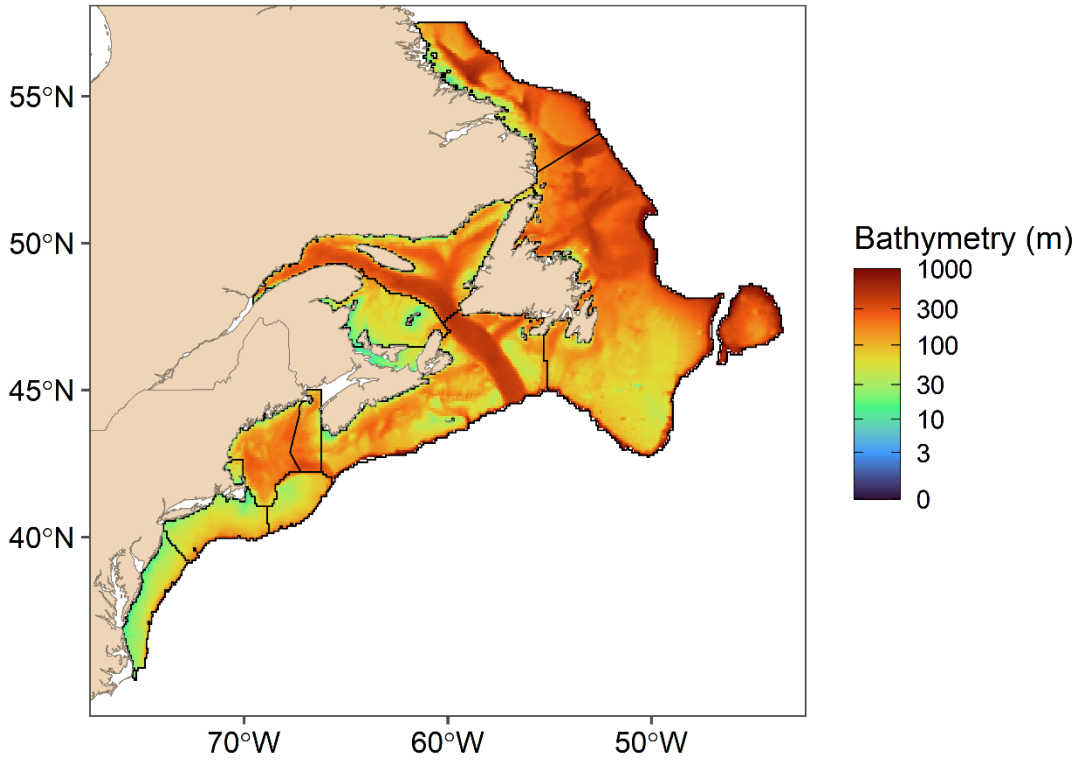

Figure A.1.5. Bathymetry (m) extracted from GLORYS12v1 and used as covariate in SDMs. Black lines delimit regions used to report results (see right panels in Figure 1 for Canada and Figure A.3. 5 for the transboundary area)

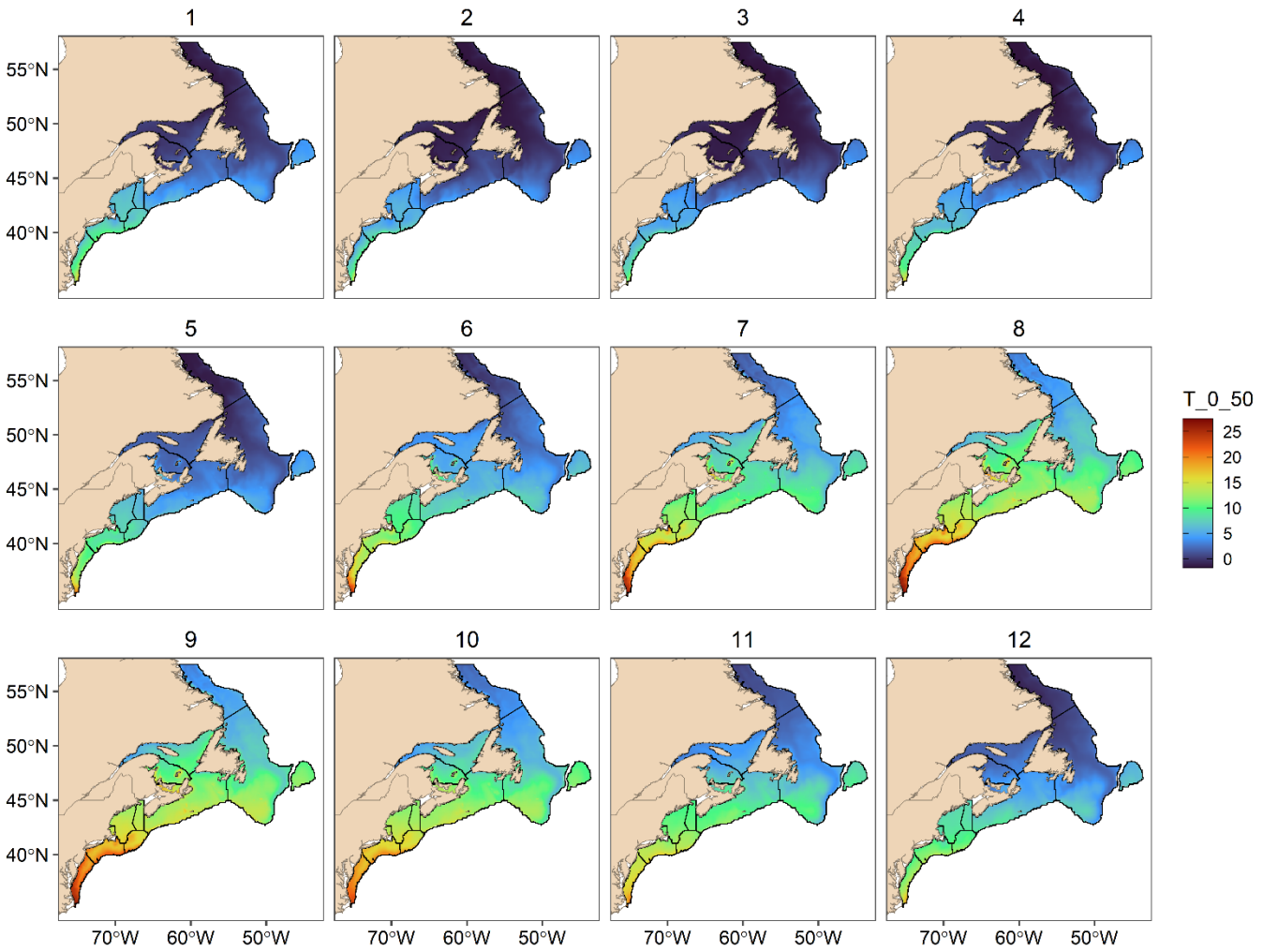

Figure A.1.6. T_0-50 (°C) from GLORYS12v1 monthly product averaged for each month during1999-2020. Black lines delimit regions used to report results (see right panels in Figure 1 for Canada and Figure A.3. 5 for the transboundary area).

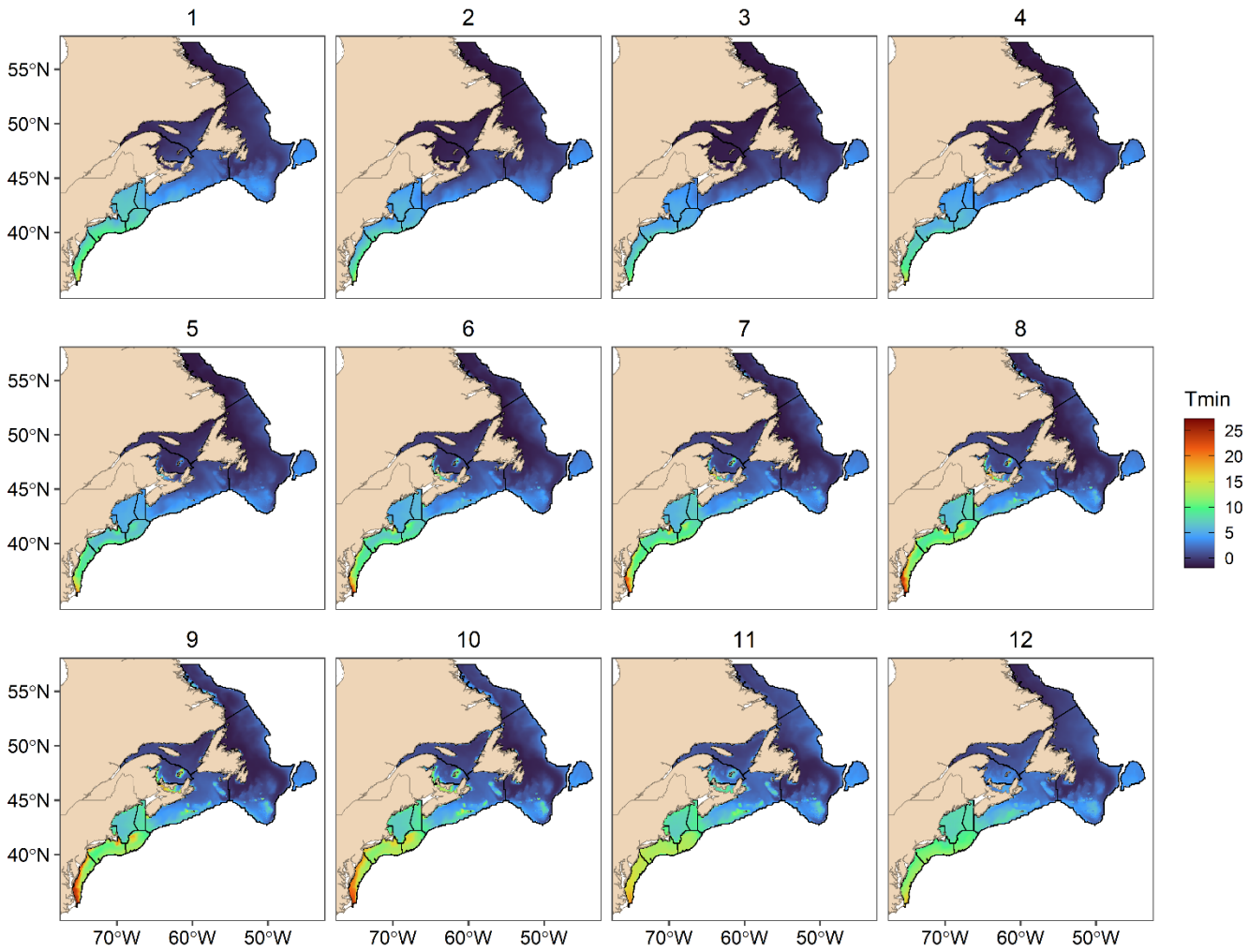

Figure A.1.7. Minimum temperature (Tmin °C) from GLORYS12v1 monthly product averaged for each month during1999-2020. Black lines delimit regions used to report results (see right panels in Figure 1 for Canada and Figure A.3. 5 for the transboundary area).

APPENDIX 2

Table A.2.1. Equations for the determination of the gradient of size based on temperature for each stage of each species. The months to calculate the T_0_50 during the active stages are indicated. The results of the Campbell et al. (2001) equations are multiplied by a scaling factor to account for stage-specific difference in size with C. finmarchicus. The result is divided by a carbon to DW ratio.

Taxa	Stage	Months T_0_50	Equations Campbell et al. (2001)	Scaling			Carbon to DW
C. finmarchicus	CIV	May-August	-4.71 * T_0-50 + 94	-	-	/	0.52
	CV		-18.8 * T_0-50 + 332	-		/	
	CVI		-6.26 * T_0-50 + 262	-		/	
C. glacialis	CIV	May-June	-4.71 * T_0-50 + 94	*	2.5	/	0.52
	CV		-18.8 * T_0-50 + 332	*	1.6	/	
	CVI		-6.26 * T_0-50 + 262	*	1.8	/	
C. hyperboreus	CIV	May-June	-4.71 * T_0-50 + 94	*	5	/	0.6
	CV		-18.8 * T_0-50 + 332	*	5	/	
	CVI		-6.26 * T_0-50 + 262	*	8	/	

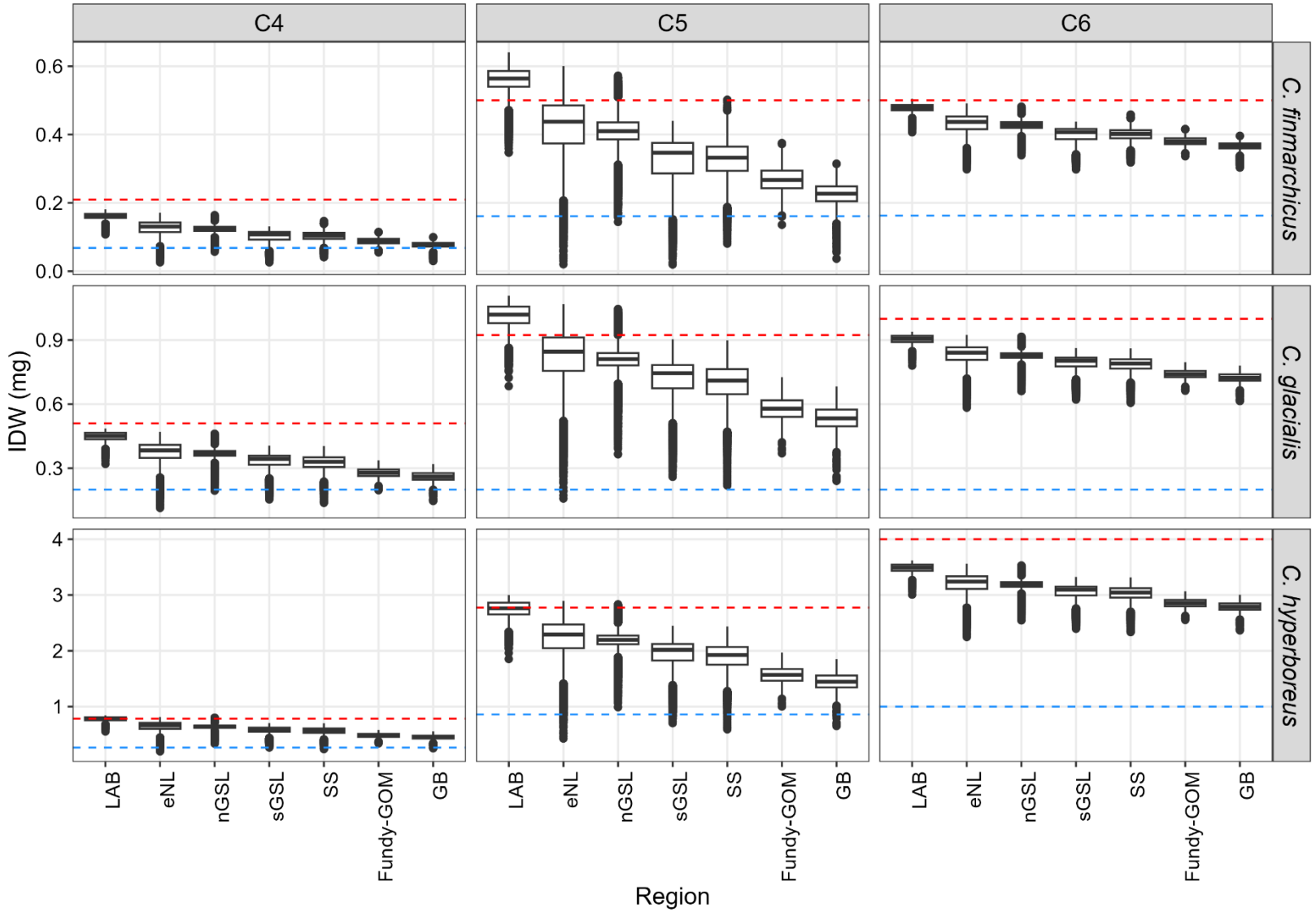

Figure A.2.1. Boxplot of estimated individual dry weight (IDW, mg) by species, stage and Region with T_0-50. The red and blue dashed lines represented the 10 and 90% quantile of individual dry weight in Helenius et al. (2022). Estimated IDW outside of these dashed lines are constrained to these maximum values.

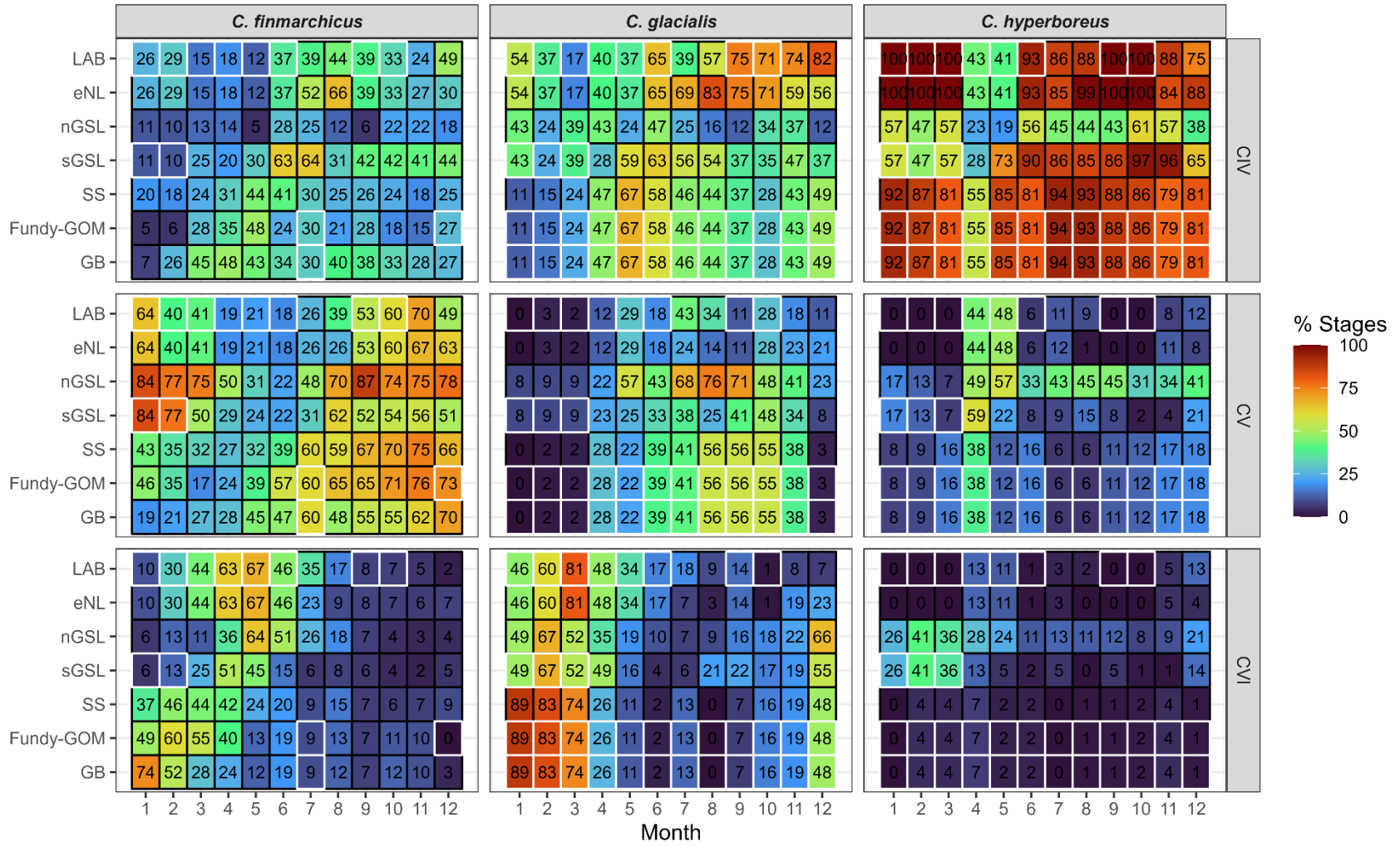

Figure A.2.2. Monthly climatology of the percentage of copepodite stages CIV, CV, CVI on the total CIV-CVI abundance averaged for each region for each species. White boxes indicate that no zooplankton samples were available and the proportions were imputed from adjacent regions.

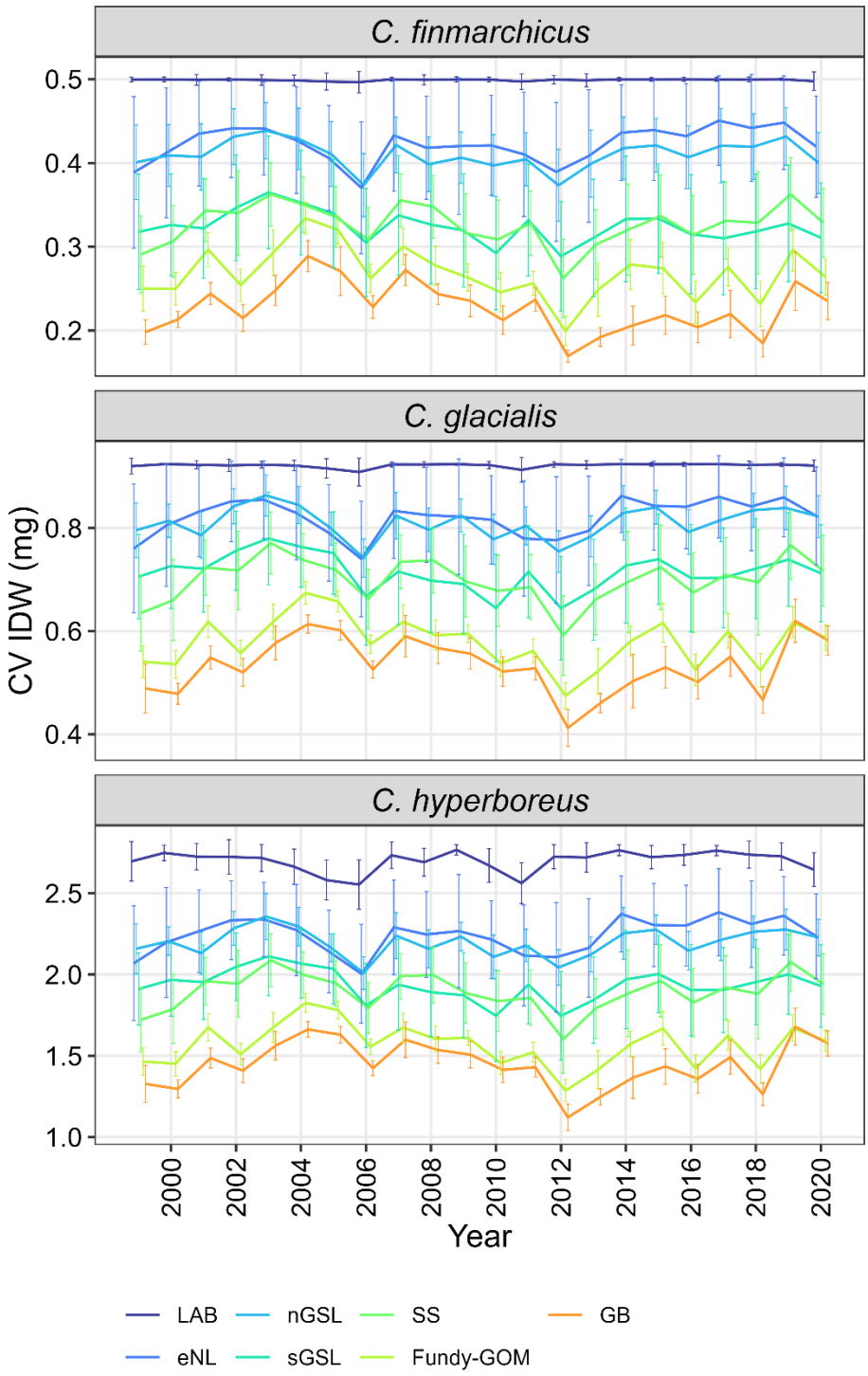

Figure A.2.3. Interannual variation of the IDW of CV predicted by temperature after the outliers were constrained. The solid line represented the annual mean and the error bar, the standard deviation across each region area.

APPENDIX 3

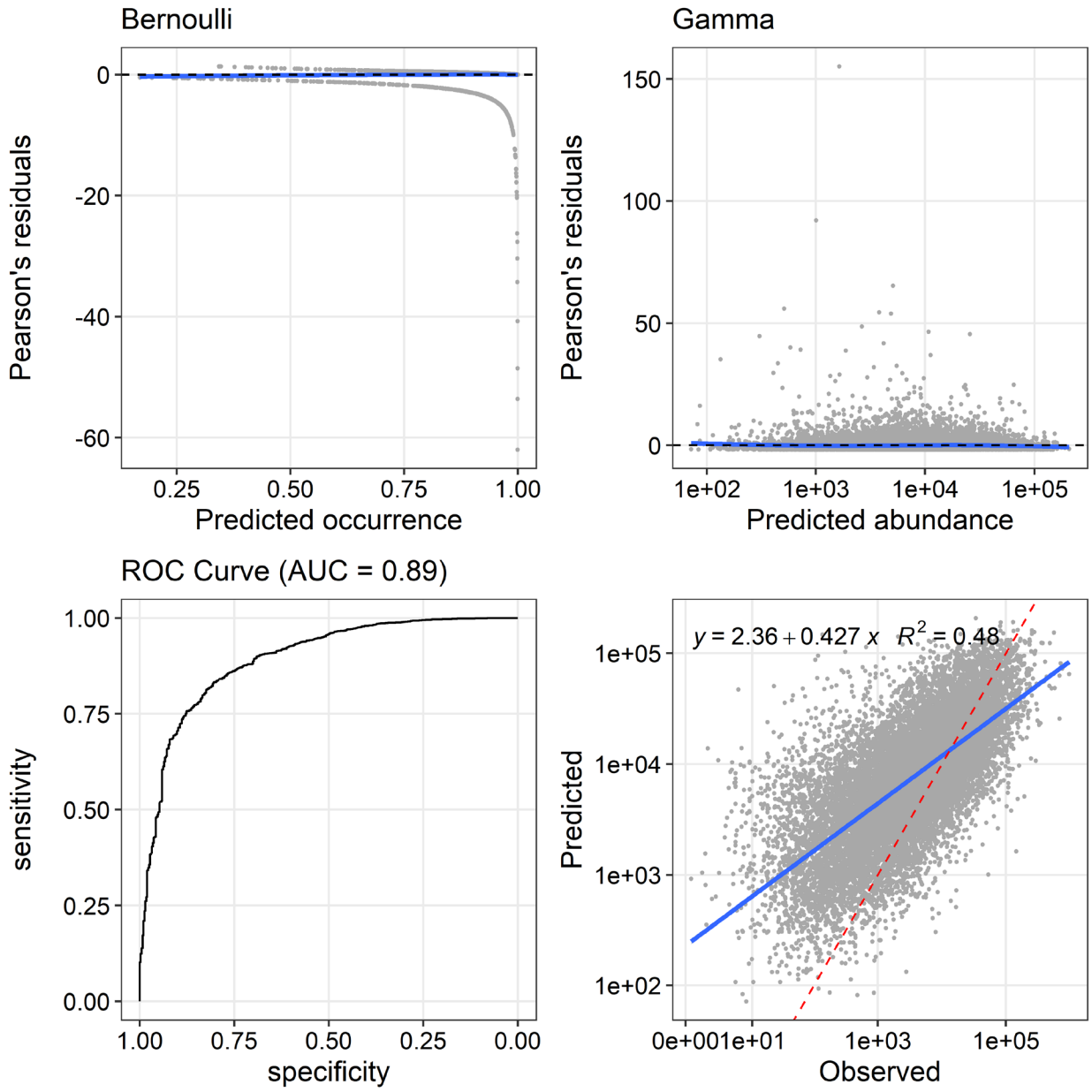

Figure A.3.1. Validation of the Bernoulli (left) and Gamma model (right) for C. finmarchicus. Homogeneity is verified in the upper panels. The smoother on the Pearson's residuals against the predictions (blue) should be near 0 (black dashed line). The accuracy of the predictions is verified with the ROC curve for the Bernoulli model (left, see also Table 2 for TSS) and the Gamma model was validated by a linear relationship between abundance predictions and observations.

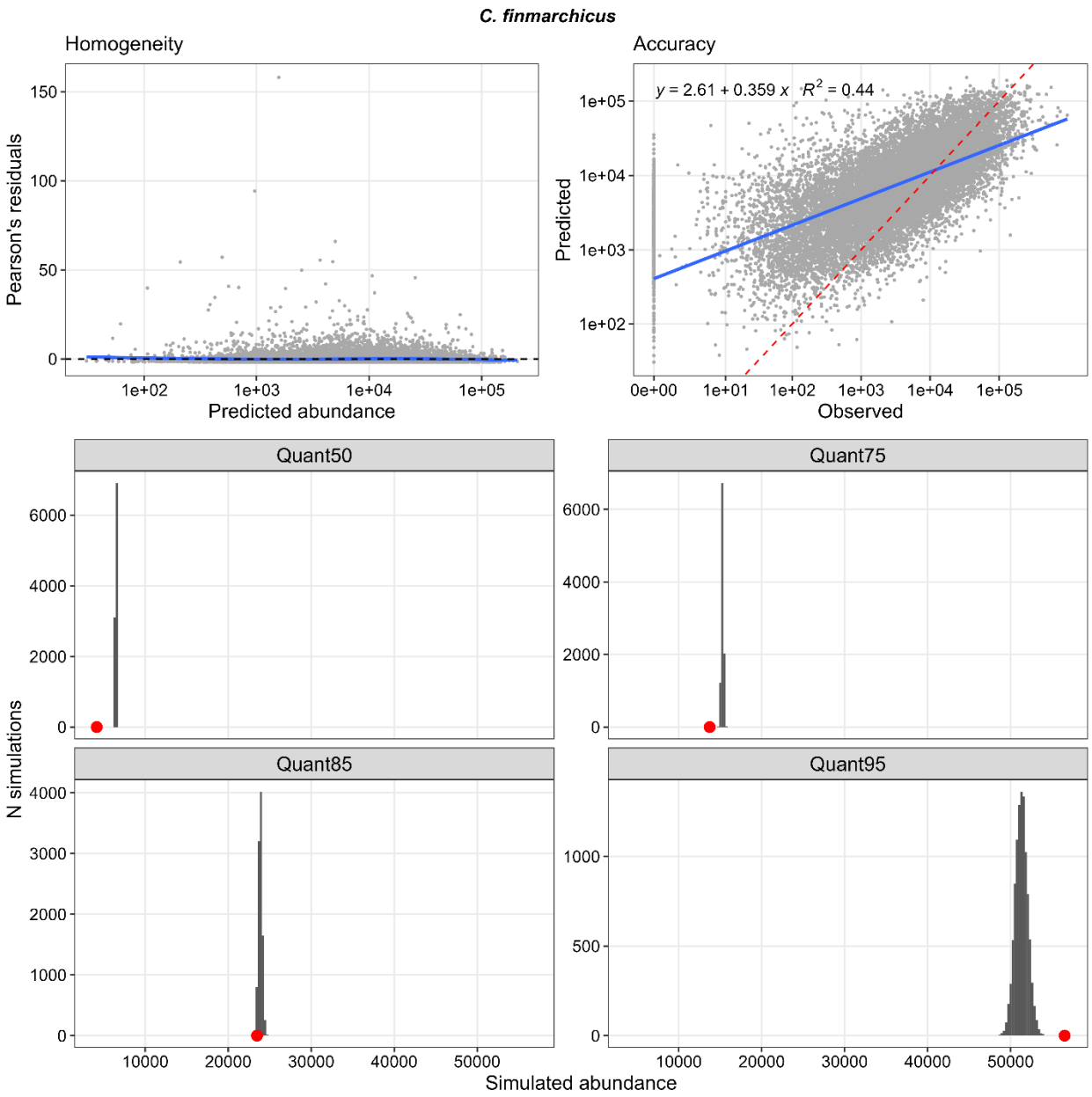

Figure A.3.2. Validation of the ZAG model (π x μ) for C. finmarchicus. Homogeneity and accuracy are verified in the upper panel, see Figure A.3. 1 for details. On the 4 bottom panels, the ZAG simulation distribution (grey histograms) was verified against the observations (red circle) for each of the 50,75,85 and 95 quantiles.

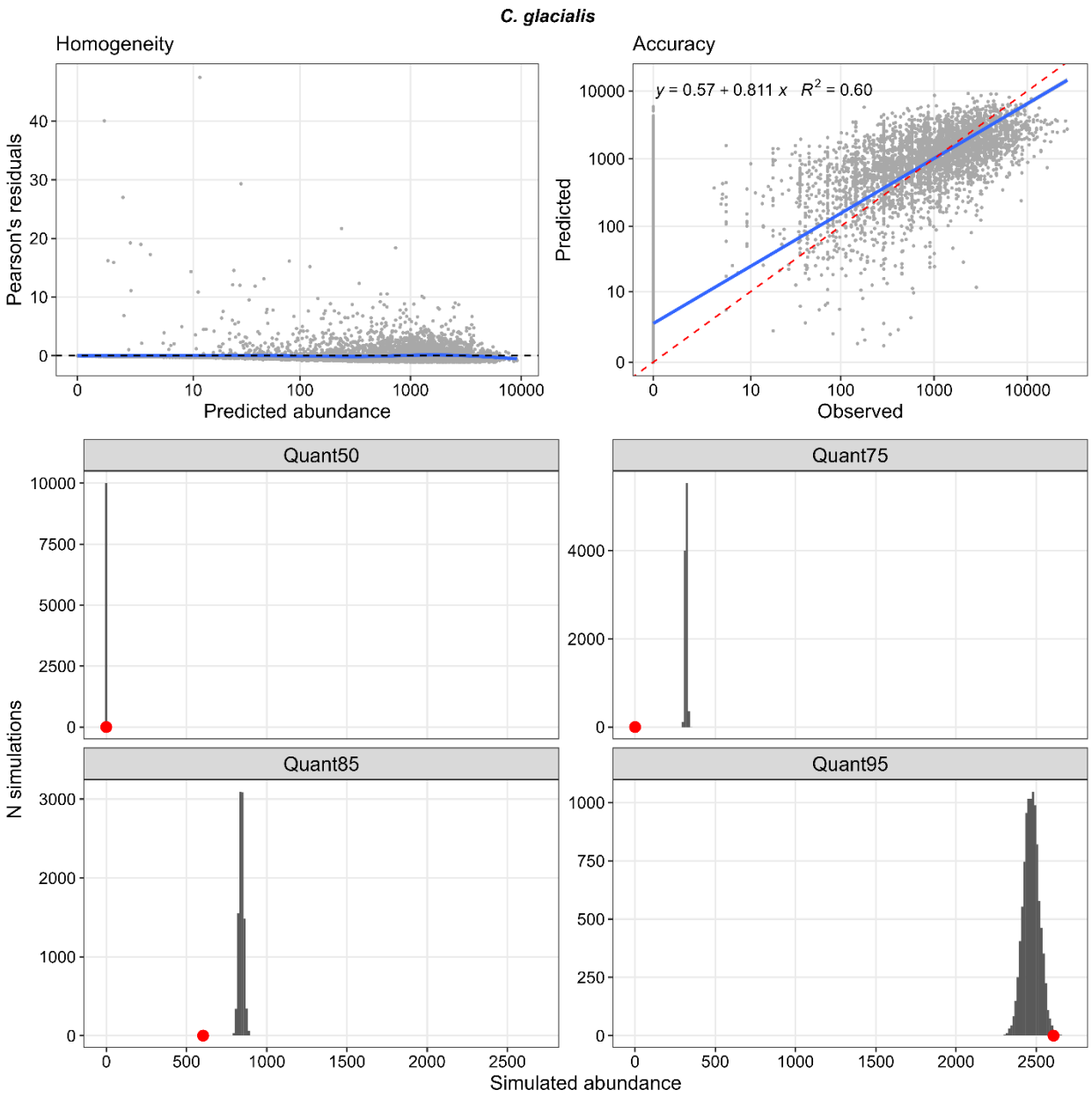

Figure A.3.3. Validation of the ZAG model (π x μ) for C. glacialis. Homogeneity and accuracy are verified in the upper panel, see Figure A.3. 1 for details. On the 4 bottom panels, the ZAG simulation distribution (grey histograms) was verified against the observations (red circle) for each of the 50,75,85 and 95 quantiles.

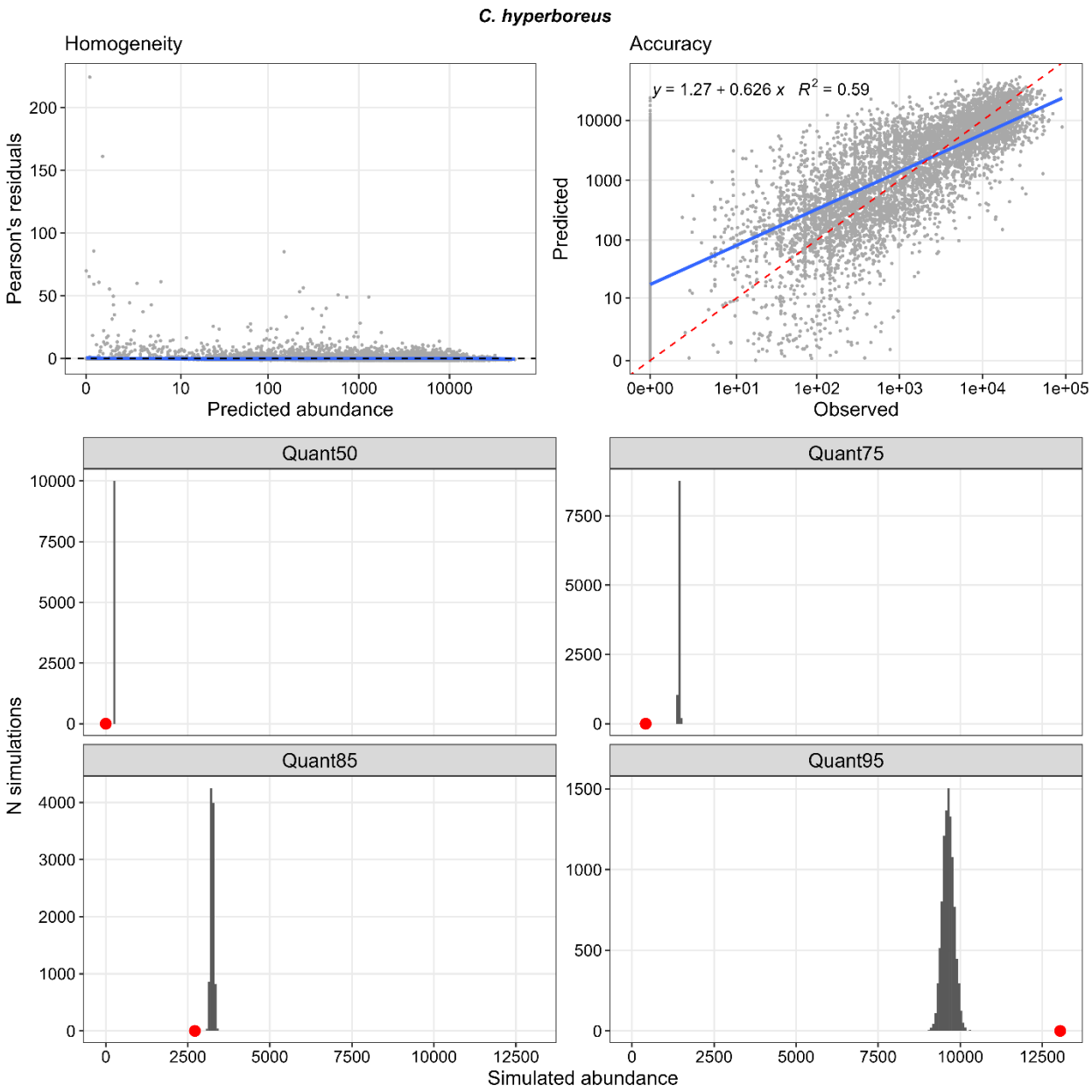

Figure A.3.4. Validation of the ZAG model (π x μ) for C. hyperboreus. Homogeneity and accuracy are verified in the upper panel, see Figure A.3. 1 for details. On the 4 bottom panels, the ZAG simulation distribution (grey histograms) was verified against the observations (red circle) for each of the 50,75,85 and 95 quantiles.

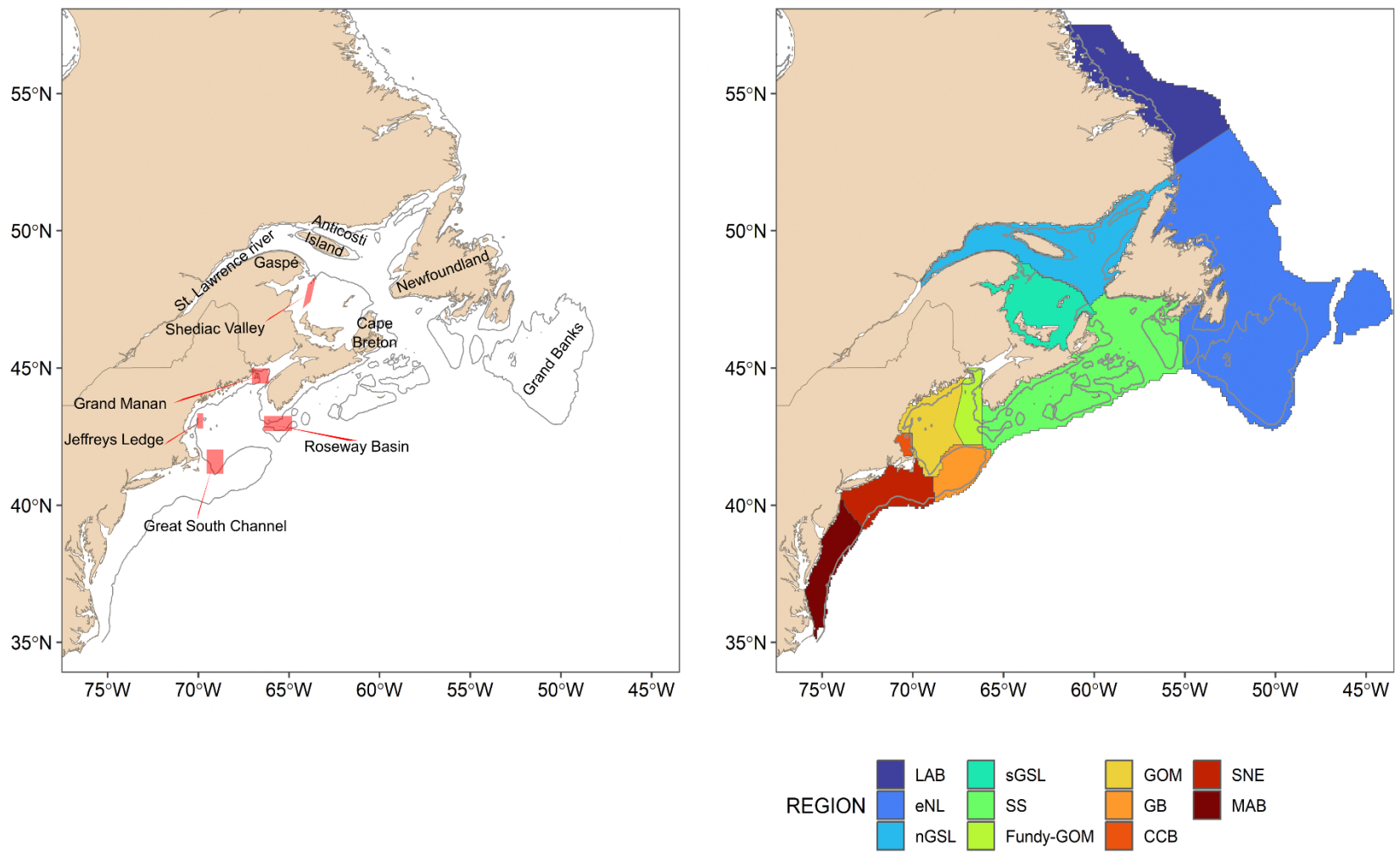

Figure A.3.5. Left panel: Study area with geographic landmarks. Right panel: Maps for regions used to report results. Model 2 also used these regions but with Fundy and SS, and LAB and eNL pooled in 2 larger regions to account for the position of AZMP fixed stations. Grey lines represent 100-m isobaths.

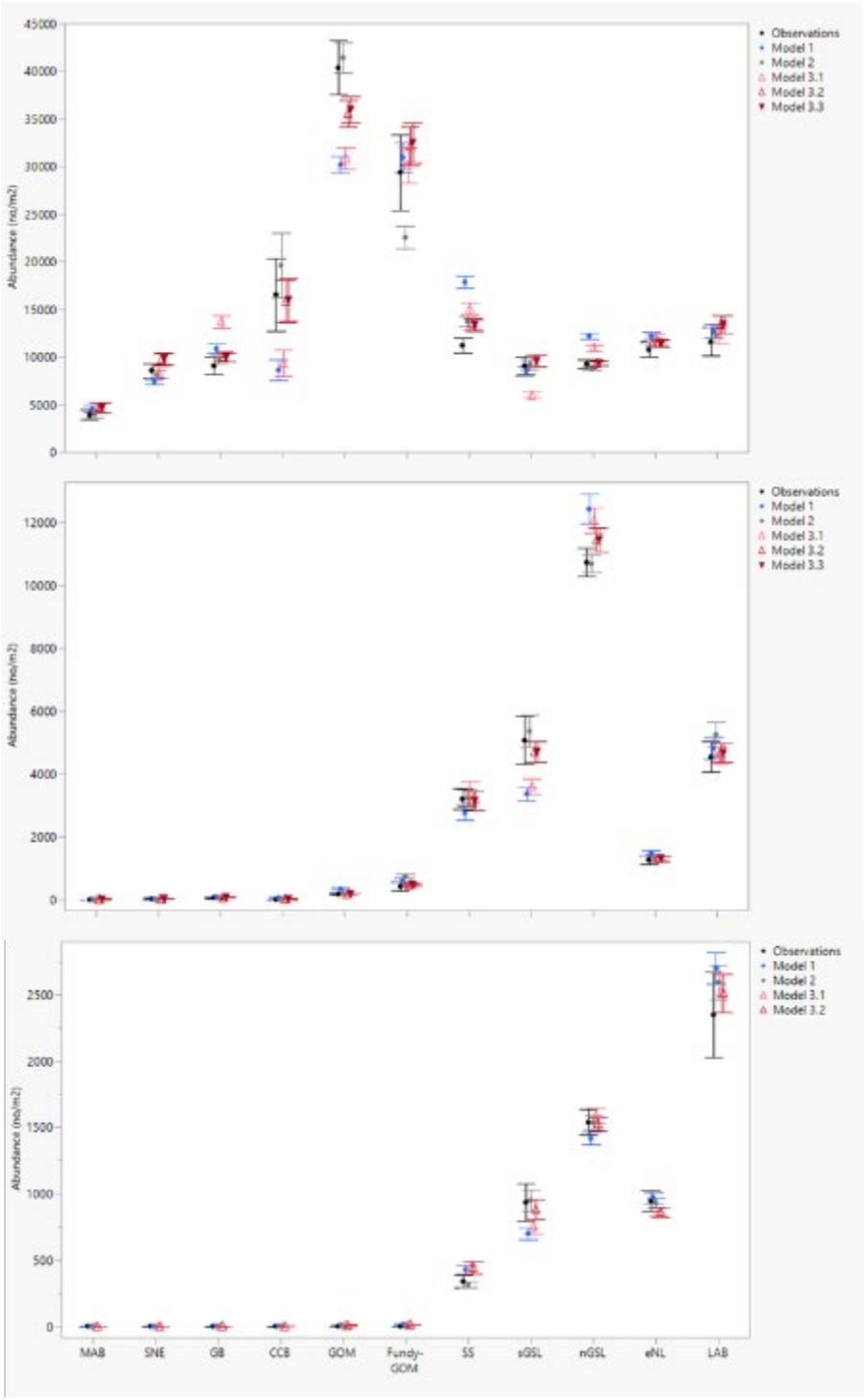

Figure A.3.6. Average observed and predicted abundance and 95%CI of Calanus finmarchicus (top), C. hyperboreus (middle) and C. glacialis (bottom) in different regions during 1999-2020. See text for description of the different models. Model 3.3 was not performed for C. glacialis.

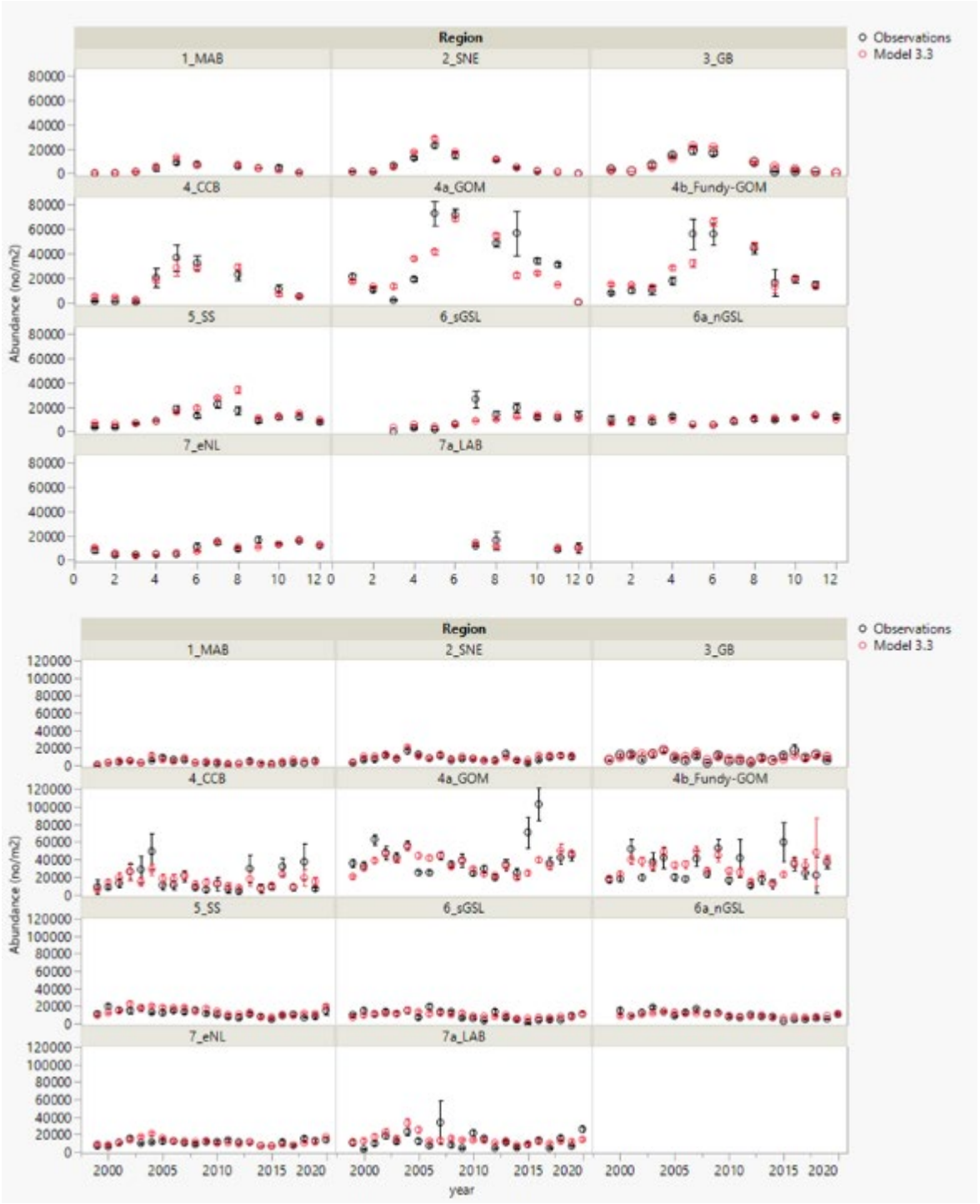

Figure A.3.7. Calanus finmarchicus. Monthly (top) and annual (bottom) averaged observed and predicted (Model 3.3) abundance in different regions during 1999-2020. Error bars = s.e.

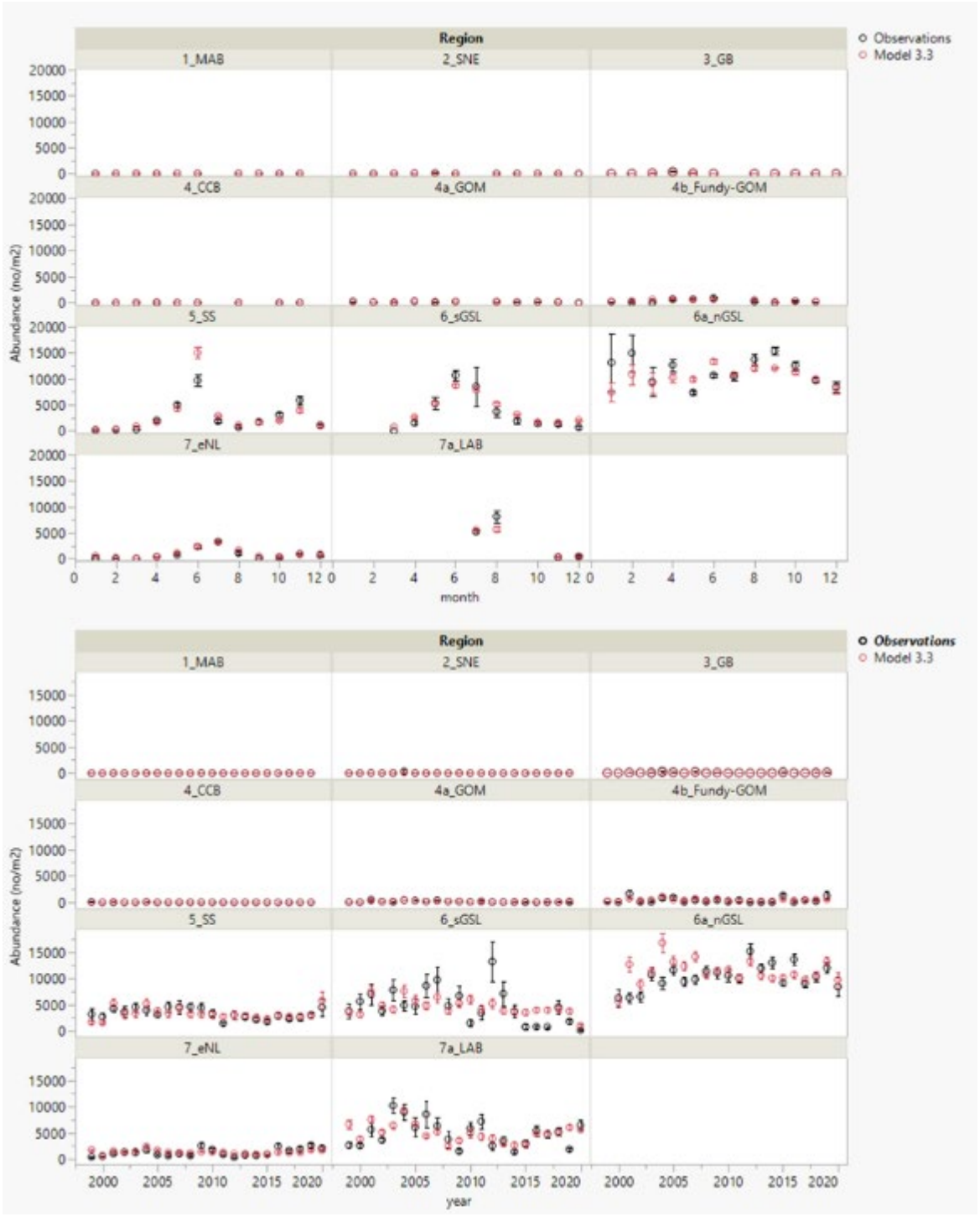

Figure A.3.8. Calanus hyperboreus. Monthly (top) and annual (bottom) averaged observed and predicted (Model 3.3) abundance in different regions during 1999-2020. Error bars = s.e.

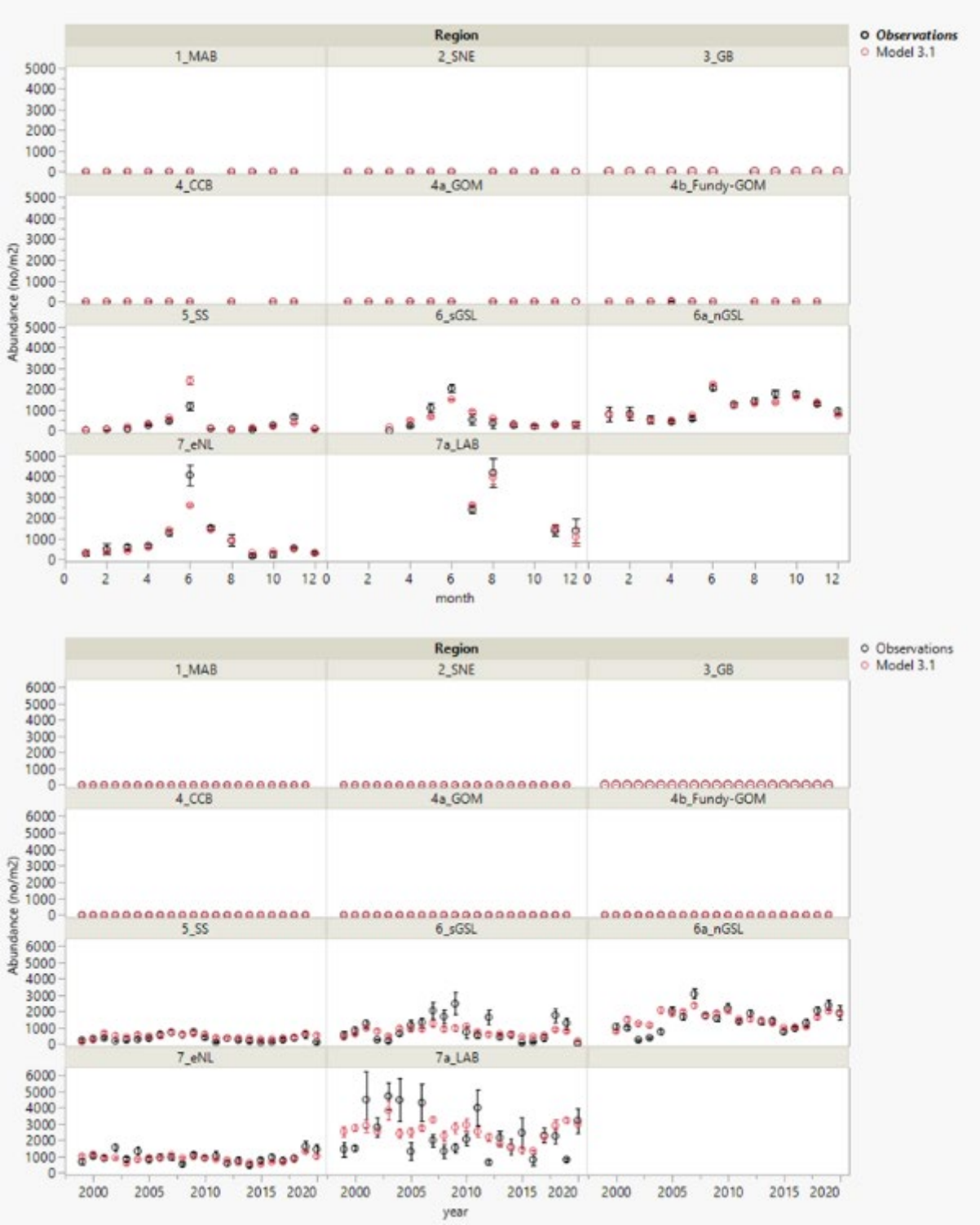

Figure A.3.9. Calanus glacialis. Monthly (top) and annual (bottom) observed and predicted (Model 3.1) abundance in different regions during 1999-2020.

APPENDIX 4

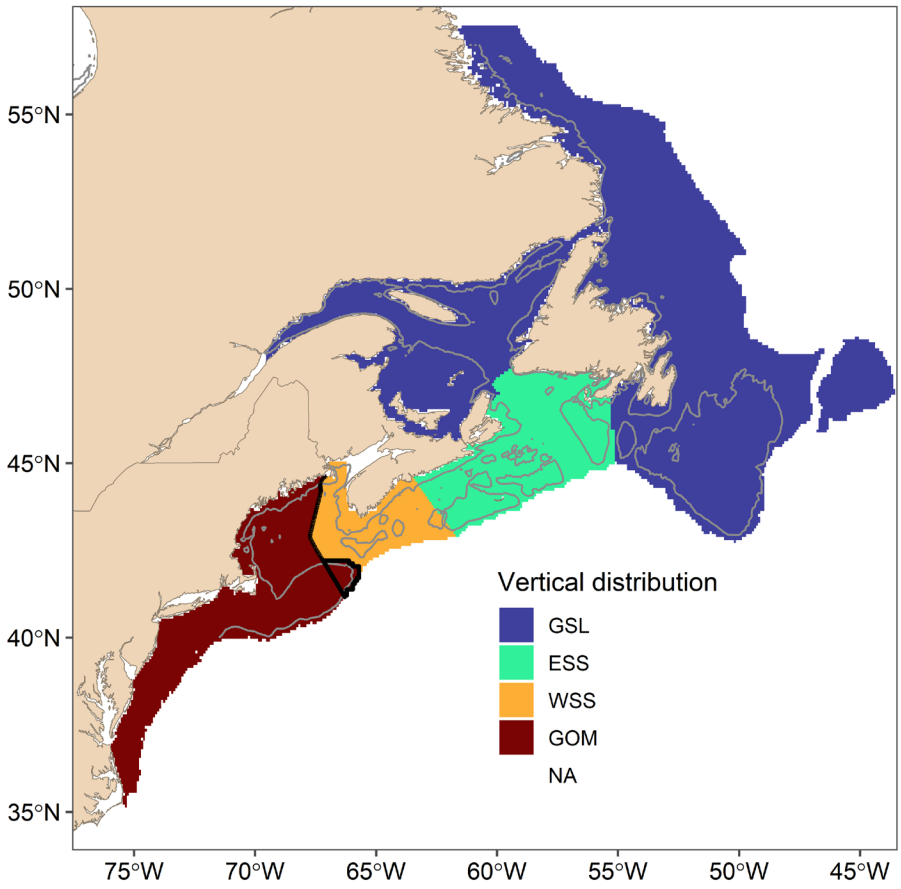

Figure A.4.1. Map of vertical distribution regions used in predictions. The vertical distribution model from the GSL was applied in the LAB and eNL region and the vertical distribution model for the GOM was applied in the GOM and northeast USA shelf. The black bold line separates the Canadian part of GB.

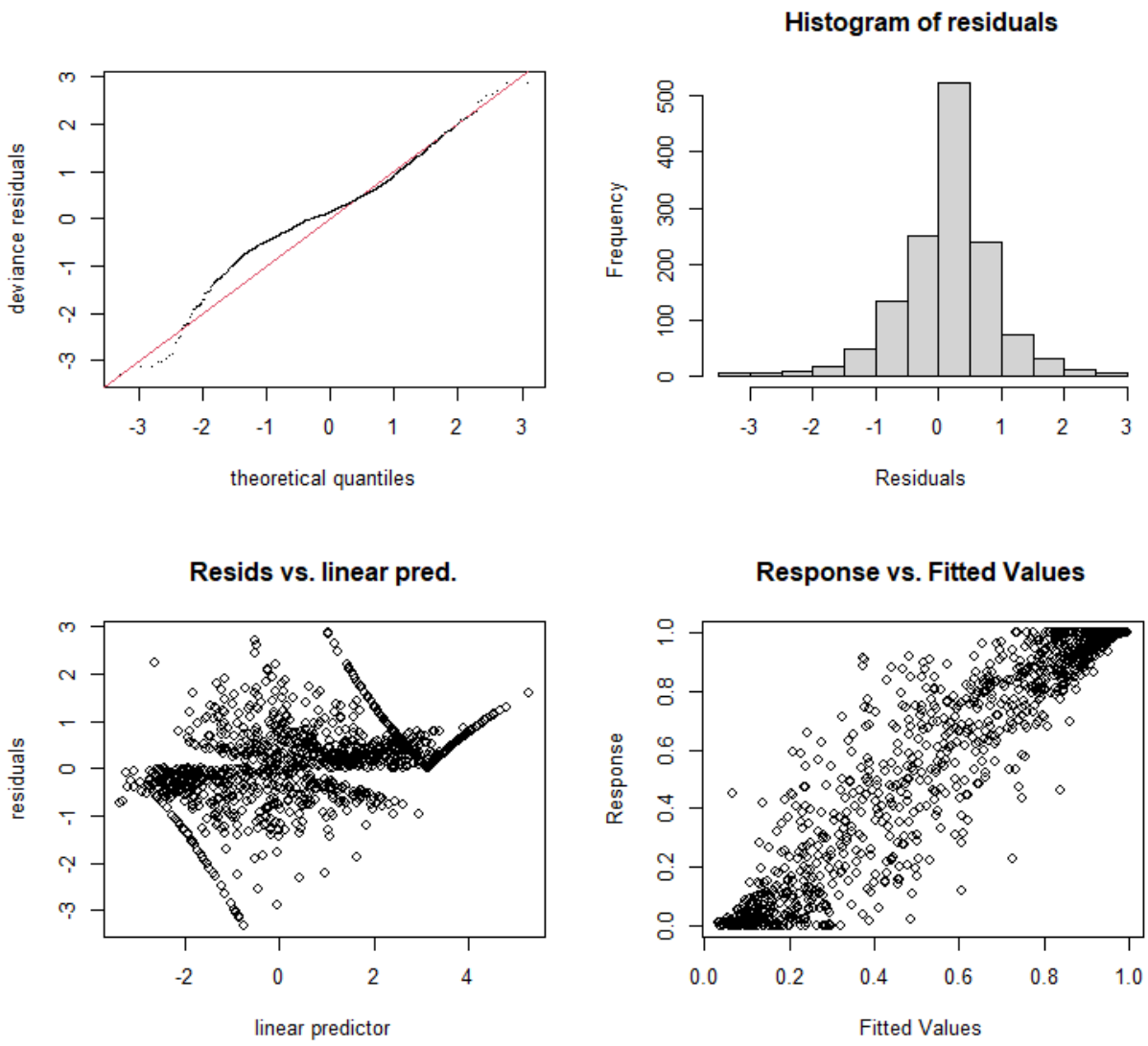

Figure A.4.2. Validation of the GOM vertical distribution GAM for C. finmarchicus CIV-CVI.

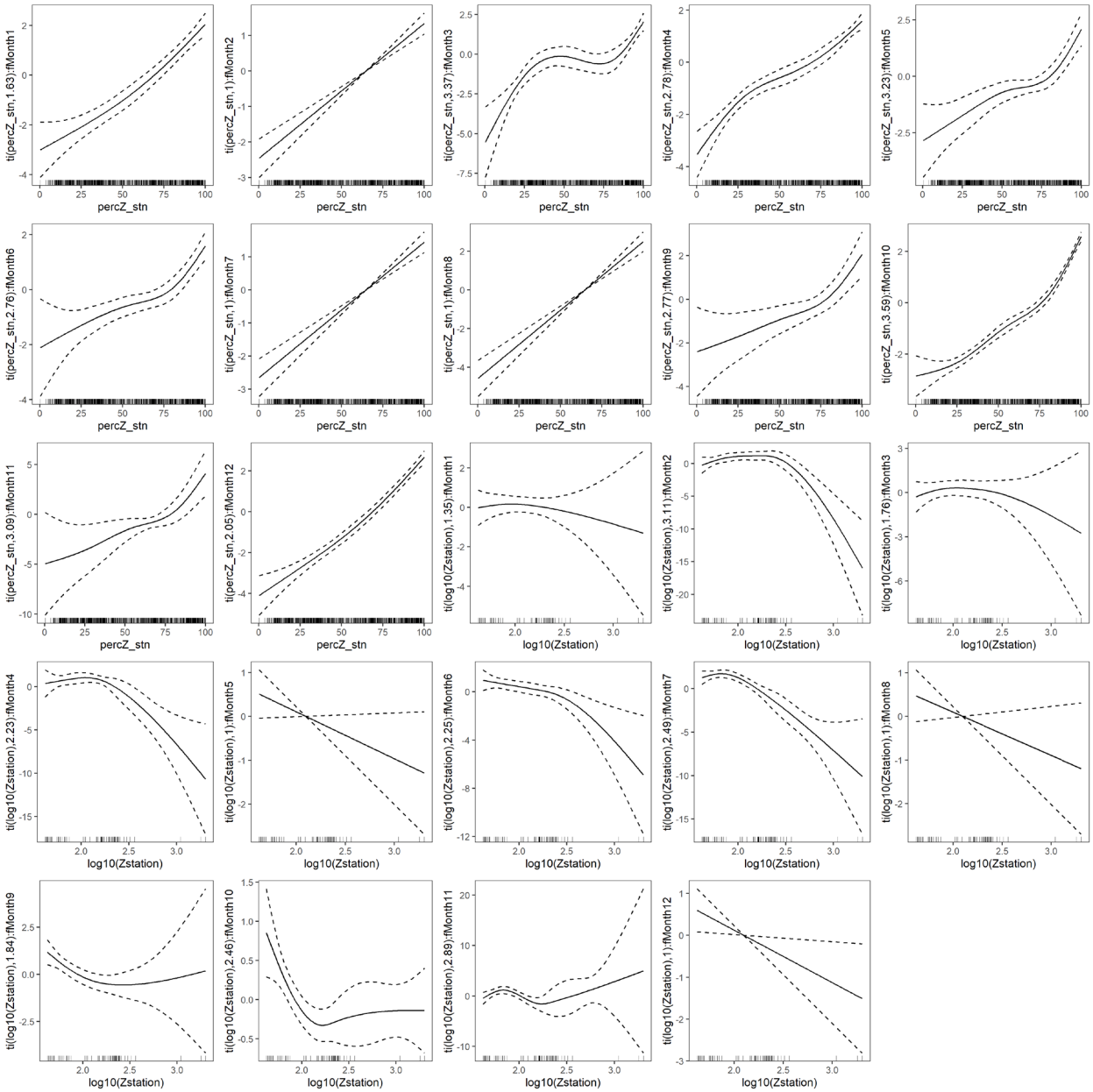

Figure A.4.3. Main effect of the GOM vertical distribution GAM for C. finmarchicus CIV-CVI. percZ_stn = %Z, Zstation = Z.

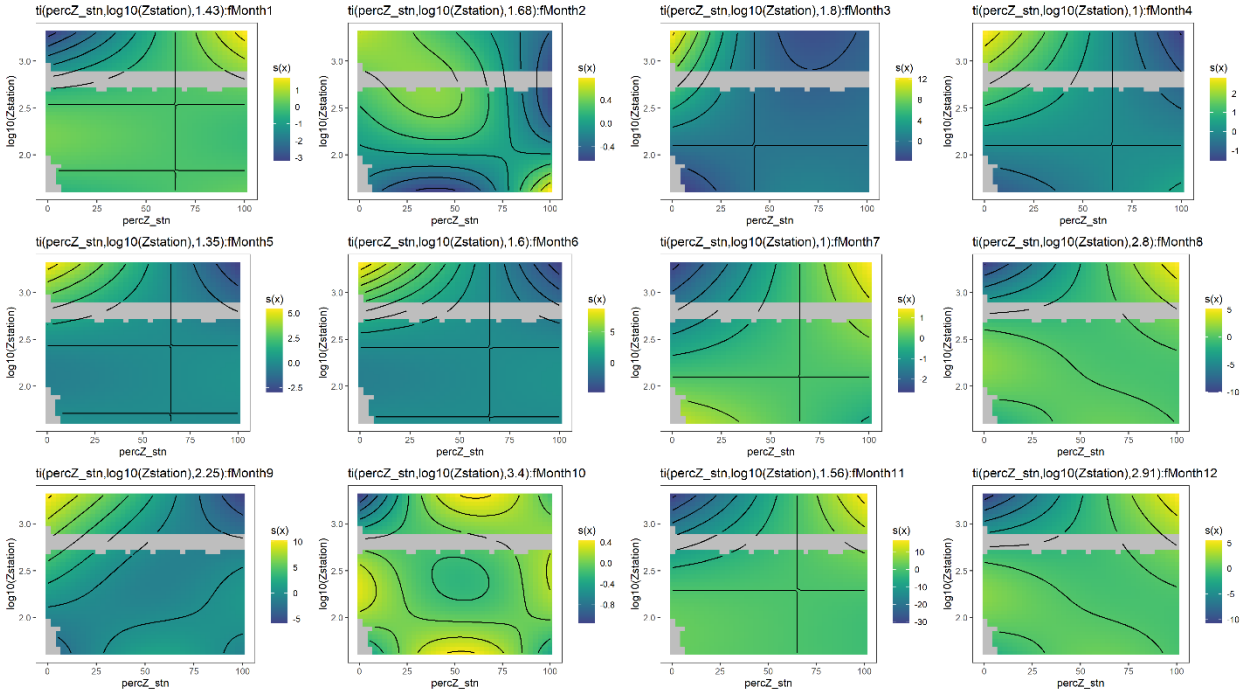

Figure A.4.4. Interaction between Zstation (Z) and percZ_stn (%Z) for each month in the GOM vertical distribution GAM for C. finmarchicus CIV-CVI.

Table A.4.1. Results of for the GOM vertical distribution GAM for C. finmarchicus CIV-CVI. P-value of smooth terms is indicated by P >0.05; ∗ P =0.05–0.01; ∗∗ P =0.01–0.001; ∗∗∗ P <0.001. a = non-significant. %Z is the percentage of the water column sampled and Z is the station depth. Months are represented by the numbers for each term.

GAM fit	Number of stations	272	
	Total N = Nstations x NZlayers	1349	
	% deviance explained	92.5	
GAM validation	Cross-validation	70/30%	100%
	Correlation	0.87	0.89
	intercept	0.09	0.16
	slope	0.81	0.73
	R^2	0.75	0.76
GAM terms	GAM terms	EDF and significance	
	%Z: 1	1.63	***
	%Z: 2	1.00	***
	%Z: 3	3.37	***
	%Z: 4	2.78	***
	%Z: 5	3.23	***
	%Z: 6	2.76	***
	%Z: 7	1.00	***
	%Z: 8	1.00	***
	%Z: 9	2.77	***
	%Z: 10	3.59	***
	%Z: 11	3.09	***
	%Z: 12	2.05	***
	Z: 1	1.35	a
	Z: 2	3.11	***
	Z: 3	1.76	a
	Z: 4	2.23	***
	Z: 5	1.00	a
	Z: 6	2.25	**
	Z: 7	2.49	***
	Z: 8	1.00	a
	Z: 9	1.84	***
	Z: 10	2.46	*
	Z: 11	2.89	**
	Z: 12	1.00	*
	%Z *Z: 1	1.43	a
	%Z *Z: 2	1.68	a
	%Z *Z: 3	1.80	**
	%Z *Z: 4	1.00	a
	%Z *Z: 5	1.35	a
	%Z *Z: 6	1.60	a
	%Z *Z: 7	1.00	a
	%Z *Z: 8	2.80	*
	%Z *Z: 9	2.25	**
	%Z *Z: 10	3.40	**
	%Z *Z: 11	1.56	a
	%Z *Z: 12	2.91	***
	s(station)	161.57	***